UNIVERSITY OF LIVERPOOL

AN EXPERIMENTAL AND NUMERICAL STUDY ON THE IMPACT OF WIND INDUCED TURBULENCE ON GASEOUS DISPERSION IN POROUS MEDIA

Thesis submitted in accordance with the requirements of
the University of Liverpool for the degree of Doctor in Philosophy

By

Alireza Pourbakhtiar

January 2018

ABSTRACT

AN EXPERIMENTAL AND NUMERICAL STUDY ON THE IMPACT OF WIND INDUCED TURBULENCE ON GASEOUS DISPERSION IN POROUS MEDIA

By

Alireza Pourbakhtiar

This research focuses on how wind turbulence influences gas transport in the porous media. It can be useful in measuring the amount of greenhouse gasses from subsurface to atmosphere or a hazardous gas like Radon emission into buildings. It can also be important in other fields of research, anywhere that gas transports through porous media.

A novel experimental arrangement is demonstrated for measuring wind turbulence-induced gas transport in dry porous media under controlled conditions. This equipment was used to measure the effect of wind turbulence on gas transport (quantified as a dispersion coefficient) as a function of distance to the surface of the porous medium exposed to wind. Two different methods for the measurement of wind-induced gas transport were compared. . In one of approaches, which is a modified version of other one, five sensors are placed inside the sample of porous material at same intervals which can measure the oxygen concentration values. Approaches are used for measuring diffusion and wind-induced dispersion. Tracer gases of O_2 and CO_2 with average vertical (perpendicular to the surface of porous medium) wind speeds of 0.02 to 1.06 m s^{-1} were applied at room temperature condition. Five different fractions of soil are utilized to find out how the particle size can affect the gas transport in a specific

wind condition at the surface of soil as the porous media. It is shown that gas dispersion was 20–100 times higher due to wind action.

Ten wind conditions (plus calm condition with zero wind speed) are selected and three perpendicular components of wind as well as wind fluctuations are characterized. Oxygen breakthrough curves as a function of distance to the wind-exposed surface of the porous medium were analysed numerically with a finite-difference based model to assess gas transport. Potential relationships between breakthrough time and wind speed characteristics in terms of average wind speed, wind speed standard deviation and wind speed power spectrum properties in three dimensions were investigated. Statistical analyses indicated that the wind speed had a very significant impact on breakthrough time and that the characteristics for the wind speed component perpendicular to the porous medium surface were especially important.

For the experiments, the penetration depth (Z_{50}) is introduced. Linear inverse relation between penetration depth and empirical factor is determined. Wind characteristics can affect the gas transport speed and penetration depth inside porous media for particle sizes above 1mm. At particle size below 0.5 mm the effect of wind on gas transport is negligible.

The relation between different wind speed characteristics such as wind speed or its power spectrumand particle shape and size on gas transport is analysed.

The main component of wind which affects the gas transport was found to be the vertical one. An expression (Eq. 26) for calculating the wind-induced dispersion coefficient has been developed which is dependent on wind speed. The direct

calculation of the empirical factors and wind induced dispersion coefficient of porous media at the surface is more accurate by fitting the empirical and numerical parameters.

DECLARATION

I hereby certify that this dissertation constitutes my own product, that where the language of others is set forth, quotation marks so indicate, and that appropriate credit is given where I have used the language, ideas, expressions or writings of another.

I declare that the dissertation describes original work that has not previously been presented for the award of any other degree of any institution.

Alireza Pourbakhtiar

ACKNOWLEDGEMENTS

First of all I express my appreciation to my parents who were always backing me and encouraging me.

It is my pleasure to acknowledge the role of individuals who had guided me during my PhD studies. I express my gratitude to Dr. Konstantinos Papadikis who were the supervisor of my PhD studies in last year with his great supports I appreciate my former supervisors, Dr. Tjalfe Poulsen for his guidance and ideas for my PhD. Also, thanks to Dr. Stephen Wilkinson and Dr. Jonathan Bridge for their encouragement and support.

I acknowledge stuff of department of Civil Engineering at Xi'an Jiaotong-Liverpool University and its soil mechanic laboratory.

Alireza Pourbakhtiar

CONTENTS

LIST OF PUBLICATIONS

1. Pourbakhtiar, A., Poulsen, T. G., Wilkinson, S. and Bridge, J. W., Effect of wind turbulence on gas transport in porous media: experimental method and preliminary results. (2017). Eur J Soil Sci, 68: 48–56. DOI:10.1111/ejss.12403**.** ***(Editor's Choice) ****

2. Poulsen, T., Pourber*, A., Furman, A., Papadikis, K., Relating wind-induced gas exchange to near-surface wind speed characteristics in porous media, (2017). Vadose zone journal, Journal, 2017. 16(8), DOI: 10.2136/vzj2017.02.0039.

3. Pourbakhtiar, A., Poulsen, T., Papadikis, K., Wilkinson, S., Relation between wind-induced gas transports in porous media and medium characteristics, (2018). Gas transport in porous media.

- "A. Pourber" is the pseudonym that was used for the author "Alireza Pourbakhtiar". They represent the same person.

LIST OF TABLES

LIST OF FIGURES

NOMENCLATURE

Latin Symbols

A_k: Empirical Parameter

As: Cross-sectional Area, m^2

B_k: Empirical Parameter

C_k: Empirical Parameter

C_p: Pressure Coefficient

C, C_g: Mass of chemical vapour per volume of soil air space, Gas concentration, m^3/m^3

CV: Coefficient of Variation

d: Particle size, m

D_0: Molecular Diffusion Coefficient in free air, m^2/s

D_{10}: Intercepts for 10of the cumulative mass, m

D_{50}: Intercepts for 50% of the cumulative mass, m

D, D_g^a: The Binary Gaseous Diffusion Coefficient in free air, m^2/s

D_g^s = diffusion coefficient of gas in soil, m^2/s

D_m: Coefficient of Molecular Gas Diffusion, m^2/s

D_w: Wind-induced Dispersion Coefficient, m^2/s

f: Wind Speed Fluctuation Frequency

H: Height of Sample, m

h: Hydraulic Head, m

J: Gas Diffusion Flux, mol/m^2s

K_S: Hydraulic Conductivity, m/s

K_a: Gas Permeability of Porous Media, m^2

K_{air}: Air Conductivity, m/s

L: Length of Sample, m

P: Pressure, Pa

Q: Gas Flow, m^3/s

r: Roundness

R: Major Axis of Ellipse, m

Ra: Mean Deviation Roughness, m

R_q: Root Mean Squared Roughness, m

R_v: Max Valley Depth Roughness, m

R_p: Max Peak Height Roughness, m

R_t: Max Height Profile Roughness, m

R_{sk}: Skewness Roughness, m

R_{ku}: Kurtosis Roughness, m

Rc: Coefficient of Retardation, m

s: Standard Deviation

S: slope of relative normalized dispersion coefficient

T: Time, s

T: Temperature, K

T: Turbulence Intensity

t_b: Breakthrough Time, s

t_{b0}: Relative Breakthrough Time

u: Wind Component in Direction X

v: Wind Component in Direction Y, m/s

V_{pore}: Volume of Voids, m^3

V: Volume, m^3

V: Total Wind Speed, m/s

V_x: Resultant horizontal wind components, m/s

V_z: Vertical Component of Wind Speed, m/s

w: Wind Component in Direction Z, m/s

Wi: Wind Condition Number i

X: Vertical Direction to Material Surface

Y: Horizontal Direction to Material Surface

z: Distance or Depth, m

Z: Horizontal Direction to Material Surface

Z_{50}: Penetration Depth, m

Greek Symbols

ε: Gas-filled Porosity

η: Dynamic Viscosity, Pa.s

λ: Average Length of Fluid Paths, m

ρ: Air Density at Atmosphere Pressure, kg/m^3

τ: Tortuosity

Φ: Total Porosity

Φ(*f*): Power Spectral Density, W/Hz

Subscript

atm: Atmosphere

k: Kaimal

l: Linear

w: Wind-induced

x: direction of x

y: direction of y

z: direction of z

Abbreviations

FDM: Finite Deference Method

SSE: Sum of Squared Error

RMSE: Root Mean Square Error

Chapter 1 INTRODUCTION

1.1 Background and novelty

Exchange of gaseous compounds between the subsurface and the atmosphere is an important mechanism controlling processes such as uptake of atmospheric CH_4 by natural soils, and intrusion of volatile contaminants from contaminated soil sites into outdoor and indoor urban environments. Thus, gas exchange has a potentially strong impact on both our global and local environment. Greenhouse gases play an important role in global warming. Soil is a source of some greenhouse gases such as methane (CH_4), carbon dioxide (CO_2) and nitrous oxide (N_2O). It is found that humidity, temperature, air pressure and vegetation tare of the affecting factors in those emissions. (Oertel et al. 2016). Nazaroff (1992) found that the difference between indoor and outdoor temperature controls the advective flow of Radon (Rn) from soil into the buildings. Several studies showed the effect of wind action on gas transport through soil for example in landfill gas emissions (Poulsen & Moldrup 2006). In addition, there are studies, which modelled the effect of wind gustiness on gas transport in porous media (Farell et al. 1966, Colbeck 1981). Poulsen & Moldrup (2006) showed that wind-induced gas transport in porous media is a dispersive process. Knowledge about the impact of wind speed characteristics and porous media properties on wind-induced gas dispersion in porous media is poor.

One of the issues in Carbon capture and storage projects (CCS) is the possibility of leakage from storage reservoir to surface and then atmosphere. Developing reliable methods to monitor and characterize potential CO_2 leakage is important for safety of

storage reservoir and risk assessment of the project (Basirat et al, 2013). Furthermore, the emission of methane, which is an important greenhouse gas, can result from land management such as from rice paddy soil and landfill sites that receive organic matter (Topp & Pattey, 1997). Contaminated soil is a source of hazardous vapours, which emits from soil into buildings and makes indoor contaminant vapour concentrations. An example is Radon (Rn); a radioactive gas that can move from soil to the atmosphere with the potential to affect human health. Radon and other volatile organic compounds produced in soil can enter building on the contaminated land due to depressurisation created by wind entering the building or the temperature differences between outdoor and indoor (Wang & Ward, 2002). Fig. 1-1. is a schematic diagram of a house exposed to Radon entry from its contaminated subsurface due to air flow.

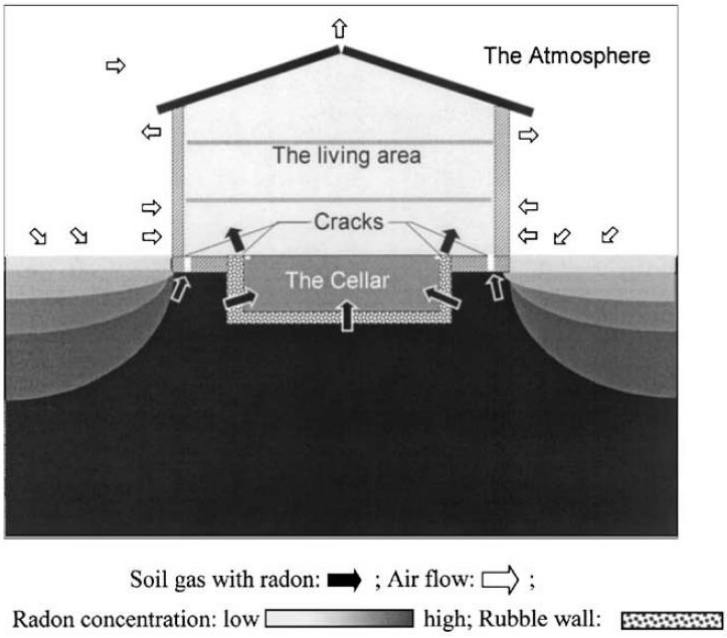

Fig. 1-1. Radon entry into a building, Schematic diagram of a conceptual house (Wang & Ward, 2002).

Transport of gas from subsurface of mars to atmosphere is another problem, which scientists are investigating. Transport of volatiles in subsurface through porous soil needs to be known for balancing mass flows in mars (De beule et al, 2013). Modelling of transport of methane gas in subsurface of gas (Stevens, et al. 2015) and investigating CO_2 gas flow in polar regions of mars (Thomas et al, 2011) are two of the researches in this field. The issue is also important in chemistry and physics in fields such as gas transport in nano-porous media. Several studies have tried to identify the affecting parameters in soil gas emissions.

1.2 Aims and Objectives

Three main objectives of this study are first to measure the variation in gas concentration of the porous medium in response to wind turbulence at different distances from the surface exposed to wind, and second to use these measurements to determine wind-induced dispersion coefficient (D_w) as a function of distance to the surface exposed to wind. Measurements were made by two different methods: (i) gas concentrations were measured at both ends of a porous medium column, following the approach used in previous research. To assess the effect of distance, columns of different length were used with one end exposed to wind turbulence, and (ii) gas concentrations were measured at several distances from the surface exposed to wind simultaneously within the same column. The results are used to compare the two methods of measurement and to assess the relation between the wind-induced dispersion coefficient D_w and distance below the surface exposed to wind. This is necessary to simulate and model the process of gas transport due to wind action. Furthermore, the

wind induced dispersion coefficient as a function of distance from the wind-exposed surface is determined. (iii) Another objective of this study is to identify and evaluate the strength of possible relationships between soil-atmosphere gas exchange and wind speed characteristics, including simple ones and wind power spectrum, under a range of wind conditions in a set of porous media.

Although published results (Fukuda, 1955; Scotter & Raats, 1968, 1969; Poulsen & Sharma, 2011) suggest that wind-induced gas transport in porous media is likely related to wind speed characteristics, medium physical properties and distance to the wind-exposed surface, the specific relations between these parameters are at present very poorly understood. Therefore, another purpose of this study is to investigate the links between wind-induced gas transport inside porous media (apparent wind-induced gas dispersion coefficient), wind speed characteristics (average wind speed, wind speed variability, wind direction) and porous medium physical properties (particle size, air permeability, hydraulic conductivity, porosity, etc.). Investigations were based on experimental gas transport data for a set of five porous media and ten wind conditions. Parameters of wind-induced dispersion coefficient models were considered with respect to their links to wind speed characteristics and porous medium properties, as well as their accuracy in approximating experimental porous medium gas concentration data.

The results of current research contribute to establishing a firm understanding of the factors governing the subsurface-to-atmosphere gas exchange. This will allow for improved estimates of for instance atmospheric greenhouse gas balances and loadings

of unwanted (hazardous) compounds in our local (urban) atmospheric environment including the indoor environment.

Wind turbulence induced pressure fluctuations induce short-term vertical and horizontal gas movements in the subsurface, which then contribute to the overall gas exchange. Understanding the relationship between wind fluctuation characteristics and subsurface gas movement is thus of key importance when estimating for instance gas loadings to the atmosphere. Short-term gas pressure fluctuations are usually characterized by their average amplitude and frequency and/or their power spectrum (the combination of frequencies and amplitudes making up the pressure variations). The first key research question is therefore:

How does subsurface-atmosphere gas exchange depend on the amplitude, frequency and power spectrum of the wind induced pressure fluctuations near the ground surface?

Pressure fluctuation amplitude, frequency and power spectrum are controlled both by the wind conditions in the un-obstructed atmosphere (well above the ground surface) and by obstacles present on the ground such as buildings, plant cover, rocks etc.

Estimates of gas exchange may be based on numerical modelling using subsurface characteristics and surface pressure fluctuation time series as inputs. However, for practical applications this approach is not feasible because the exact pressure time series are usually not known. To be practical, the estimation should be based on simple mathematical expressions allowing rapid and easy estimation of gas exchange.

The aim of this research is, based on empirical data and theoretical relations, to develop a set of mathematical expressions that will allow for fast, easy and acceptable estimations of average subsurface-to-atmosphere gas fluxes. This will take into account the wind induced pressure fluctuations, physical characteristics of soil (porosity and grain size etc.) and the gas concentration profiles in the subsurface and the atmosphere. More specifically this research has three distinct aims:

1) To build an empirical database for identifying the impact of wind induced pressure fluctuation characteristics (pressure fluctuation amplitude, frequency and power spectrum) and properties of porous medium on the magnitude of the time averaged gas flux through porous medium.

2) To use these two data sets for developing a set of empirical mathematical expressions that will allow for estimating gas exchange inside porous media in response to wind induced pressure fluctuations based on pressure fluctuation and media characteristics.

3) To verify and validate these mathematical expressions using additional independent empirical laboratory measurements in combination with numerical modelling and to demonstrate their use for predicting subsurface-to-atmosphere gas exchange or any gas transport through porous media under a variety of applications.

1.3 Thesis structure

After introduction, in Chapter 2, literature study about gas transport through porous media in general and wind-induced gas movement through that is discussed. Next chapter is the theoretical part where all the applied concepts including soil

classification, particle characterization, gas transport mechanisms and wind characterization. Chapter 3 is followed by experimental methodology in Chapter 4 where the applied laboratory experiments for measuring the amount of gas transport is illustrated and approach for measuring wind speed and turbulences are expressed. In Chapter 5, mathematical procedures and calculations for modelling the gas transport through porous media is discussed. How-to characterize the wind turbulences is another part of that chapter. Chapter 4 is where the results of the experiments and modelling are presented. Relating wind and particle characteristics to the amount of gas transport is illustrated. Following the results, the main conclusions of the research are stated and afterwards, some suggestions for future study are recommended. After references used for the research, the thesis is finished by appendix of result of measurements of gas concentrations, wind turbulences and particle properties.

Chapter 2 THEORETICAL FRAMEWORK

2.1 Porous Media

Porous media are materials, which contains voids such as soil. The pores are filled with liquid or gas, which for a dry porous media all the voids are filled with air. Soil as a porous media is being considered in current research.

According to Unified Soil Classification System (ASTM D2487-11), soils are classified to four ranges, which can be seen in Table 2-1.

Table 2-1. Soil classification

Soil Type	Grain Size range (mm)
Gravel (G)	76.2 to 4.75
Sand (S)	4.75 to 0.075
Silt (M)	0.075 to 0.002
Clay (C)	< 0.002

The required range of porous media for experiments can obtain by sieving. Key particle sizes are D_{60} and D_{10}, which are equal to the diameter that 60% and 10% of the particles are finer than, respectively.

Porosity is defined as the volume of voids over the total volume of a sample as the Eq. 1 and has a value between zero to one. Usually porosity increases as the particle size of

porous media decreases. In addition, rounded particles have higher porosity than angular ones.

$$\phi = \frac{V_{pore}}{V_{total}} \quad (1)$$

where V represents the volume.

Another important property of porous media that is relevant to current study is gas permeability of porous media, which is defined as the measure of ability of that to allow gas to pass through it. Amount of gas permeability of soil is related to porosity and particle shape. If the relation between gas flow and drop in pressure of gas within the porous media is approximately linear then Darcy's law is applicable.

Darcy's law is the important principle that describes how fluid moves in the subsurface. That is an equation, which quantifies a fluid flow in a porous media such as soil. It is based on the physical meaning that the amount of flow between two points is related to the difference in pressure between the points, the distance between the points, and the interconnectivity, called permeability; of flow pathways in the soil between those points. Darcy's law can be written as below:

$$Q = -K_s A \frac{dh}{dl} \quad (2)$$

where

Q = rate of water flow (volume per time)

K_s = hydraulic conductivity

A = column cross sectional area

dh/dl = hydraulic gradient, that is, the change in head over the length of interest

Gas permeability in a porous medium, k_a, is determined by measurement of the drop in pressure ΔP across a sample of the medium with length L and cross-sectional area A_s exposed to a gas flow Q followed by Darcy's law (Kirkham, 1947),

$$k_a = \frac{Q\,\eta\,L}{A_s\,\Delta P} \tag{3}$$

where η is the dynamic viscosity of the gas (Pa.s). One another useful parameter of a porous media is tortuosity (τ). A common definition of tortuosity is the ratio of the length of the actual path of the fluid particles to the shortest path length in the direction of the flow. Tortuosity is always greater than one and decreases with increasing porosity. Since streamline in a porous media is not straight, this dimensionless parameter is introduced as below:

$$\tau = \frac{\lambda}{L} \tag{4}$$

where λ is average length of fluid paths and L is geometrical length of sample.

2.2 Gas Transport Mechanisms

Four mechanisms control the gas transport in porous media: (i) molecular gas diffusion because of gas concentration gradient, (ii) Convection as slow varying and stable advective gas flux controlled by pressure gradient (for instance gas production), (iii) gas dispersion associated to advective gas flow and (iv) gas mixing due to wind turbulence-induced pressure fluctuations. Dispersion has the similar mechanism as the advective

flow but the difference is different paths of gas flow because of nature of porous media (Poulsen and Sharma, 2011).

Diffusion occurs whenever there is a gradient in the concentration of gas. It means diffusion is net movement of a substance from a region of high concentration to low concentration. Particles randomly move around, and it results in mixing or mass transport without bulk flow. Convection, the other mechanism, is fluid flow. It is bulk movement of gas in response to difference in air pressure inside soil, same as transport of liquid like water inside soil. Dispersion is the third mechanism which has been investigated less than to other mechanism in researches. Different pathways and/or velocities make particles which are in advection process to be dispersed. A major mechanism of gas transport is diffusion of gas phase in soil air space. In free air, the gas diffusion flux J is expressed by Fick's law of diffusion:

$$J = D_g^a \frac{\partial Cg}{\partial z} \quad (5)$$

where

D_g^a = The binary gaseous diffusion coefficient in free air

C_g = mass of chemical vapour per volume of soil air space, called gas concentration

z = distance or depth.

At atmospheric pressure and temperature of 25^{o}C, for gases with low molecular weight, D_g^a varies between about 0.15 and 0.25 cm^{2}s^{-1}. It decreases with increasing size of diffusing molecule. The diffusion coefficient need to be modified for gas transport

through soil by a tortuosity factor τ to gain soil gas diffusion coefficient D_g^s, because of longer path for gas and smaller cross-sectional area for gas passing due to solid barriers.

Standard method to measure diffusion coefficient in laboratory is diffusion chamber (Rolston & Moldrup, 2002), in which a soil column after being devoid of gas is open and at one surface is exposed to closed air chamber containing a specific concentration of the gas of interest. Over time, the gas diffuses from chamber into the soil at a rate, which can leads to calculating the diffusion coefficient of gas into that soil. The gas transport equation, called "advection-dispersion equation" is as below:

$$R\frac{\partial Cg}{\partial t} = D_g^s\frac{\partial^2 C_g}{\partial z^2} - V_z\frac{dC_g}{dz} \quad (6)$$

Where:
C_g = Concentration of gas
R = Coefficient of retardation (dimensionless)
D_g^s = diffusion coefficient of gas in soil
V_z = Average gas velocity
z = depth
t = time.

where the first term after equal sign is dispersion part and second term is advection term.

For a porous medium where gas concentration and wind conditions in the atmosphere at its surface exposed to wind are uniform, net gas transport in the porous medium is one-dimensional (Poulsen *et al*., 2001) and Equation (6) becomes:

$$\frac{\partial C}{\partial t} = \frac{\partial^2 (D_{\mathrm{tot}} C)}{\partial z^2} = \frac{\partial^2 ((D_{\mathrm{m}} + D_{\mathrm{w}}) C)}{\partial z^2} \quad , \tag{7}$$

where z is the distance from the surface exposed to wind. D_{tot}, D_m and D_w are total diffusion coefficient, molecular diffusion coefficient and wind-induced dispersion coefficient, respectively.

A key factor controlling gas exchange is advection which is result of difference in pressure of soil air phase and atmosphere. The process can be described by Darcy's law:

$$J_c = -k_{air} \frac{dP}{dz} \tag{8}$$

which

J_c = air flux density (m s^{-1})

K_{air} = air conductivity (m s^{-1})

P = air pressure in head units (m)

z = distance (m).

The coefficient of molecular diffusion in the porous medium (D_m) can be estimated from the molecular diffusion coefficient in free air (D_0) with for instance the Penman (1940) model,

$$\frac{D_m}{D_0} = 0.66\varepsilon \ , \tag{9}$$

or the Millington & Quirk (1961) model

$$\frac{D_m}{D_0} = \frac{\varepsilon^{10/3}}{\phi^2} \ , \tag{10}$$

where ε is gas-filled porosity and ϕ is total porosity (assumed to be equal in media with no liquid phase).

Air conductivity is a function of soil air content, pore structure, air density and air viscosity. Pressure differences are caused by the passage of weather systems (intermediate term variations) and wind turbulence (short term variations). More reasons that can affect the natural pressure are temperature effect, barometric pressure effects, rainfall effect, and mass flow of gases into buildings and remediation of volatile pollutants. Temperature can change the pressure in two ways. First is because of difference in temperature between different parts of soil which causes contraction and expansion of air in pore spaces and tendency of warm air to move upward and second is the difference of temperature between soil and atmosphere. Rommel (1922) concluded that wind cannot be responsible for more than 0.1% of aeration inside vegetated soils, but recent experiments suggest that bulk flow of air in soil in response to pressure fluctuations caused by wind may not be negligible in porous soil (Farrel et al., 1966). Wind can penetrate to depth of several centimetres. Fluctuations in air pressure at the soil surface can cause mixing of air within the surface that enhances gas transport beyond it due to diffusion alone (Scotter et al., 1967). A schematic diagram illustrating the mechanism of wind induced gas exchange is shown in Fig. 2-1.

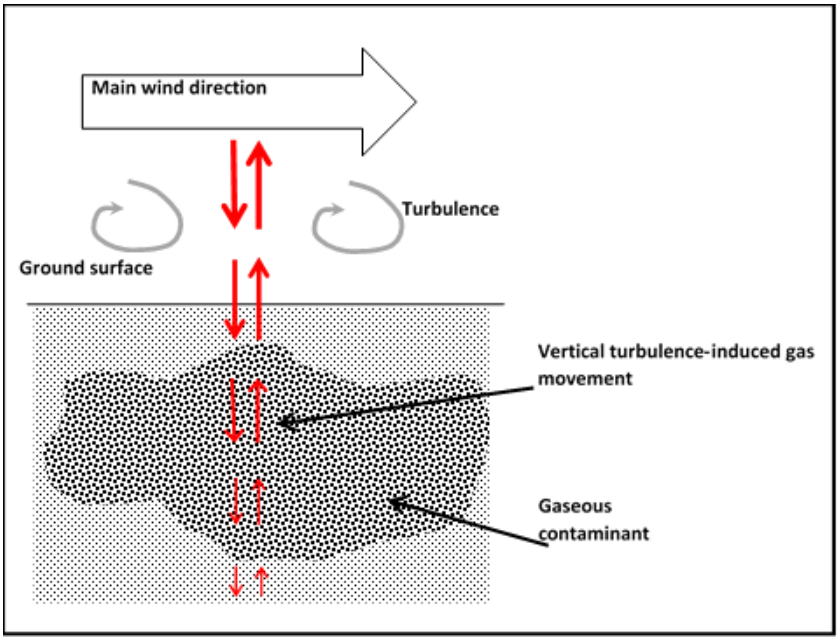

Fig. 2-1. Wind action effect on gas transport from subsurface to atmosphere.

Solute dispersion refers to the spatial spreading of a solute plume over time. The spreading is actually a mixing and consequent dilution of the solute plume with the resident fluid. Dispersion includes diffusive and mechanical mixing components. (Costanza-Robinson M. & Brusseau, M.L., 2006).

A part of gas transport which is due to wind-induced pressure fluctuations is main matter of concern in current research. The magnitude of wind-induced pressure on and around any obstacle can be expressed as follows (Clancy, 1975):

$$\Delta P = 0.5 C_p \rho U^2 \quad (11)$$

Where ΔP is magnitude of wind-induced pressure, C_p is a pressure coefficient that depends on surface roughness, ρ is air density at atmospheric pressure and V is mean free-wind speed.

Gas exchange between subsurface and atmosphere is controlled by subsurface properties (such as porosity, pore size and microbial activity), climatic factors (such as wind speed and wind turbulence), and the conditions of the surface (such as plant cover, presence of buildings and other obstacles to wind flow). While the impacts of subsurface properties on gas exchange is very well understood, comparatively little knowledge about the impacts of climatic factors and surface conditions on gas exchange is available. Various soil properties affect soil gas emissions, such as humidity, temperature, air pressure and vegetation (Oertel et al., 2016). Advective flow controlled by wind and the difference between indoor and outdoor temperatures are the main factors in the transport process of radon from soil to air and buildings (Nazaroff, 1992). Oliver & Khayrat (2001) found that in addition to lithology, factors such as elevation, soil depth and particle size could affect the spatial variation in radon in the soil atmosphere.

2.3 Wind Speed Characterization

Wind speed can be regarded as a stochastic parameter and characterized by its mean (V) and standard deviation (s) in any given direction. Often turbulence intensity (T) = s/V (Cheung et al. 1983) is used instead of s as T is independent of V and therefore, gives a better characterization of the wind speed variation intensity. This is the same concept as the coefficient of variation (CV) which is used in this study for quantifying the wind speed fluctuations magnitude.

The wind speed fluctuations may alternatively be characterized by their power spectrum (De Karman and Howarth, 1938; Van Der Hoven, 1956; Kaimal et al., 1972, 1976). Van

der Hoven (1956) models a power spectrum analysis of horizontal wind speed over a range of frequencies. Kaimal et al. (1972) described the behaviour of spectra of turbulence in the surface layer using wind fluctuation. Later (1976) they studied structure of turbulence in the convective boundary layer. The power spectrum expresses the magnitude (energy content) of the wind speed fluctuations as a function of fluctuation frequency. The power spectrum can be calculated based on measured wind speed data by expressing the data as a sum of sine wave functions with different amplitude and frequency using Fourier analyses. The resulting empirical power spectrum often exhibits significant scatter depending on the wind speed conditions. Empirical power spectra are, therefore often approximated by theoretical power spectrum models that allow easier subsequent analyses of the experimental data. The Kaimal power spectrum model (Kaimal et al. 1972, 1976) given in Eq. (12) is one of the most widely used models.

$$\Phi(f) = \frac{A_K}{(1 + fB_K)^{5/3}}, \tag{12}$$

where f is the wind speed fluctuation frequency, $\Phi(f)$ is the power spectral density and A_K and B_K are empirical parameters.

Chapter 3 LITERATURE REVIEW

3.1 Experimental studies: Effect of wind in gas transport through soil

Understanding of the potential impact of wind action on soil-atmosphere gas exchange is very important when assessing for instance methane emissions from landfills, water evaporation from agricultural soils or soil greenhouse gas balances and turnover under natural conditions. Such knowledge may also be used to reduce greenhouse gas emission for instance via designed top covers for enhanced biodegradation of methane emitted from closed landfill sites. Fukuda (1954) did one of the leading researches about effect of wind gustiness on air movement in soil. Fukuda (1954) emphasized the effect of wind gustiness on transmission of air pressure into soil as well as volume of air transported though soil surface. He suggests a theoretical formula, which measures pressure transmission and air movement, derived from Darcy's law and verified it by experimental work. He concludes that depth of soil which air due to wind gustiness can penetrate is very slight for instance in sandy soil with mean diameter of 0.5-0.25 mm of particles, it penetrates just about 5 mm below the surface. Fukuda (1955) modeled wind as a sinusoidal pressure wave and derived an equation for predicting behavior of soil air movement using a one-dimensional analysis.

Hanks & Woodruff (1958) believed that since diffusion involves movement of gases in the air due to concentration gradient of the gas, any disturbance which causes mass movement of air would affect the rate of transfer. They showed wind has a definite effect on water vapor transfer in soil and increases the evaporation (Fig. 2-2). They

found that the rate of water evaporation increased two to six times for soil mulches and 10 to 15 times for gravel and straw when wind speed was increased from 0 to 40 km per hour. While effects of long and intermediate term pressure variations on gas exchange are well understood, impacts of wind induced pressure fluctuations on gas exchange are much less studied.

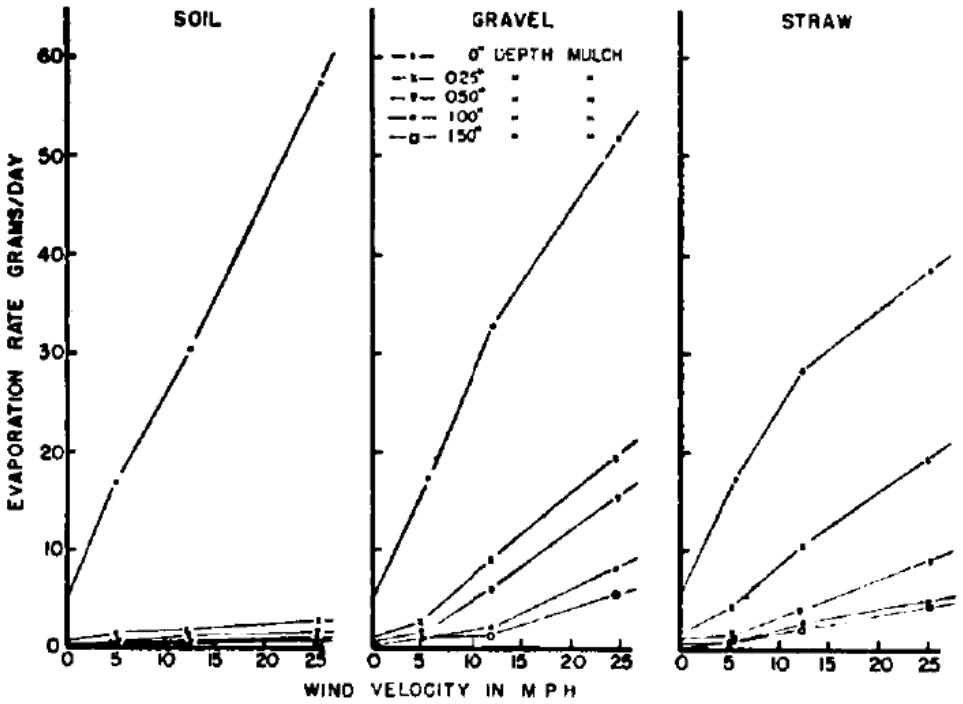

Fig. 3-1. Influence of wind speed on evaporation rate (Hanks & Woodruff, 1957)

Farrell et al. (1965) showed the limitations of Fukuda's researches. They stated that Fukuda's research only deals with the case which soil is of infinite depth and treatment ignores horizontal gradients in atmospheric pressure at the surface of soil. Based on their research the effective diffusion coefficient in soil as a porous media is a function of macroscopic velocity of the fluid. Air movement within the soil was reported greater than what previously was assumed and for example in wind speed of 24.14Kph. Surface

air can penetrate coarse soil (gravel and sand) to depth of several centimeters, about ten times more than what Fukuda suggested. Their analysis assumes that the oscillations in air pressure can be described as sinusoidal pressure waves, but they derived the second equation using a two-dimensional analysis. Finally, they concluded that the influence of wind could not be ignored anymore.

Scotter & Raats (1986) used an apparatus for measuring the dispersion made by oscillating flow inside porous media. Fig. 2-3 shows a diagram of the apparatus used by them.

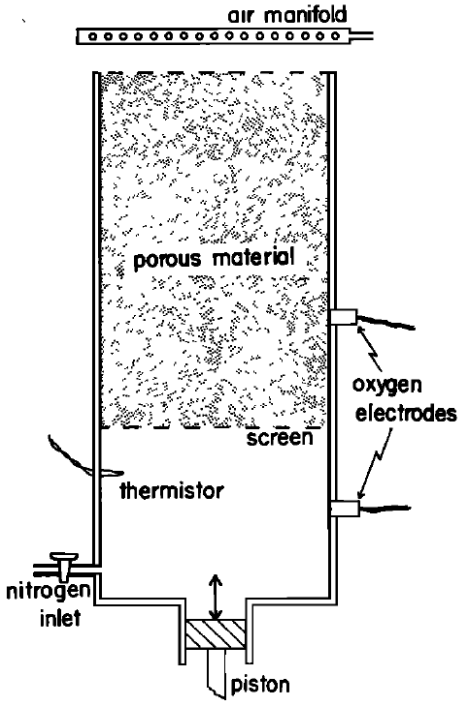

3-2. Schematic diagram of apparatus for measuring dispersion in porous media due to oscillating flow (Scotter & Raats, 1986).

Ishihara et al. (1992) carried out laboratory experiments to investigate the mechanism of water vapor transport in subsurface influenced by a turbulent wind. They found out that when the layer is low permeable the mechanism of gas transport is molecular diffusion as well as turbulent diffusion. The turbulent diffusion is determined by horizontal and vertical components of air fluctuation but with increasing the depth, vertical component would be the only affective one. For high permeable porous material, the turbulent diffusivity decays exponentially with depth.

Novak et al. (2000a, 2000b) studied turbulent exchange processes in a straw mulch. A result showed under high wind conditions most of the drag occurs very near the top of the mulch. Wang & Ward (2002) also conducted a research on factors affecting the soil radon entry into houses including ambient temperature, wind speed and direction. They proposed points in building design that could decrease the hazard gas entry into building. Takle et al. (2003) measured pressure fluctuations at and below a soil surface in the vicinity of CO_2 flux chamber. In their field experiment they tried to examine the role of pressure pumping caused by atmospheric pressure fluctuations on surface fluxes of CO_2. They found out that the presence of chamber did not introduce pressure perturbations that could lead to biases in measurement of surface fluxes of CO_2. Concurrent measurements of CO_2 fluxes from the soil surface reveal systematic increases with increasing the root-mean-square pressure, pumping rate and mean wind speed (Takle et al., 2004). Massman & Frand (2006) investigated the exchange of natural soil gases in permeable media induced by atmospheric pressure fluctuations. Poulsen et al. (2003), Poulsen & Moldrup (2006), evaluated effect of atmospheric

pressure on landfill gas emissions and also effect of wind-induced pressure fluctuations on exchange of gas between soil and atmosphere in the same landfill. They used a stochastic modeling to generate random fluctuations with statistical properties. The model included wind turbulence-induced gas transport, diffusion-induced gas transport as well as advective gas transport made by pressure gradients caused by weather system. They reported 40% of gas emissions are wind turbulence-induced. Two main factors controlling it were soil-air permeability and amplitude of wind-induced pressure fluctuations. Increasing in water content of soil would increase the effect of wind-induced gas transport. One of the results of the above studies is that wind-induced gas transport in porous media is a multi-dimensional process, and that the use of sinusoidal functions to represent one-dimensional wind action generally underestimates gas transport. The above studies show further that wind-induced gas transport decreases with increasing distance from the surface exposed to wind action.

Poulsen et al. (2008) proposed a method for measuring gas dispersion in soil as a mechanism, which was less investigated before based on oxygen (O_2) and nitrogen (N_2) transport. Gas dispersion coefficient was determined by fitting oxygen concentration data of experiments to advection-dispersion equation. See Fig. 2-4

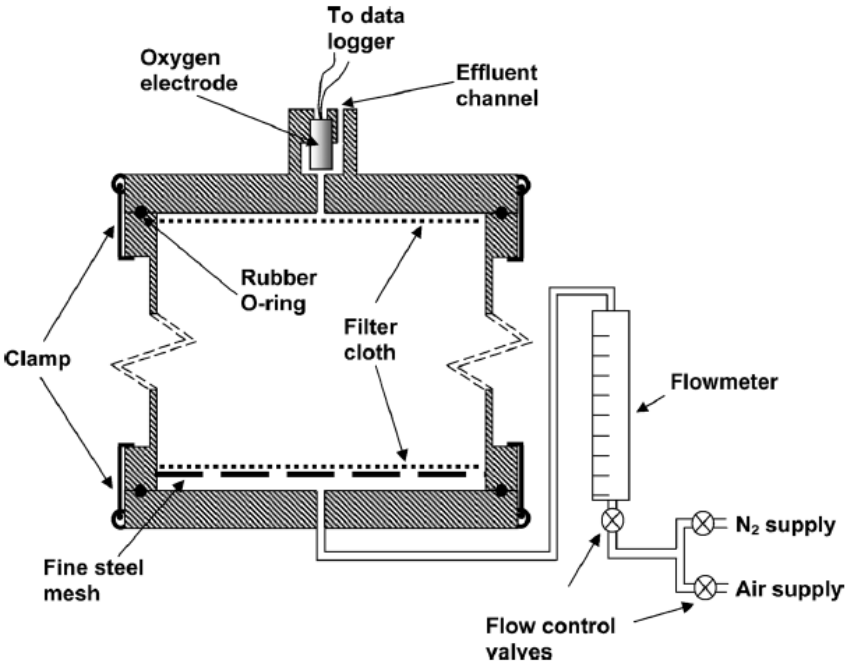

Fig. 3-3. Schematic drawing of apparatus used for measuring gas dispersion coefficient by Poulsen et al. 2008.

They fitted the data to the advection-dispersion equation to achieve gas dispersion coefficient. Result showed that gas dispersion coefficient was linearly proportional to gas pore velocity for constant pore gas velocity and dry bulk density.

They presented the breakthrough curves (Fig. 2-5) which are relative oxygen concentrations, C/C_0 as a function of time, for displacement of air with nitrogen and vice versa. The corresponding pore gas velocity (u) was calculated based on gas-filled porosity of the column.

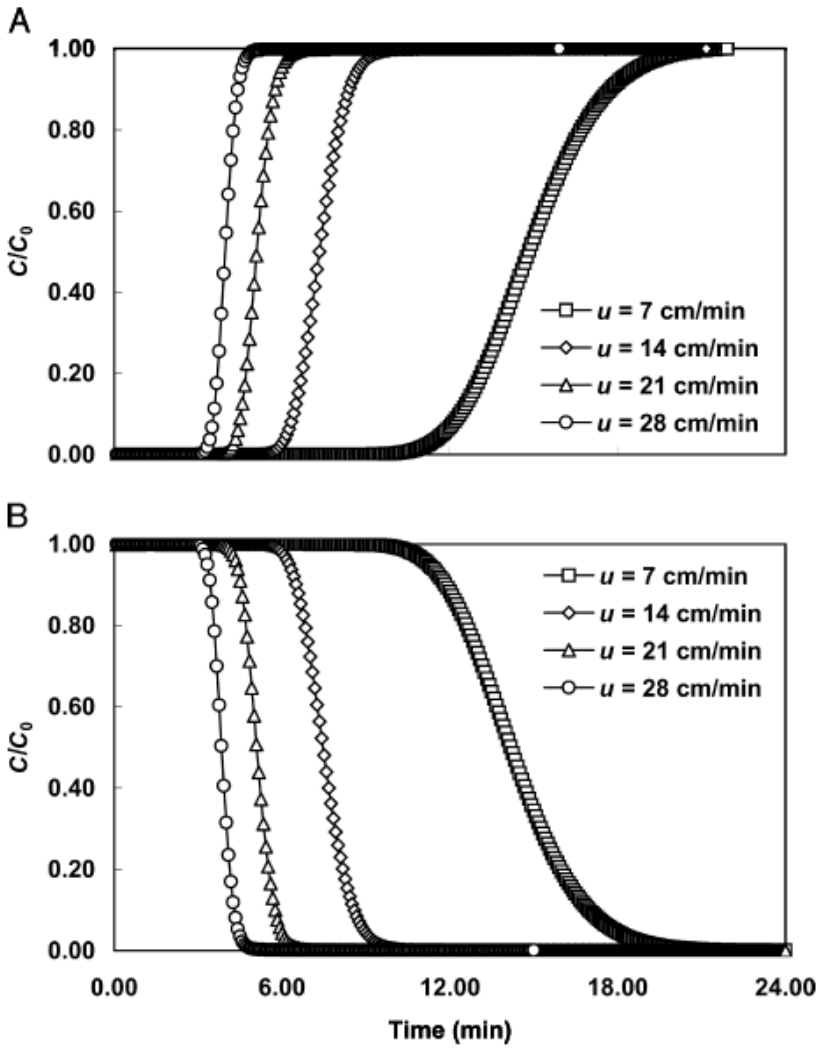

Fig.3-4 Relative oxygen concentration as function of time for displacement of nitrogen with air (A) & air with nitrogen (B) at different pore gas velocities. C/C0 indicates relative oxygen concentration (Poulsen et al. 2008).

Later, Poulsen and Sharma (2011) measured pressure fluctuation-induced gas dispersion coefficient (D_p) and showed that it is independent of any background steady gas flow. D_p increases with increasing A (amplitude of wind-induced pressure fluctuations), f (fluctuation frequency) and k_a (porous medium gas permeability). Maier et al. (2012) stated that the fluctuation of wind results in gas transport by advection and dispersion in addition to the molecular diffusion.

The gustiness of wind at the surface of the porous medium generates velocities of pore gas that fluctuate rapidly in magnitude and direction (Maier et al. 2012). The velocities also vary spatially within the porous medium because of differences in pore size. This results in mixing of the gas within the porous medium but does not usually generate net advective gas fluxes. This means that wind turbulence-induced gas movement in porous media behaves like a dispersive process (Poulsen & Moldrup, 2006).

Haghighi & Or (2015a) studied evaporation from surface of soil. They suggested that the relief and roughness of natural surfaces interacting with airflows affect rates and distributions of vapor fluxes into the atmosphere. They quantified interactions of sinusoidal wavy porous surfaces affecting vapor transport into turbulent airflows. In that research, evaporative mass loss measurements and observed thermal patterns were in agreement with model predictions for turbulent exchange over various sand surface geometries. For a practical range of air velocities (0.5–4.0m/s), the evaporative mass loss) was reduced by up to 60% for low surface aspect ratio (amplitude of wavy building block over wavelength of wavy building block and high wind velocity, and enhanced by up to 80% for high aspect ratio and low wind velocity. Haghighi & Or (2015b) showed that results from evaporative of sand surfaces with isolated cylindrical elements subjected to constant turbulent airflows were in good agreement with model predictions for localized exchange rates.

One other recent research in this field was carried out by Goffin et al. (2015). They tried to improve the understanding of soil CO_2 efflux mechanism, especially by investigating, through modeling. They showed that intra-day variation of F_s and CO_2 is better

represented when the more complex CO_2 production expression is considered compared to the more detailed description of CO_2 transport. Finally, they conclude that there should be more concentrations on the potential factors affecting the CO_2 production, rather than on the transport process description.

There are many uncertainties persist in estimates of soil– atmosphere exchange of important trace gases, Redecker et al. (2015) expressed that significant source of uncertainty is the combined effect of wind and pressure on these fluxes. Furthermore, they described that wind and pressure effects are mediated by surface topography. They considered how such spatial variability in air pressure and wind speed affects fluxes of trace gases. They applied a nested wind tunnel in which wind speed and pressure may be controlled, set in a larger, linear wind tunnel. The influences of both wind speed and pressure differentials on fluxes of CO2 and Methane within three different ecosystems were quantified. They found that trace gas fluxes are correlated with both wind speed and pressure differential near the surface boundary. They discussed that wind speed is the better proxy for trace gas fluxes because of its stronger correlation and because wind speed is more easily measured.

A small number of experimental studies (Poulsen and Sharma, 2011; Maier et al., 2012; Redecker et al., 2014; Mohr et al., 2016) indicate that increasing near surface mean wind speed and mean temporal pressure gradient (*dP/dt*) results in increasing soil gas flux and soil-atmosphere gas exchange. In addition, Poulsen and Sharma (2011) observed positive correlation between gas exchange and wind induced pressure fluctuation amplitude, and negative correlation between gas exchange and pressure

fluctuation frequency. Because pressure fluctuations are generated by fluctuations in the wind speed, it is likely that the amplitude and frequency of the wind speed variations are also important for controlling gas exchange. Redecker et al. (2014) further found that wind speed was a better predictor of soil-atmosphere gas fluxes than the wind induced pressure gradient based on measurements in three different types of soils. This suggests that the focus of future investigations on the impact of wind characteristics on wind induced soil-atmosphere gas exchange should be on the characteristics of wind speed rather than pressure fluctuations.

3.2 Numerical studies

Scotter and Ratts (1968) described that sine waves provide a simplified model of irregular pressure fluctuation induced by air turbulence, but calculations based on this model need to indicate the order of magnitude of fluxes and effect of variations in wavelength, amplitude and frequency of oscillations and permeability and depth of soil need to be predicted (Fig. 2-2). They claimed Farrell et al. give a little attention to problem of relation between sinusoidal fluxes and hydrodynamic dispersion and hence rate of gas transport in soil. Using experimental dispersion coefficient, they evaluated the dispersion resulting from mean flow, numerically. They suggested that dispersion in real soil with real wind condition over the surface results in larger relative fluxes compared to previous results.

Acharya & Prihar (1969) also carried out a research on water evaporation from soil. Kimball and Lemon (1970) started to enhance a theory for soil air movement due to

pressure fluctuations. They derived an equation, which calculates the air pressure in the soil using variance spectrum of air pressure at the soil surface. Fluctuations can lead to movement of air in soil which results in increasing in exchange of gases between soil and atmosphere. Before, Scotter & Raats (1968) showed that rate of exchange between soil and atmosphere depends on velocity and displacement amplitude of soil air movement. Kimball & Lemon (1970) derived the third equation for calculating those variables, which models the wind as a series of superimposed, traveling, sinusoidal pressure using a three-dimensional analysis. Their equations provide soil air velocity and displacement, but they stated that field measurements are absent in their research. Colbeck (1981) modelled the effect of the wind gustiness on gas transport in porous media. Pritchard & Currie (1982) measured binary diffusion coefficients and proposed their experimental method as a suitable and reliable one. Their research didn't involve investigating the gas diffusion in porous medium, but their research is valuable for achieving the binary gas diffusions which is necessary in calculating any gas diffusion through porous medium.

Riley et al. (1999) described a novel modeling technique to study the effect of wind on radon transport in soil close to buildings. Their research was based on mathematical modeling which was compared with analytical solutions and measurement of radon entry into an experimental basement structure. They concluded that wind fluctuations have small to moderate effect in entry rate of radon into the buildings. Fluctuation wind direction dominates the impact on rates of radon entry up to 30% compared to steady state.

In general, modelling of wind-induced gas transport has been done by simulating the velocities of advective pore gas as functions of location (depth) and time within the porous medium. For real (random) wind velocity or pressure fluctuations, this is computationally intensive because minor steps are required to resolve the fluctuations (Saffman, 1960; Poulsen & Sharma, 2011).

Computationally intensive simulations can be avoided, therefore, by modelling wind turbulence-induced gas transport as a purely dispersive process with a cumulative location-dependent dispersion coefficient, D_{tot}, that represents the sum of molecular diffusion, D_m, and wind-induced mixing, D_w (Poulsen et al., 2001; Poulsen & Sharma, 2011). This approach, however, requires knowledge about the relation between D_w and distance from the surface exposed to wind. Experimental investigations of D_w are limited at present, however. The author is aware of four earlier studies only that focus on this property. Scotter & Raats (1968, 1969) and Poulsen & Sharma (2011) measured D_w in columns of porous media under fluctuations in sinusoidal pressure induced by an oscillating piston (one-dimensional gas transport). Maier et al. (2012) carried out similar experiments, but used a fan combined with a chopper wheel, which is a wheel-shape frame with shutters inside to generate more realistic conditions of wind turbulence.

Redecker et al. (2015) suggested a conceptual model of the soil profile that has a "mixed layer", with fluxes controlled by wind speed, wind duration, porosity, water table, consumption and gas production.

3.3 Lacks in the literature studies

Most of our current knowledge about the impacts of short-term pressure fluctuations on gas exchange is based on either numerical modeling (Scotter & Raats, 1968, 1969; Poulsen et al. 2003; Poulsen & Moldrup 2006; Poulsen & Sharma 2011) or laboratory experiments carried out under controlled conditions with artificially generated pressure fluctuations (Scotter et al. 1967; Scotter & Raats, 1968, 1969; Poulsen and Sharma, 2011, Maier et al. 2012). Based on these results it is therefore difficult to fully assess gas exchange under natural wind and ground surface conditions. As gas exchange, however, do take place under natural wind conditions, and in locations with very different ground surface conditions, research is required to explore the connections between wind turbulence characteristics, ground surface characteristics, and gas exchange rate.

Although there are researches trying to show the effect of wind action on gas transport in porous media, there was no research at present that measures the variation in gas concentration of the porous medium in response to wind turbulences at different depths from the surface. In this research, this is done and then utilized and second to determine D_w as a function of distance to the surface exposed to wind.

Although it is widely accepted that the characteristics of the near surface wind speed or wind induced pressure fluctuations are of key importance in controlling the gas exchange, only a relatively limited number of studies have focused on identification of these key characteristics under real (experimental) wind conditions. The present

understanding of the relations between wind speed characteristics and soil-atmosphere gas exchange is, therefore, very limited.

Wind speed is usually regarded as a stochastic (random) parameter and can therefore, in a simple manner be characterized by a mean value and a standard deviation (or alternatively a coefficient of variation). While including effects of mean wind speed and wind speed fluctuation amplitude, this approach, however, does not represent the wind speed fluctuation frequency distribution. This is so because mean wind speed and wind speed standard deviation are largely independent of wind speed fluctuation frequency. Fluctuation frequency may instead be characterized by the wind speed power spectrum (De Karman and Howarth, 1938; Van Der Hoven, 1956; Kaimal et al., 1972, 1976), describing the relation between the magnitude of the wind speed (proportional to the energy in the wind) as a function of the fluctuation frequency. Wind speed fluctuation frequency is potentially important because low frequency fluctuations tend to penetrate deeper into the soil than higher frequency fluctuations. Low frequency fluctuations will therefore potentially have a larger impact on gas exchange than fluctuations with higher frequencies for the same energy level. Because wind speed is a 3-dimensional vector, overall wind speed characterization must include mean, standard deviation (or coefficient of variation) and power spectrum in each of the three directions to sufficiently characterize the wind speed. At present, however, there are no comprehensive studies on the level of correlation between soil-atmosphere gas exchange and the above discussed wind speed characteristics in three dimensions. In fact, the authors are not aware of any studies on the relation between soil-atmosphere

gas exchange and wind speed power spectrum. Thus, there exists, in the scientific literature, at present no comprehensive experimental assessment of the importance of wind speed characteristics (including power spectra) and soil-atmosphere gas exchange. There is, thus, a need for more comprehensive and in-depth studies of the links between wind-induced soil-atmosphere gas exchange and wind speed characteristics.

Former studies measured gas concentrations as a function of time at both ends of the columns. None of these studies, however, assessed the variation in D_w with position inside the columns of the porous medium, but measured average D_w values only across the entire columns. Therefore, to the best of the authors' knowledge there is no experimental assessment in the scientific literature at present of the relation between D_w and distance to the surface of the porous medium exposed to the wind or the effect of column length on the dispersion coefficient. To provide such knowledge would require measurements of gas concentration at different positions within the porous medium.

Although published results suggest that wind-induced gas transport in porous media is likely related to wind speed characteristics, medium physical properties and distance to the wind-exposed surface, the specific relations between these parameters are at present very poorly understood. A few studies have shown that wind-induced gas transport may be approximated as a dispersion process (Poulsen and Moldrup, 2006; Maier et al., 2012). Apart from the studies discussed above, the authors are not aware of any other investigations into the impacts of wind action and porous medium properties on wind-induced gas transport inside near-surface porous media. At present, knowledge about the impact of wind speed characteristics and especially porous medium properties on

wind-induced porous medium gas transport and gas exchange with the atmosphere is relatively poor.

Chapter 4 EXPERIMENTAL METHODOLOGY

4.1 Porous media

Five different dry porous materials were used in this research. They were at five different ranges of particle size which was prepared after sieving. Gas permeability of each material is determined by Eq. 2. The sample's column diameter was 25cm while the sample's length ranged between 15 and 35 cm depending on particle size. The validity of Darcy's law was verified by checking that the relation between Q and ΔP was approximately linear in all cases.

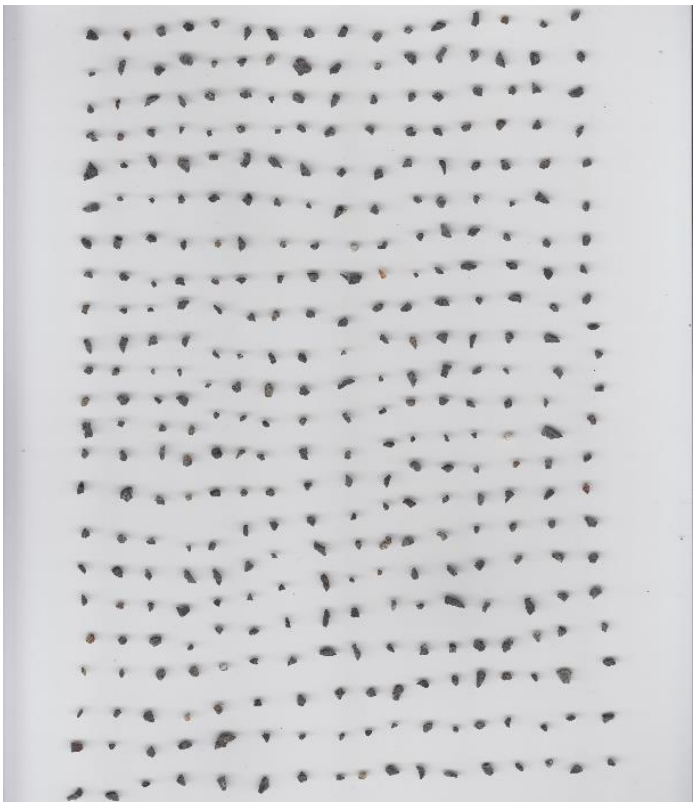

Fig. 4-1. Image of material fraction 2.

The saturated hydraulic conductivity (K_S) for each material was determined by the constant head method, using samples with diameter 10cm and length 30cm. For each material, the steady-state hydraulic head (h) was measured at six locations inside each sample for three different values of water flow (Q_w). These measurements were then used in combination with Darcy's law to calculate the corresponding values of K_S.

Image of several particles of each fraction were scanned as it can be seen for a sample of material fraction 2 in Fig. 4-1. The particle shape was characterized by roundness and roughness. After measuring the diffusion coefficient in porous media (D_m) and diffusion coefficient in air (D_0) amount of tortuosity can be calculated using Eq. 13.

$$D_m = \phi/\tau\, D_0. \quad (13)$$

Grain size distribution of all five fractions is achieved by sieving test. The results can be seen in figure 4.2.

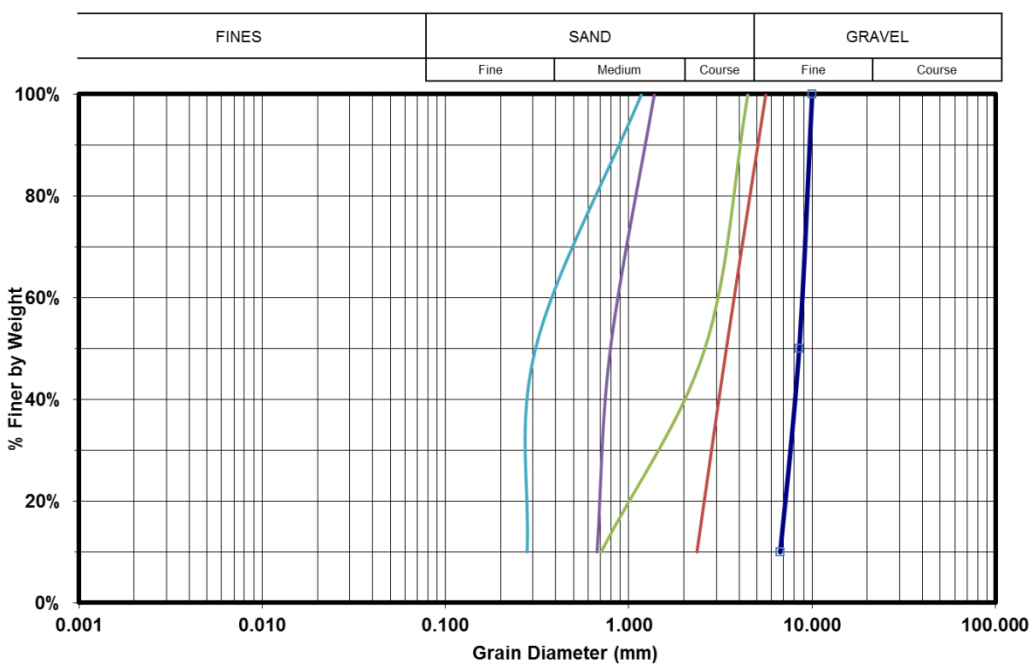

Figure 4-2. Grain size distributions of five fractions of materials used in the study. From left to right, curves respectively represent the grain size distribution of porous material 5 to 1.

Saturated hydraulic conductivity (K_S) was determined by the constant head method, using samples with diameter 10cm and length 30cm. For each material, steady-state hydraulic head (h) was measured at six locations inside each sample for three different values of water flow (Q_w). These measurements were then used in combination with Darcy's law to calculate corresponding values of K_S. All measurements of K_S were carried out in triplicate. For each material, total porosity (equal to gas-filled porosity), φ, was calculated based on the 181 sample weight, assuming a particle density of 2.65 g/cm3 for all five materials which is quartz particle density. Fluid saturation method is applied to measure the volume of pores and hence gain the total porosity be dividing that to the bulk volume.

4.2 Image analysis

Initial assessments were made to quantify the particles used in the columns in order to try to isolate the parameters of the particles that are most important in determining the effects of surface wind turbulence. The process for the automated measurement of particles (Tang et al. 2017) involves initially a selection of particles to be assessed based on image parameters (saturation, hue, brightness). Ideally, the original imaging conditions should be set such that the partition would be easy.

This produced the best contrast between the particles and the surrounding medium (Fig. 4-3). With the resulting image, the particles could be easily separated on the basis of brightness or colour. This generates a binary image from which measurements can be made (Fig. 4-3). The images are then reviewed for errors (e.g. particle number 10 in Fig. 4-3 B) and these can be removed from the data prior to analysis. At this scale, the major measurements that can be made are of particle scale characteristics. The major measurements relate to particle size (area, perimeter), particle shape (circularity, ferret lengths, aspect ratio, roundness) and presence absence of holes (solidity).

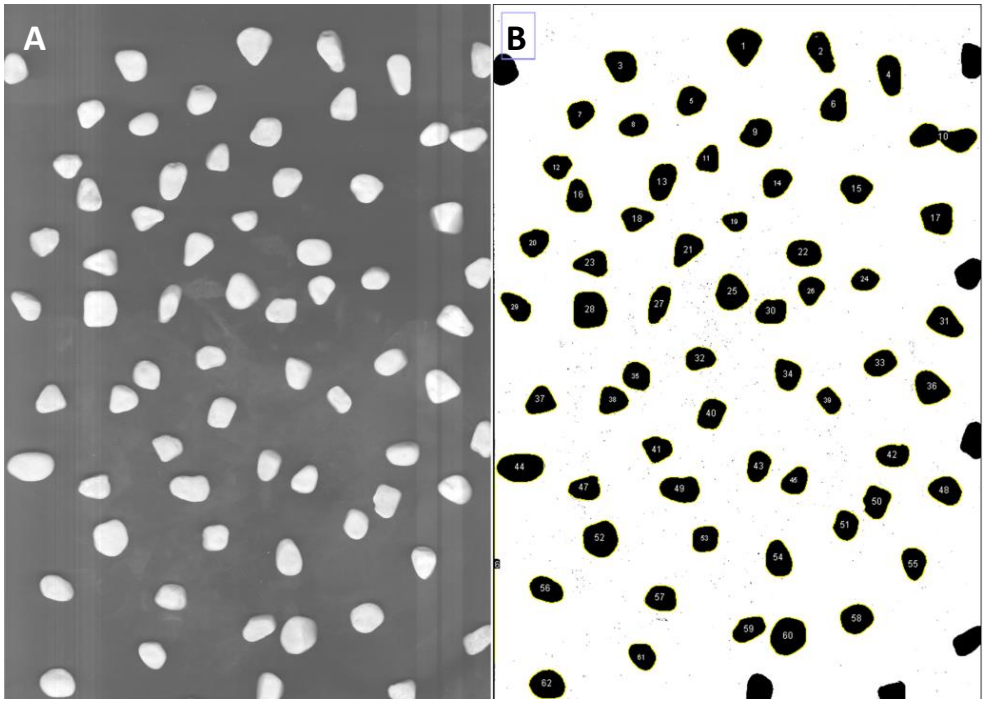

Fig. 4-3. A, Image of particles. B, Auto-identification of particles using a binary threshold prior to analysis

Through empirical, observational studies, it has been established for over 100 years that there is a relationship between particle size and gas flow, e.g. Hazen's formula (Hazen 1911). The relationship between other particle parameters and flow is much less dominant, and difficult to measure. The key impact of variations in particle shape is to create variations in packing and openness of the voids (hence influencing the void ratio). Roughness has been shown to influence flow (Natrajan & Christensen 2010), in the first instance by altering laminar to turbulent flow. The roughness of particles across 5 grain sizes were quantified as a part of the Xian Jiaotong-Liverpool University (XJTLU), department of civil engineering surface roughness project. This project created a library of particle roughness measurements for the standard construction sand

used for a wide range of research projects. Each individual particle is imaged using an optical microscope with a stepping motor (Fig. 4-4).

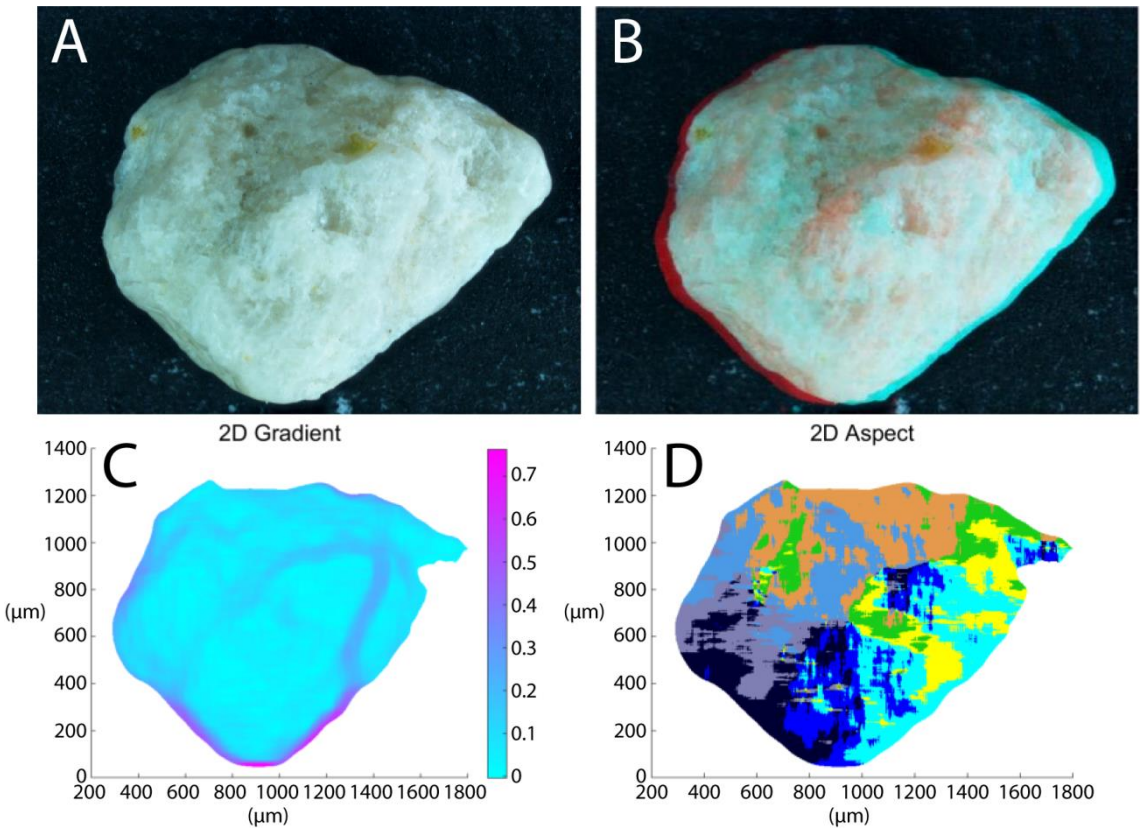

Fig. 4-4. Sample 3D analysis of a single grain of sand. A) Image of the surface of the sand grain taken in the optical microscope. B) 3D view of the surface of the sand grain using red cyan filter. C) Gradient map of the surface of the sand grain. D) Aspect map of the surface of the sand grain.

By identifying the focused pixels in an image a height map can be generated for the surface of the particles by comparing the height of pixels with the heights of their immediate neighbours, gradient maps (Fig 4-4C) and aspect maps (Fig. 4-4D) can be generated. This allows a visual assessment and categorisation of any large-scale roughness features prior to measurement. Precise measurements of the roughness of particles can be made from the surface measurements. For these measurements, the

selection of a datum (reference plane) is important. In the assessment of roughness of the sand particles a best fit parabola is shown here (Fig. 4-5). Several other reference plane options, such as circular or locally smoothed (Gaussian filter), are available alternatives. However as long as the same approach to the reference plane is used valid comparisons can be made between particles and with their application in soils. The roughness measurements for the sample particle are shown (Fig. 4-5). The complete particle library is available on request. In appendix C, images of all fractions are presented.

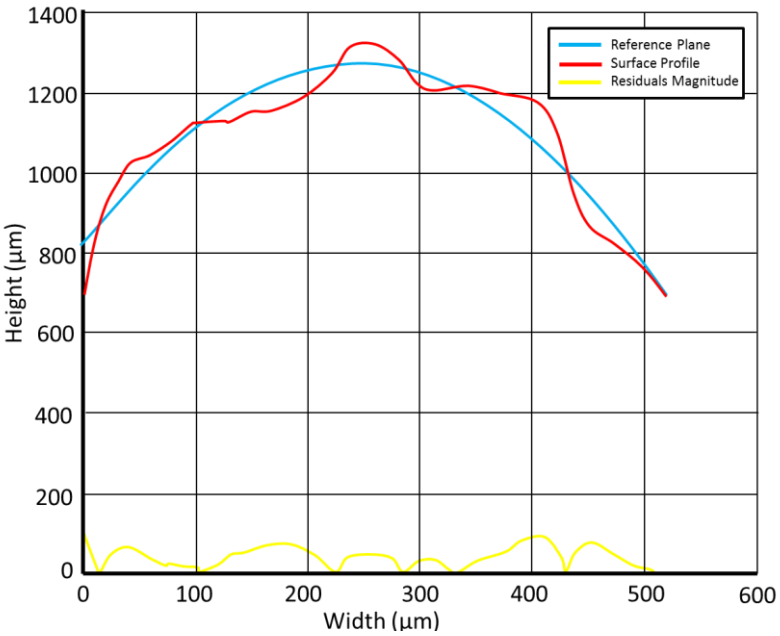

Fig. 4-5**.** Measurement of the roughness of the midplane of the surface of the sand grain. Only the top of the particle is shown, all values are in micrometre. In this approach the reference plan used is the best fit parabola. The magnitude of residuals is shown.

Particle shape was characterized by roundness, r, as given by (Russ, 2007)

$$r = \frac{4\,A_{\mathrm{p}}}{\pi\,R^2} \tag{14}$$

where A_p is the area of a two-dimensional image of the particle and R is the major axis of the best fitting ellipse into area (A_p) of a two-dimensional particle image. The roundness was determined applying the software package ImageJ (National Institutes of Health, Bethesda, MA, USA). For roughness Java coding were applied at another project and results were used here. Total 2580 particle images from five fractions of porous materials were analysed for determining roundness and roughness.

Another particle shape parameter applied in this study was surface roughness. Roughness is deviation of normal vector of surface from its ideal form and it has different parameters. The most common one is used here, which is actually one-dimensional arithmetical mean deviation of the surface profile, R_a is calculated as below, based on ISO 4287:1997 standard:

$$R_a = \frac{1}{n}\sum_{i=1}^{n} |y_i| \tag{15}$$

where n is the number of points that are equally spaced along the trace and y_i is the vertical distance from point i to the mean line.

All types of roughness which are also calculated in this study are in table 4-1:

Table 4-1. All types of measured Roughness, and their formula

Roughness description	Formula
Arthimetical mean deviation	$R_a = \frac{1}{n}\sum_{i=1}^{n} \lvert y_i \rvert$
Root mean squared	$R_q = \sqrt{\frac{1}{n}\sum_{i=1}^{n} y_i^2}$
Max valley depth	$R_v = \min(y_i)$
Max peak height	$R_p = \max(y_i)$
Max height profile	$R_t = R_p - R_v$
Skewness	$R_{sk} = \frac{1}{nR_q^3}\sum_{i=1}^{n} y_i^3$
kutosis	$R_{ku} = \frac{1}{nR_q^4}\sum_{i=1}^{n} y_i^4$

4.3 Experimental Setup

The experimental set-up is developed based on those used by Scotter & Raats (1968), (1969); Poulsen *et al*. (2008); Poulsen & Sharma (2011) and Maier *et al*. (2012). It was designed to enable measurements of gas (oxygen) concentration on samples of variable thickness at several locations within each sample. It consists of a 56-cm high, 25-cm inner diameter PVC column divided into two separate chambers by a perforated metal plate with 1-mm diameter holes that cover 30% of the surface of the plate. The upper chamber was used to hold a porous medium sample of the desired depth. Samples with depths less than the depth of the chamber were supported by an additional perforated

metal plate. This plate was adjustable to any elevation within the chamber so that surface of the sample was level with the top of the column. A 1.5 m × 1.5 m wooden board with a hole the same diameter as the column was installed horizontally, and level with the top edge of the column to minimize unwanted patterns of standing wind turbulence around the column. The lower chamber was connected to a pressurized source of CO_2 through a precision ball flow meter, Model LZM-15ZT (Yuyao Kingtai Instrument Co., Ltd, Yuyao, China). A differential pressure sensor (AB Micatrone, Solna, Sweden) and Omega differential pressure sensor model PX2650 (Omega engineering, Norwalk, USA) was connected to the lower chamber to facilitate measurements of pressure gradient across the sample. The column was fitted further with several KE-50 galvanic oxygen electrodes (Yuasa Power Supply Ltd, Kyoto, Japan) connected to a Campbell Scientific CR 1000 data logger (Campbell Scientific, Logan, UT, USA). To reduce the effects of preferential gas transport, oxygen sensors were not installed directly above one another but at different positions along the inner wall of the column (Fig. 4-5C). The column was further fitted with a Gill Wind master ultrasonic anemometer (Gill Instruments Ltd. Lymington, UK) for three-dimensional wind speed measurements at 20Hz recording frequency.

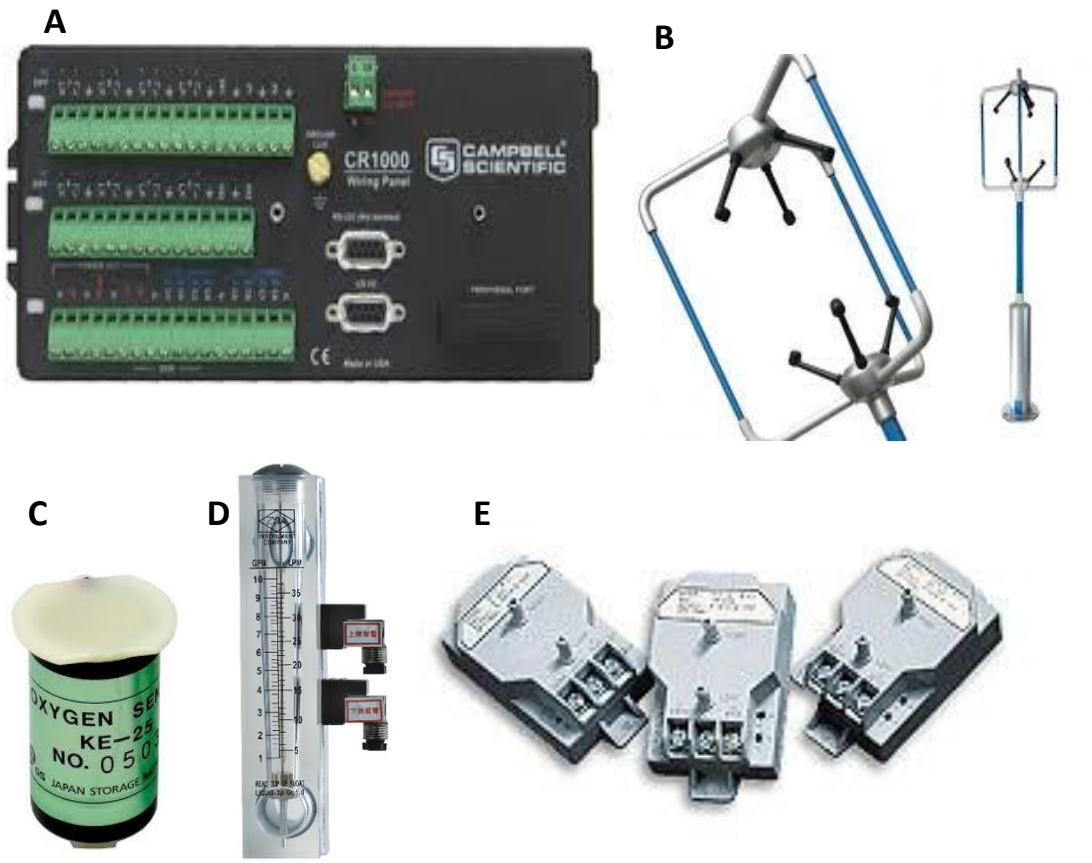

Fig. 4-6. A, CR1000 data logger, B, Anemometer, C, Oxygen sensor used in the experiments, D, Flow meter, E, Differential pressure sensor.

The main axis of the anemometer was placed 10 cm above the surface of the sample. A fan was used to create the desired wind conditions by adjusting the fan speed and inclination, and also distance between the fan and column. A schematic diagram of the set-up is shown in Fig. 4-6.

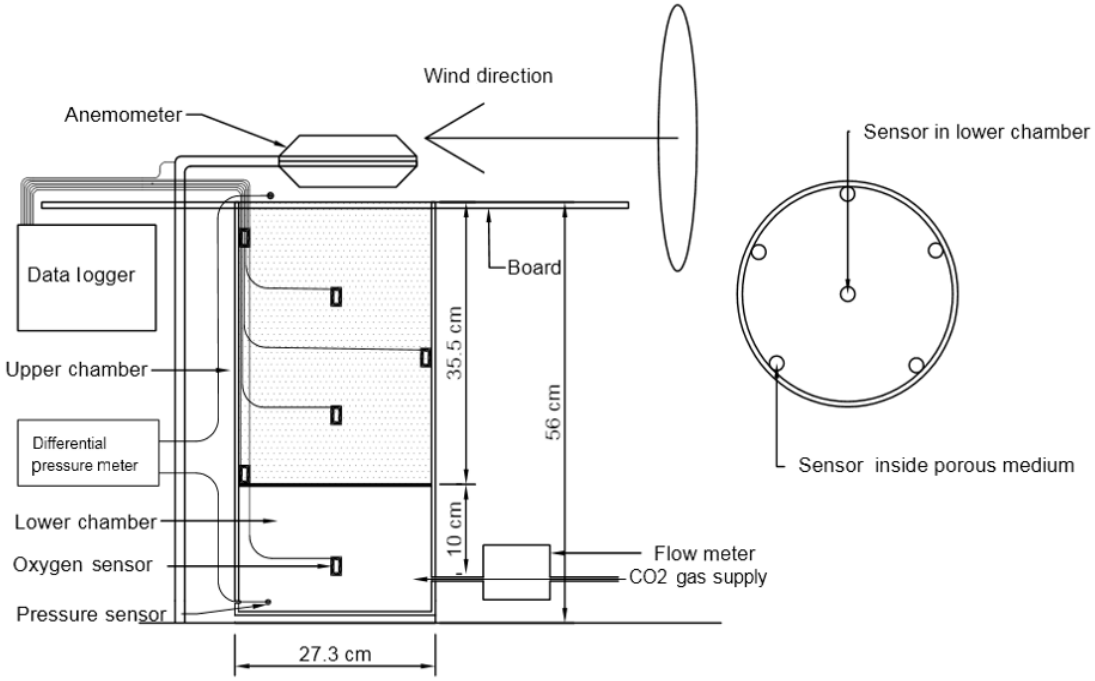

Fig. 4-7. Schematic diagram of the experimental set-up. Cross-section of the setup

As it can be seen in Fig. 4-7, a flow meter is connected to the entrance pipe for measuring amount of CO_2 flow into the chamber. That is used for calculating the gas permeability of each porous media. A differential pressure meter is also placed with sensors above and below the sample to see how the pressure difference is related to the gas transport.

4.4 Experimental Procedure

The dry porous medium was packed into the upper chamber of the column in 5-cm increments to ensure a homogeneous medium. During each experiment, the column was saturated initially with CO_2. Carbon dioxide was used rather than N_2 because it is heavier than air, which avoids the effects of buoyancy-driven flow that occurs when N_2

is used, which is lighter than air. During the saturation process, the top of the column was closed with a non-air tight lid. The level of CO_2 saturation (replacing the atmospheric air) was monitored by an oxygen sensor placed on top of the porous medium (at saturation the sensor would read zero O_2). At saturation, the CO_2 supply was switched off, the fan was turned on and the lid was removed by sliding it horizontally to minimize disturbance to the gas phase inside the column during its removal. Atmospheric air would then re-enter the column by molecular diffusion and wind-induced mixing, and the progress of air entry was recorded by oxygen electrodes at one-second intervals. Experiments were continued until oxygen concentrations had reached approximately 21% throughout the column. That amount is the percentage of O_2 in air by volume. Room temperature was recorded during all experiments. Oxygen was used as an indicator of the amount of air that has entered the column.

Two sets of experiments (A and B) were carried out. In set A, six different sample thicknesses (5, 10, 15, 20, 25 and 30 cm) were considered. These experiments were carried out with one oxygen sensor at the bottom of the sample and another placed in the lower chamber at 46-cm depth (to ensure full oxygen penetration). This approach is equivalent to that used in earlier research (Scotter & Raats, 1968, 1969; Maier *et al*., 2012; Poulsen & Sharma, 2011). The experiments were carried out in triplicate for four different wind conditions to give a total of 72 experiments and 144 oxygen breakthrough curves. Table 4-2 compares two methods of experiments, A & B.

Table 4-2. Comparing the methods of experiments.

Experiment types	Method A	Method B
Sample depths	5, 10, 15, 20, 25, 30 cm	Constant: 35.5 cm
Number of sensors inside sample	2	5

In all set B experiments, a sample thickness of 35.5 cm (corresponding to the height of the upper chamber) was used. In all experiments, five oxygen sensors were placed inside the sample at depths of 5.5, 13, 20.5, 28 and 35.5 cm and one sensor was placed in the lower chamber at a depth of 46 cm. This number of sensors was chosen as a 'trade-off' between accuracy in the estimates of the D_w-depth relations and the amount of computation time required to determine D_w. Set B experiments were carried out in triplicate for 13 different wind conditions to give a total of 157 experiments and 942 oxygen breakthrough experiments. Wind conditions were chosen based on the possible settings of the fan to have different range of near-surface wind speeds and turbulence intensities (represented by the standard deviation in wind speed).

The flow meter installed at the gas supply of the chamber and also the pressure meter which measures amount of pressure of gas flow into the chamber, can help us to achieve required data to be used in Eq. 3 for calculating the gas permeability of each fraction of porous media. This is done by reading the data for different gas pressure and correspondent flow meter value.

Differential pressure meter is another sensor, which can lead us in gaining the relation between pressure difference due to the wind fluctuation and gas transport through

porous media. For different wind conditions, amount of pressure difference is read and recorded.

Chapter 5 DATA ANALYSIS

5.1 Wind Speed Characterization

For characterizing wind speed in this research, different approaches have been used. Those include simple wind speed characterizations consisting of wind speed in three directions horizontal longitudinal (X), horizontal transversal (Y), vertical (Z) respectively u, v, w, and the standard deviation (s_x, s_y, s_z) of wind speed as a parameter that can show the fluctuations of the wind. Result of measurement of wind in three vertical components and resultant vector for one of wind conditions is shown in Fig. 5-1. Diagrams of other measured wind speeds are available in appendix A.

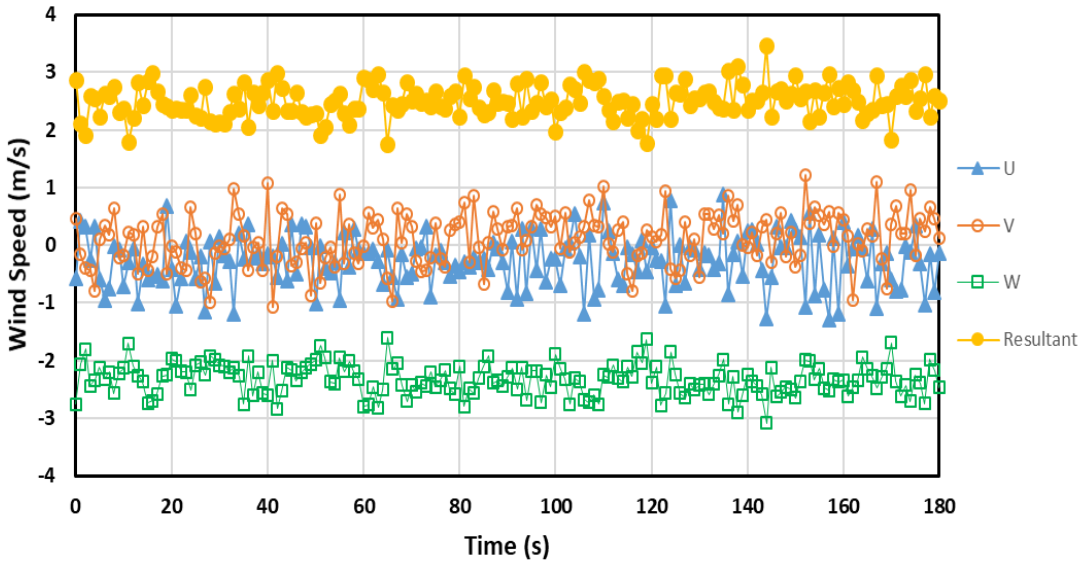

Fig. 5-1. Wind speed recorded measurements in 3 minutes sample for wind condition 5

For the first material fraction (The coarsest), 12 different wind conditions were applied. In that part of research which was used as the pilot study to the best methods for measuring effect of wind on gas transport and also to select wind conditions. Two of the

wind speed conditions are eliminated in the rest of study and a total of 11 wind conditions (10 different wind speed and one zero wind condition) remained as the selected ones. Method B was chosen for the rest of experiments on other materials and the changing factors in fitting procedure were the empirical factors of the achieved equation.

For the 12 wind speeds, their average values and the standard deviation as a factor of wind fluctuation in three main directions are measured. They can be seen in Table 5-1. To easily distinguish the different wind speeds, they are placed in order of increasing vertical component of wind in Table 5-1. It should be mentioned that, the two wind conditions that were eliminated for the next fraction experiments, are wind conditions 2.1 and 8.1. (Since they don't represent a different wind condition rather than the remained ones, they are eliminated in the rest of study).

Table 5-1. Wind conditions used in the experiments in this study. V_z, V_x and V are near-surface vertical, horizontal and total wind speeds, respectively (average wind speed out and standard deviations in parentheses).

Wind condition	Average V_z (s_z) /ms^{-1}	Average V_x (s_x) /ms^{-1}	Average V (s) /ms^{-1}
W0	0(0)	0(0)	0(0)
W1	0.02 (0.43)	1.67(0.31)	1.73(0.31)
W2	0.12(0.46)	1.80(0.36)	1.86(0.36)
W2.1	0.13(0.46)	1.92(0.32)	1.98(0.32)
W3	0.15(0.61)	1.98(0.39)	2.08(0.40)
W4	0.30(0.75)	2.40(0.50)	2.53(0.52)
W5	0.31(0.61)	2.33(0.46)	2.43(0.46)
W6	0.36(0.60)	0.97(0.49)	1.19(0.50)
W7	0.52(0.58)	2.74(0.42)	2.85(0.43)
W8	0.66(0.60)	3.06(0.45)	3.19(0.47)
W8.1	0.67(0.69)	3.27(0.54)	3.41(0.51)
W9	0.83(0.59)	2.64(0.42)	2.83(0.42)
W10	1.06(0.67)	1.55(0.63)	1.98(0.67)

While average horizontal, longitudinal wind speed (V_X) varies over one half order of magnitude, both average horizontal transversal (V_Y) and vertical (V_Z) wind speed vary over 2 orders of magnitude. In contrast, s is more constant and varies between approximately 0.4 and 1.0 ms^{-1} for all wind conditions and wind directions.

Power spectral density is another approach for characterizing wind speed fluctuation frequencies used in the current study. Kaimal power spectrum at Eq. 12 is selected for the theoretical modeling of power spectrum of wind. Experimental values are gained

using Fourier analysis routine in Microsoft Excel. Having the folding frequency, which is half of sample frequency; one can calculate frequency increment using Eq. 16:

$$\mathbf{\Delta}f = f_c / N, \quad (16)$$

where N is the number of frequencies and f_c is the folding frequency. Folding frequency is equal to half of sampling rate and sampling rate is equal to inverse of time step of the time series data of the wind speeds.

The complex coefficient is normalized by multiplication by 1/N. The absolute value of complex number is calculated by function of IMABS in excel. Multiplication of the absolute number in factor of $\sqrt{2}$ produces the magnitude of Fourier coefficient. Finally, the power of each frequency is the square of that magnitude.

After fitting Eq. (12) to the experimental power spectra obtained in this study (to obtain estimates of A_K and B_K) it was observed that the Kaimal model as given in Eq. (12) did not fit the experimental data well in the frequency range chosen in this study. The fitting accuracy, however, was greatly improved by including one additional fitting parameter into the model and using $Log_{10}(f)$ instead of f in Eq. (12), which was therefore modified accordingly to yield:

$$\Phi(Log_{10}(f)) = \frac{A_K}{(1+Log_{10}(f)B_K)^{5/3}} + C_K, \quad (17)$$

where C_K is the additional empirical parameter that is proportional to the energy content in wind speed fluctuations at high frequencies. It was also observed that fitted

combinations of A_K, B_K, and C_K in some cases are non-consistent, i.e., that several combinations of A_K, B_K, and C_K with differing values would yield similar fitting accuracies when fitted to the same experimental power spectrum. The reason was that the objective function (here chosen as the sum of squared differences between experimental and calculated spectral density values) was relatively flat in the optimal region caused by a relatively large variability in the experimental power spectral density values with frequency for some experimental power spectra. It was further observed that the experimental wind speed power spectra for the wind conditions used in this study could be approximated by a relatively simple piecewise linear function in the $\mathrm{Log}_{10}(f)$ domain given as:

$$\Phi(Log_{10}(f)) = A_L Log(f) + B_L \quad for\ f < \frac{C_L - B_L}{A_L} \tag{18a}$$

$$\Phi(Log_{10}(f)) = C_L \quad for\ f \geq \frac{C_L - B_L}{A_L}, \tag{18b}$$

where A_L and B_L are the slope and intercept of the best fit straight line to the experimental power spectrum for f < 0.18 Hz, respectively, and C_L is the average of experimental power spectral density for $f \geq 0.18$ Hz. As Eq. (18) was observed to yield more consistent parameter values than Eq. (17), Eq. (18) was included in this study together with Eq. (17) for characterizing wind speed fluctuations.

Initially mean wind speed (V), wind speed standard deviation (s) and wind speed coefficient of variation (CV) in all three directions (X, Y, Z) were calculated for each individual replicate wind speed time series for each of the 11 wind conditions. These values were then averaged for each of the corresponding 11 wind conditions.

Experimental wind speed power spectra were also calculated for each individual replicate wind speed time series and averaged in the same manner. Values of A_K, B_K, C_K, $\mathrm{Log}_{10}(B_K/A_K)$, A_L, B_L and C_L for each wind condition were then estimated by fitting Eqs. (17) and (18) to the corresponding experimental power spectra, respectively. Fitting was done by minimizing the sum of squared errors (SSE) between experimental $\Phi(\mathrm{Log}_{10}(f))$ values and $\Phi(\mathrm{Log}_{10}(f))$ values calculated by Eq. (17) or (18), respectively. The SSE is calculated as:

$$SSE = \sum_{i=1}^{N} \left(\Phi(\mathrm{Log}_{10}(f))_{e,i} - \Phi(\mathrm{Log}_{10}(f))_{c,i}\right)^2 \quad (19)$$

where N is the total number of experimental $\Phi(\mathrm{Log}_{10}(f))$ values in the experimental power spectrum being fitted and subscripts *e* and *c* refer to experimental and calculated values, respectively.

Wind induced gas transport can alternatively and in an easier way be quantified by the amount of time required to reach a certain concentration (C) at a given location for a given set of experimental initial and boundary conditions. An often-used value is the time required to reach 50% of a pre-selected final steady state gas concentration (C_s) applied experimentally at the medium surface and a specified initial (uniform) gas concentration (C_i) applied throughout the porous medium at the beginning of the experiment. This so-called breakthrough time (t_{50}) is easily determined from measured gas breakthrough curves from inside the porous medium as:

$$t_{50} = t[C = C_i + 0.5(C_s - C_i)] \quad (20)$$

Because the focus of this study is to identify possible links between wind speed characteristics and porous medium gas transport, and because breakthrough time is far simpler and much less time-consuming to determine than the lumped dispersion coefficient, while still providing adequate quantification of gas transport magnitude, breakthrough time (t_{50}) was selected in this study as the parameter of choice.

Average oxygen breakthrough curves were calculated from the individual replicate curves measured for each wind condition, material and depth. The corresponding values of breakthrough time (t_{50}) were then determined from these curves as the time required to reach an oxygen concentration of 10.5% which is selected as the half of the final percentage of oxygen in air. This was done by linear interpolation between the two nearest average measurements.

$\mathrm{Log}_{10}(t_{50})$ generally appeared much more linearly related to parameters V, s, Log_{10}(CV), A_K, B_K, C_K, $\mathrm{Log}_{10}(B_K/A_K)$, A_L, B_L and C_L in the X, Y and Z directions compared to just using t_{50} (which exhibited strongly non-linear relationships). A linear relationship allows the use of the simple and easier-to-apply parametric F-test for assessing the statistical significance of the linear correlation. It was therefore chosen here to use $\mathrm{Log}_{10}(t_{50})$ instead of t_{50} as basis for the correlation analyses. Correlation analyses for parameters V, s, Log_{10}(CV), A_K, B_K, C_K, $\mathrm{Log}_{10}(B_K/A_K)$, A_L, B_L and C_L in all three wind directions against $\mathrm{Log}_{10}(t_{50})$ were carried out for each individual depth in the five porous media across the 11 wind condition (yielding a total of 600 correlation analyses). In each case, it was tested using the F-test whether the correlation was significant at the

95% level. F-test is a statistical test to find the best-fit population. It gives the P-value which is used against or to support a null hypothesis. The P-value is evidence against a null hypothesis. Smaller P-value is the strong evidence for rejecting a null hypothesis. All analyses were carried out using the data analyses package in Microsoft Excel^{TM}.

5.2 Gas Dispersion Characterization

A one-dimensional numerical model used to solve one-dimensional equation of gas transport in porous media with an explicit forward time, central space finite difference method that was implemented in Microsoft Excel with the following initial and boundary conditions:

$C(z,t) = 0$ for $z \geq 0$ and $t = 0$, (21a)

$C(z,t) = 0.21$ for $z = 0$ and $t > 0$. (21b)

Boundary condition for the equation is C(0,t) = 0 and initial condition is C(x,0)=0.21. (It is known that 21% of air is oxygen). The idea of numerical method to solve differential equation is to replace the derivatives in the transport equation by difference quotients and consider the relationship between C at (x,t) and its neighbours a distance Δx and at a time Δt after. In the method there is also a limitation for stability of calculations that $D_w (\Delta t/\Delta x)^2 \leq 0.5$.

Boundary condition: C(0,t) = 0.21 , Initial condition: C(x,0) = 0

Difference in time:

$$\frac{C(z,t+\Delta t)-C(z,t)}{\Delta t}=\frac{\partial C}{\partial t}(z,t) \qquad (22a)$$

Central difference in space:

$$\frac{C(z+\Delta x,t)-2C(z,t)+C(z-\Delta z,t)}{\Delta z^{2}}=\frac{\partial^{2}C(z,t)}{\partial z^{2}} \qquad (22b)$$

After rewriting the transport equation using the expressions above and rearranging terms:

$$C(z,\ t+\Delta t) = C(z,t) + D\left(\frac{\Delta t}{\Delta z^{2}}\right)[C(z+\Delta z,t)-2C(z,t)+ C(z-\Delta z,t)]-v_z\left(\frac{\Delta t}{\Delta z}\right)[(C(z,t)-C(z-\Delta z,t)] \qquad (22c)$$

Therefore, having the C at three adjacent points z-Δz, z, z+Δz at time t, approximated value of C at x but a time step later, t+Δt can be calculated.

$$C(x_n, t_k) \sim C_n^k \qquad (22d)$$

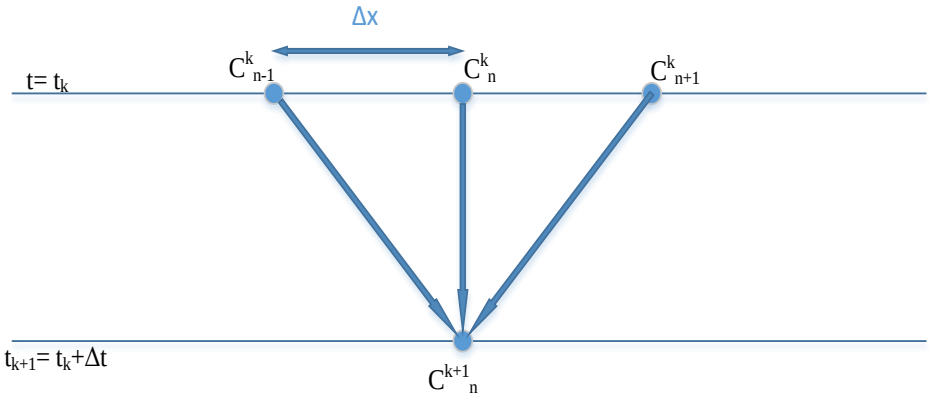

Fig. 5-2. Schematic of finite difference method in calculations

$$C^{k+1}_{n} = C^{k}_{n} + D\left(\frac{\Delta t}{\Delta x^2}\right)\left(C^{k}_{n+1} - 2C^{k}_{n} + C^{k}_{n-1}\right) \quad (22e)$$

Boundary and initial conditions are implemented. Numerical calculations are performed in excel and for each of the experiments, with different depths and different wind conditions has been used.

One-dimensional modelling is selected because only one measurement is available for each depth. This is equivalent to assuming that vertical concentration gradients only existed in the column. The model is fitted to the measured oxygen concentration data to determine values of D_w as a function of sample depth for different wind conditions.

Since experiments were carried out in different temperatures, the diffusion for zero wind condition first was modified to a diffusion coefficient in equal temperature condition. For this purpose, the first binary diffusion coefficient of CO_2 in air was exported which it can be seen at Table 5-1 (Denny, M., 1951). The table was calculated from data presented by Marrero and Mason (1972). The interpolation helped to achieve values for any other temperatures in between. Since the experiments were carried out at different temperatures, the gained values of binary diffusion coefficient and diffusion coefficient in soil, the table 5-2, could help to convert them to corresponded value at $20^{O}C$.

Table 5-2. Diffusion coefficient of CO_2 in air at one atmosphere (Denny, M., 1951)

T(^{O}C)	Diffusion coefficient of CO_2 in air (m^2s^{-1} x 10^{-6})
0	13.9
5	14.4
10	14.9
15	15.4
25	16.5
30	17.0
35	17.6
40	18.1

For experiment A, the model fitting procedure is carried out as follows: for each wind condition, the model is fitted to the oxygen breakthrough curves for the oxygen sensors placed at the bottom of the sample with 5 cm depth. In the lower chamber simultaneously by optimizing the values of D_{tot} in the porous medium and in the free air phase below. The model is then applied to the 10-cm depth sample assuming that D_{tot} for the top 5 cm of that sample is equal to that fitted to the 5-cm sample while optimizing the values of D_{tot} for the lower 5 cm of the 10-cm sample and the free air phase below that. This procedure is utilized to samples of consecutively increasing thickness to give a D_{tot} value for each 5-cm depth increment. The approach assumes that the value of D_{tot} for a given depth is independent of the thickness of the sample. For experiment B, the model is fitted to the six oxygen concentration datasets from the

oxygen sensors inside the porous medium and in the lower chamber simultaneously by optimizing D_{tot} values for each of the five depth increments represented by the sensors. Breakthrough time was reached very rapid for shallow depths, and the corresponding values of D_w are not always physically meaningful. Therefore, the model is fitted so that D_w could not increase with depth (see Fukuda, 1955). For both sets of experiments, model fitting is done by minimizing the root-mean-square error (RMSE) between measured and fitted oxygen concentrations.

$$\mathrm{RMSE} = \sqrt{\frac{1}{n}\sum_{i=0}^{n}(C^{n}_{\mathrm{measured}} - C^{n}_{\mathrm{fitted}})^2}, \tag{23}$$

where n is the number of measurements of concentration.

Function of "solver" is used for this purpose. Solver is a Microsoft Excel add-in program can be used for what-if analysis. This is done to find an optimal (maximum or minimum) value for a formula in one cell subject to constraints, or limits, on the values of other formula cells.

Generalized reduced gradient method knows as GRG Nonlinear is the selected method for the fitting procedure in current research. The procedure is like this: A model/problem is defined by a "line" (curve, really, possibly in multiple dimensions), and GRG is passed variable "starting" points that may or may not be on the solution curve. GRG will test that solution (given by the initial starting points), determine if it is "on the curve" and within the bounds/limits defined. If all variable values are not integers, GRG will take every point that is not an integer and start a new possible solution "around" the point that is not an integer (Making two for each point, one that is

an integer above and one that is an integer below the non-integer point). This is done for every given point that falls into this category and retest those solutions to see if they improve the previous one. If at least one of them does, GRG will pick the largest improvement and continue solving the problem by looping through the above steps of trying to find an all-integer solution. At some point, GRG will likely not be able to improve the solution any more after desired number of iteration. If any solution ever falls outside the bounds/limits defined in the problem, it is discarded. Smith, S. & Lasdon, L. (1992) showed the procedure and application of that method

For zero wind condition, the fitted values of D_{tot} for the porous medium and the free air space correspond to the molecular diffusion coefficients D_m and D_0, respectively. For wind conditions 1–11, the fitted D_{tot} values for the porous medium correspond to $D_m + D_w$. Values of D_w are obtained by subtracting D_m from D_{tot}. Prior to the determination of D_w, all values of D_m were standardized to a temperature of 20^oC. It can be seen in Fig. 5-3, where the measured oxygen concentration data are shown in markers for different sensors and the continuous line is the best fitted modelling gained by the procedure described above. Diagrams of relative oxygen concentrations for rest of the experiments are available in appendix B.

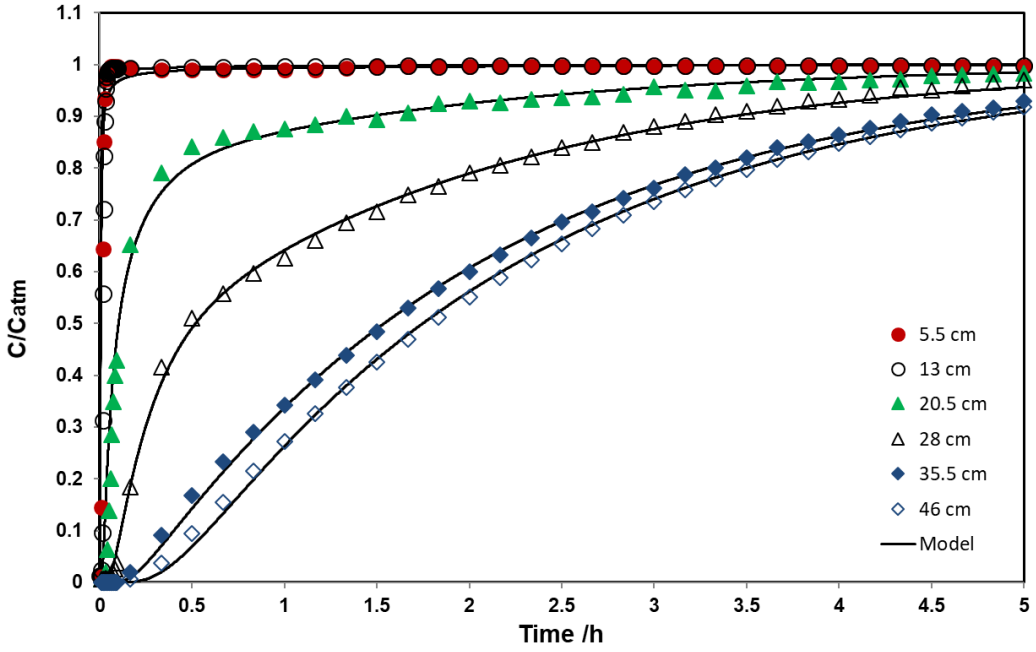

Figure 5-3. Relative oxygen concentration (C/C_{atm}) as a function of time and depth for experiment B, under wind condition where C_{atm} is the atmospheric oxygen concentration. Note that not all individual measurements (taken at 1s intervals) are shown.

Material 1, the coarsest fraction of the research, was exposed to 12 different wind speed plus zero-wind conditions (i.e. a total of 13 wind conditions). The procedure of fitting experimental and calculated data leads to finding an equation, which can be used for calculating and predicting the dispersion coefficient. For Material 1, which was used as the pilot study of the research, fitting was executed between measured oxygen concentration values and modelled ones by minimizing RMSE value, with changing five dispersion coefficients at the location of oxygen sensors in the model. For the rest of the materials (fractions 2 to 5), fitting was done by minimizing the RMSE with change in the experimental parameters of that equation directly. For those fractions, 10 selected wind speeds were utilized which together with the calm condition, produces 11 different wind conditions.

Chapter 6 RESULTS AND DISCUSSION

6.1 Particle Properties

Particle properties including particle shape analysis, size and gas permeability are measured by the corresponding tests, which are described in Chapter 5.

The gas permeability of each of the fractions is measured by a flow meter and applying the Eq. (24) & (25). The graph in Fig. 6-1 shows the flow rate and the corresponding pressure for material fraction 2 as an example. The trend line of the measured points is drawn and the slope of that like which represents the linear relation between pressure and flow rate can be calculated as below:

$$slope = \frac{\mu \Delta x}{k_a}. \tag{24}$$

Therefore,

$$k_a = \frac{\mu \Delta x}{slope} \tag{25}$$

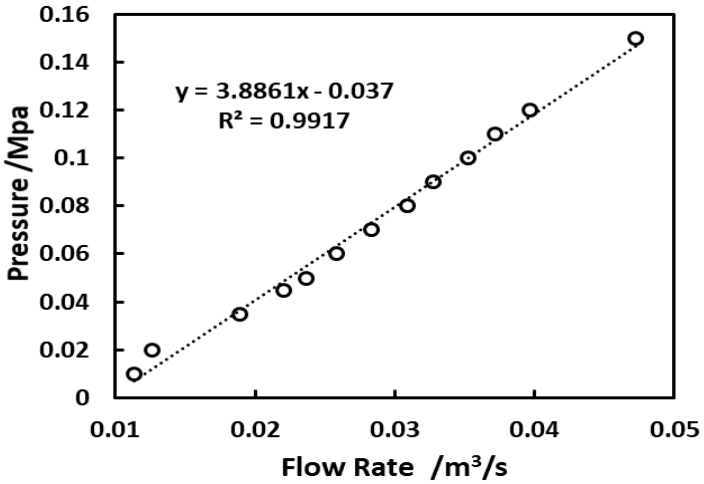

Fig. 6-1. Permeability test. Relation between differential pressure in two sides of sample and flow rate for material number 2.

Different types of roughness are measured and presented in Table 6-1. The main parameter of roughness that is used later is R_a called arithmetical mean deviation.

Table 6-1. Roughness measurements for five fractions. The measurements of different types of roughness from left to right are: mean deviation (R_a), root mean squared (R_q), max valley depth (R_v), max peak height (R_p), max height profile (R_t), skewness (R_{sk}) and kurtosis (R_{ku}).

Roughness type	R_a	R_q	R_v	R_p	R_t	R_{sk}	R_{ku}
Material 1	0.633	0.743	0.001	1.590	1.588	1.398	2.238
Material 2	0.784	1.158	0.001	2.842	2.841	1.632	3.078
Material 3	0.348	0.428	0.001	1.058	1.057	1.532	2.698
Material 4	0.0605	0.076	0.001	0.184	0.183	1.548	2.776
Material 5	0.060	0.074	0.002	0.166	0.165	1.499	2.547

All the measured and calculated parameters of five fractions of porous materials are shown in Table 6-2. However, due to the dominant effect of particle size on the results a large number of different samples with different properties need to be analysed in order to identify the significance of the effect of particle roughness.

Table 6-2. Physical characteristics and sample size for the materials used in this study

Medium	Material	D_{10}	D_{50}	ϕ	r	R_a	k_a	K_S	D_m	τ	H
		mm	mm	cm^3cm^{-3}			mm^2	mh^{-1}	cm^2s^{-1}		cm
1	Crushed marble	6.7	8.5	0.31	0.74	0.78	0.19	31	0.047	1.06	35.5
2	Crushed granite	2.35	3.41	0.43	0.69	0.21	0.096	6.4	0.042	1.64	25.5
3	Crushed granite	1.7	2.37	0.45	0.72	0.24	0.066	1.6	0.044	1.64	20
4	Very coarse sand	0.67	0.81	0.46	0.79	0.05	0.055	0.96	0.038	1.94	15
5	Coarse sand	0.28	0.31	0.46	0.73	0.07	0.053		0.040	1.84	15

Gas permeability (k_g) and saturated hydraulic conductivity (K_s) decrease by about an order of magnitude going from material 1 to material 5. The results of measuring hydraulic conductivity are used to compare them with air permeability values for all five fractions of porous material to find out if there is any relation between them. Fig. 6-2 represents a diagram which shows how increase in those two values is close to a linear relation. Each marker represents one of porous materials.

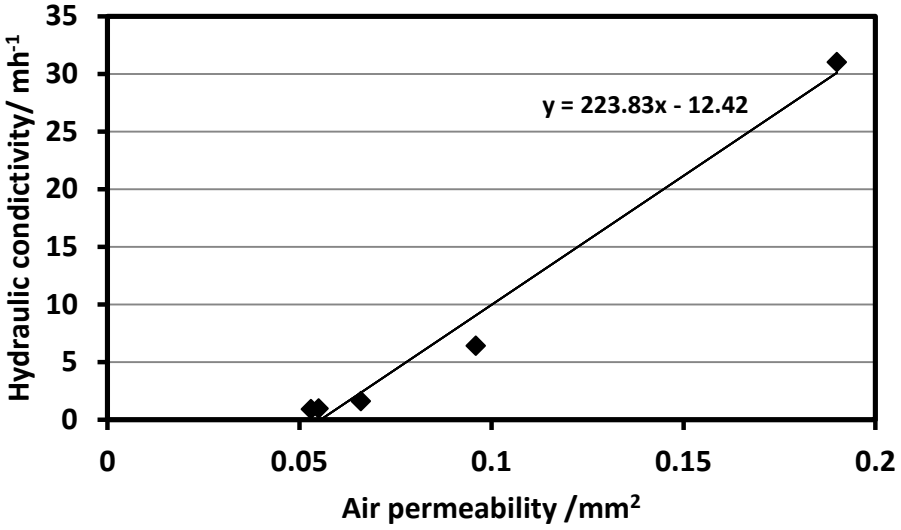

6-2. Hydraulic conductivity versus air permeability for five fractions of materials used in the experiments.

6.2 Gas Dispersion Parameters

The observed values of D_m and D_0 were independent of depth of the porous medium, as expected, and relatively constant in their agreement with theory. For example, average values of D_m and D_0 at 20^{o}C across all experiments for material five, at zero wind condition are 0.0485 $cm^2\ s^{-1}$ with a standard deviation of 0.013 and 0.12$cm^2\ s^{-1}$ with a standard deviation of 0.009, respectively. By comparison, values in the literature for D_0 as the binary diffusion coefficient of CO_2 and air at 20^{o}C are about 0.16 cm^2s^{-1}

according to Denny (1993). The deviation between these values might be explained partly by differences in experimental set-up and the sensors used. Estimates of D_m by Equations (9) and (10) did not compare well with the measured values, probably because these equations were developed for soil, which is much finer grained than the medium used here.

Fitted versus measured oxygen concentrations for all individual replicate experiments are shown in Fig. 6-3. (Each plot contains between 1 and 1.5 million data points). It can be observed that the model in general is able to obtain reasonably accurate fits to the data as indicated by the 95% confidence intervals for the data, although there are a smaller number of curves where the fits are less accurate. Overall Fig. 6-3 indicate that the modelling approach used here is adequate for fitting the measured oxygen breakthrough curves.

Fig. 6-4 shows the six oxygen breakthrough curves for two media (media 2 and 4) as a function of depth and time corresponding to six oxygen sensors inside each porous medium. In Fig. 6-4, curves represent the fitted values, whilst symbols are the measured values of oxygen concentration. It is evident that the fitted curves closely follow the measured data. It is also showing how the gas is transporting with slower rate by increasing in the depth of porous media.

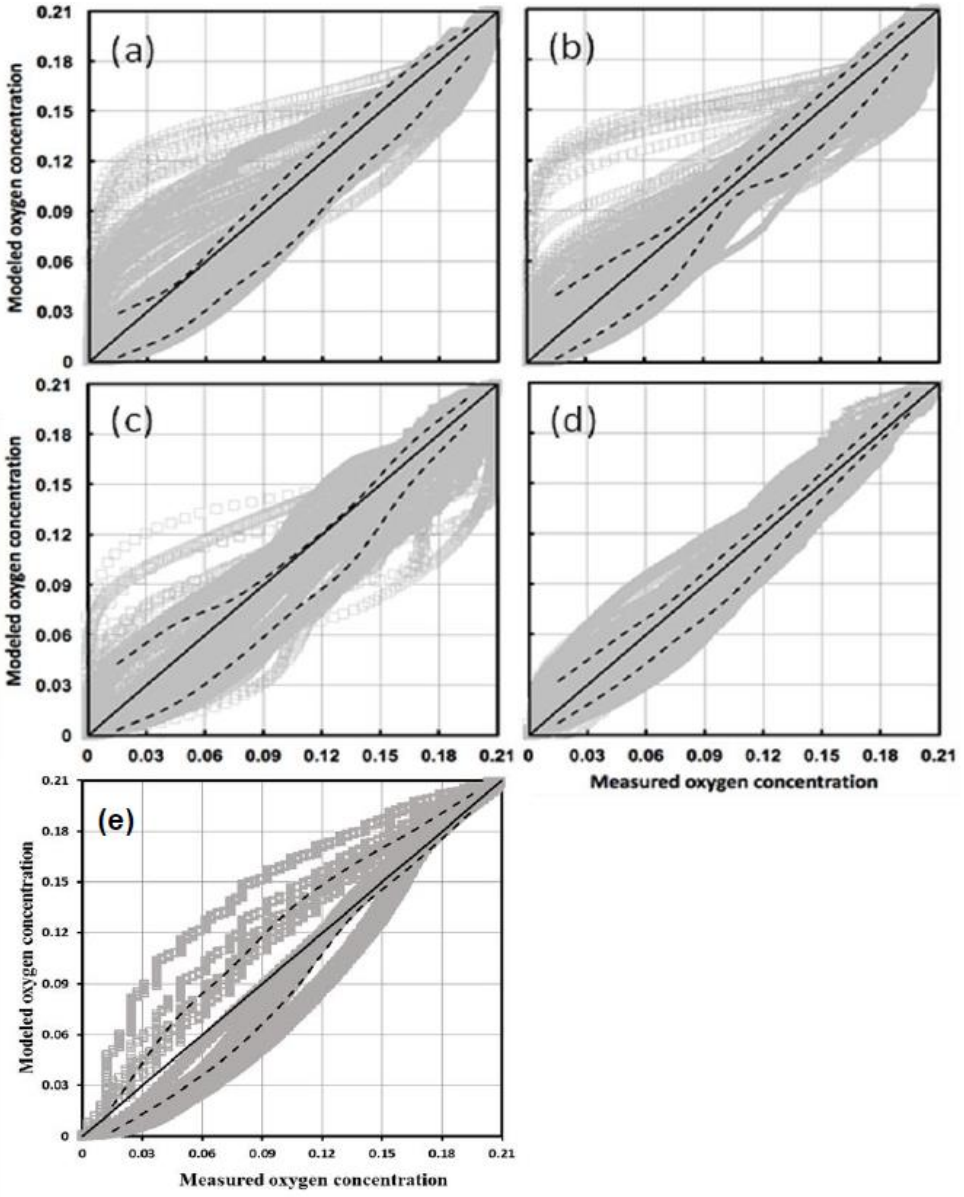

Fig. 6-3. Measured vs. fitted oxygen concentrations for (a) medium 1, (b) medium 2, (c) medium 3, (d) medium 4 and (e) medium 5. Symbols indicate individual data points; solid lines indicate ideal fits (1:1 lines) and dashed lines represent the intervals containing 95% of the fitted oxygen concentration data.

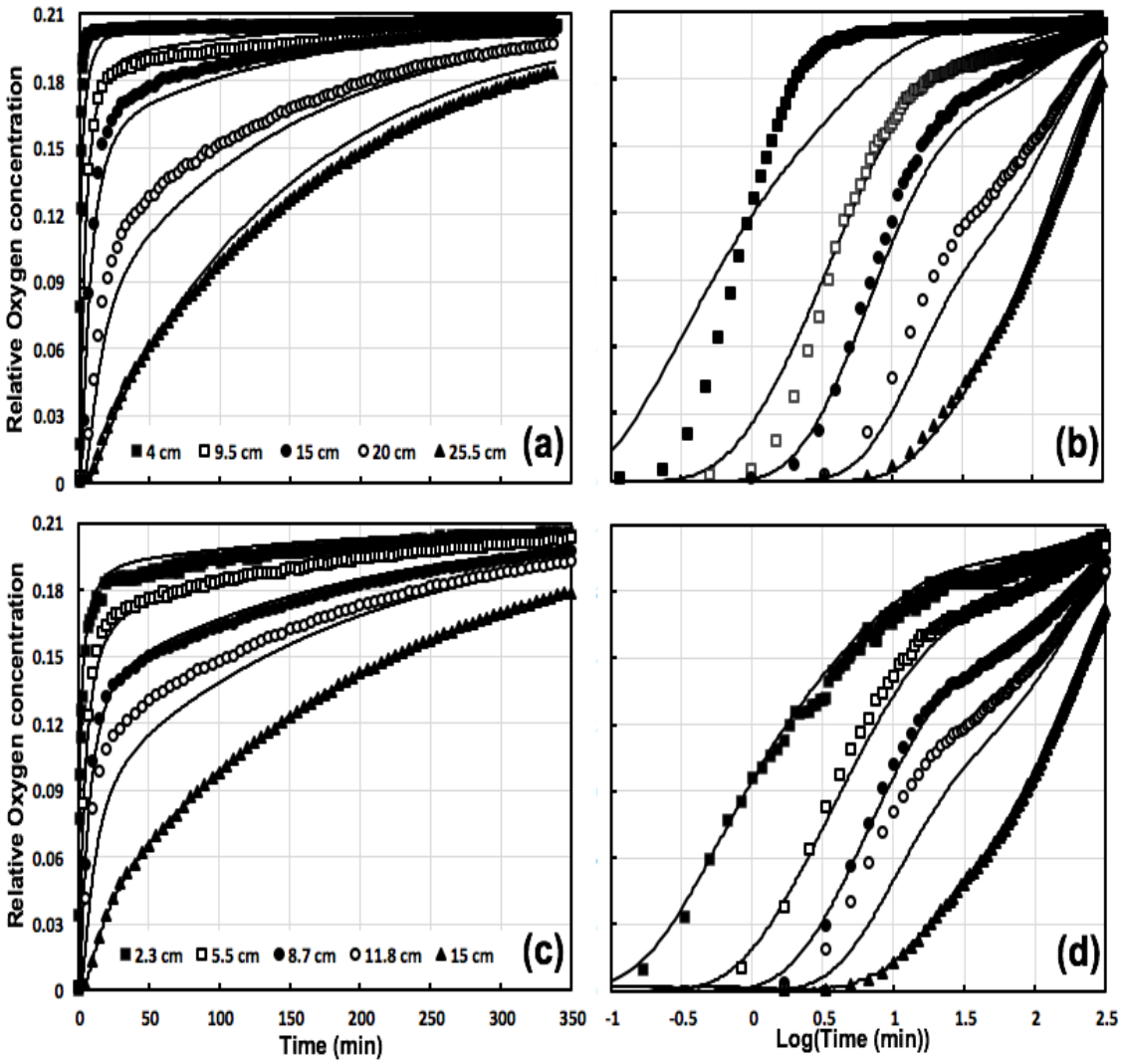

Fig. 6-4. Oxygen concentration as a function of depth and time for medium 2, wind condition 6 (a), (b) and medium 4, wind condition 9 (c), (d). Symbols indicate measured values and solid curves are fitted model (Eq. (9)) values.

Fig. 6-5 shows that wind-induced dispersion coefficients (D_w) as a function of depth for all 5 fractions. The results show the effect of wind is lowering by increase in depth and at a specific depth, the D_w is approaching zero and D_{tot} is getting close to molecular diffusion coefficient (D_m). This depth is higher, for coarser fractions of porous media. It can be observed that value for fractions 5 is almost equal to the value of the molecular

diffusion coefficient. This indicates that the effect of wind on gas transport in that fraction is negligible.

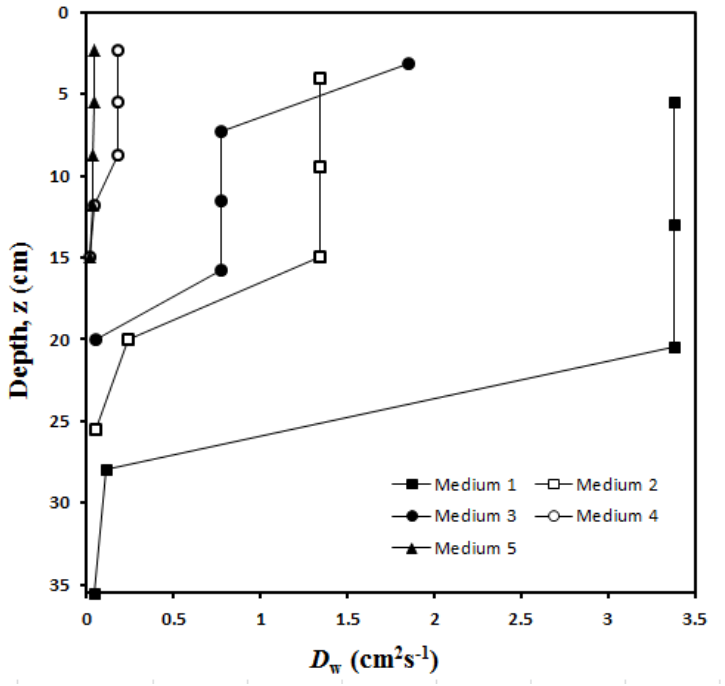

Fig. 6-5. Wind-induced dispersion coefficients (D_w) as a function of depth at wind conditions W10 for 5 porous media fractions.

Fig. 6-6 shows the six oxygen breakthrough curves for experiment B at wind condition 3 for coarsest fraction of materials (material 1), which corresponds to the six oxygen sensors installed inside and below the sample. In this case, breakthrough time is taken as the amount of time that elapsed before the oxygen concentration at a given depth reaches 50% of its final value (10.5 relative to 21% oxygen). Fig. 6-5a shows the breakthrough time (t_b) as a function of depth for the 11 wind conditions.

As expected, t_b increases with z (Fig. 6-6a). Although t_b increases almost linearly with z for wind condition 0, the t_b–z relation is strongly non-linear for the remaining 10 wind

conditions. Under windy conditions, t_b is very small for z less than about 15–20 cm and only increases for z > 20 cm. Oxygen breakthrough times are less for windy conditions than for the no wind condition for all depths investigated.

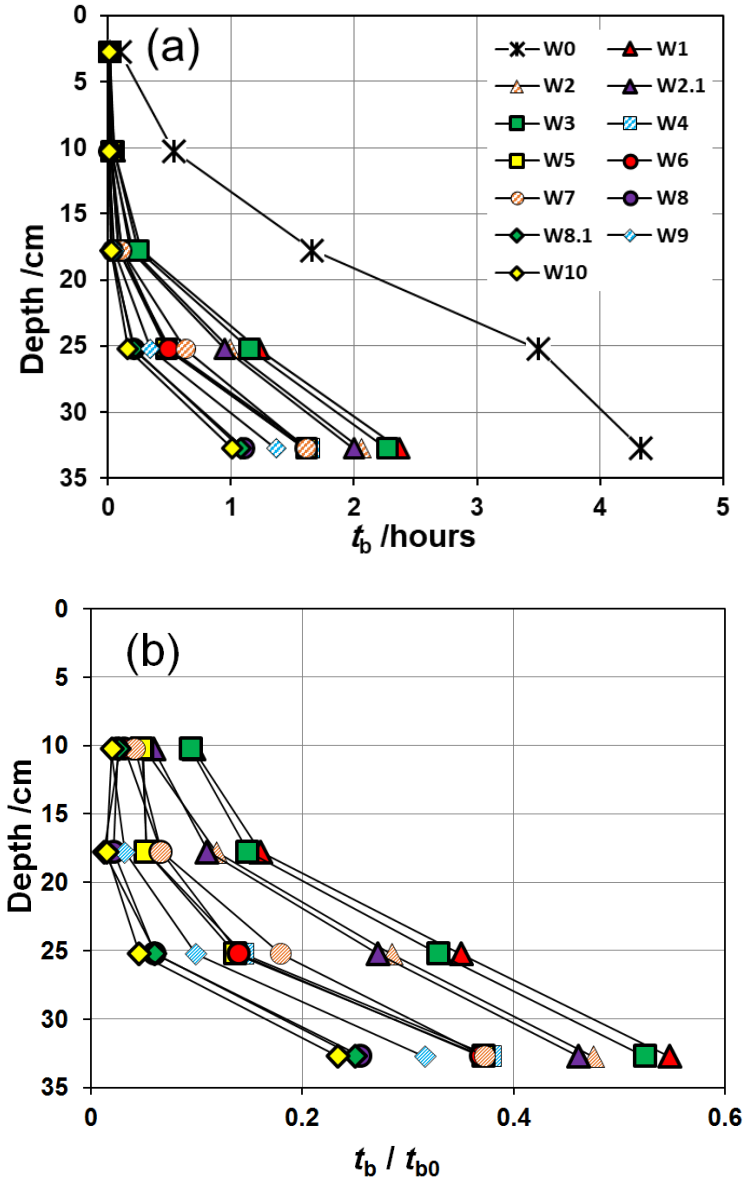

Fig. 6-6. (a) Breakthrough time, t_b (time to reach 10.5% O_2), as a function of depth below the column surface for wind conditions W0–W10 and (b) relative breakthrough time (compared to wind condition 0) for wind conditions W1–W10. Note that the y-axis is reversed to represent measurement location better.

Fig. 6-6a also indicates a strong inverse relation between t_b and wind speed. The largest effect of wind turbulence on t_b occurs at shallow depths (z < 20 cm, Fig. 6-6b). At these depths, t_b under windy conditions is 2–9% only of the corresponding t_b values under calm conditions (molecular diffusion only). For material 4 (Fig. 6-7d), however there is a general tendency that t_{50} for windy conditions is closer to t_{50} for calm conditions than for the other three materials. This suggests that for finer grained materials the relative effect of wind action on gas transport is potentially less pronounced in agreement with earlier theoretical studies. For all five porous media, t_{50} for a given depth and medium vary strongly as function of wind condition (0.5 – 2 orders of magnitude), indicating a significant dependency of breakthrough time on wind speed characteristics.

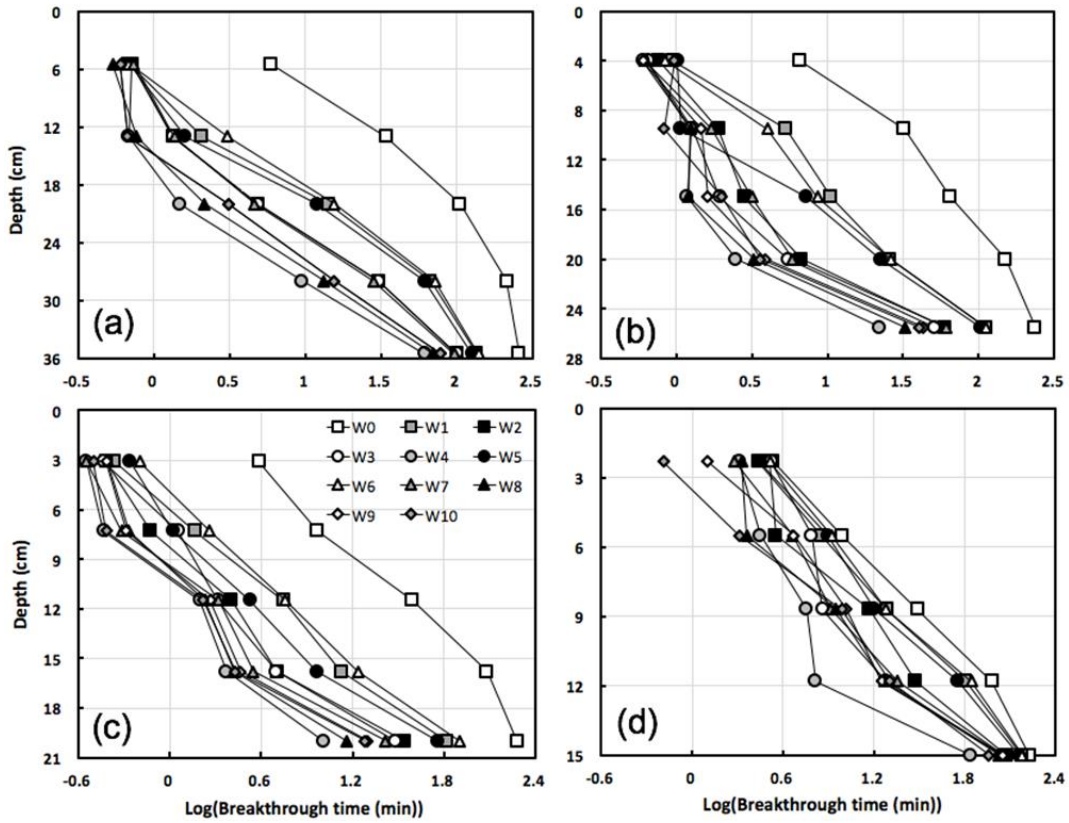

Fig. 6-7. Log_{10}(breakthrough time, t_{50}) as function of depth and wind condition for (a) material 1, (b) material 2, (c) material 3 and (d) material 4.

At larger depths, the relative effect of wind on t_b decreases, however, at z = 30–35 cm wind effect still reduces t_b to between 23 and 55% of that observed under calm condition (zero wind). Note that breakthrough times at 2.5 cm were very small (Fig. 6-7a), therefore, the values of relative breakthrough time at this depth were variable and not always physically meaningful. They were excluded therefore from Fig. 6-7(b). The results in Fig. 6-7 indicate that even though wind turbulence penetrates to a limited depth only, it can have a potentially large effect on gas transport at much larger depths.

6.3 Wind Speed Characteristics

Values of applied wind speeds in horizontal and vertical components are presented in table 5.1. Average values of V, s and $Log_{10}(CV)$ for the 11 wind conditions are given in Table 6-3. Examples of wind speed measurements in the X, Y and Z directions for wind condition 6 are shown in Fig. 6-8a, 6-8b, and 6-8c, respectively. The corresponding experimental wind speed power spectra for the X, Y and Z directions for wind condition 6 are shown in Fig. 6-8d, 6-8e, and 6-8f, respectively. Note that the power spectra were calculated using much longer (300s) wind speed time series than shown in Fig. 6-8a – c.

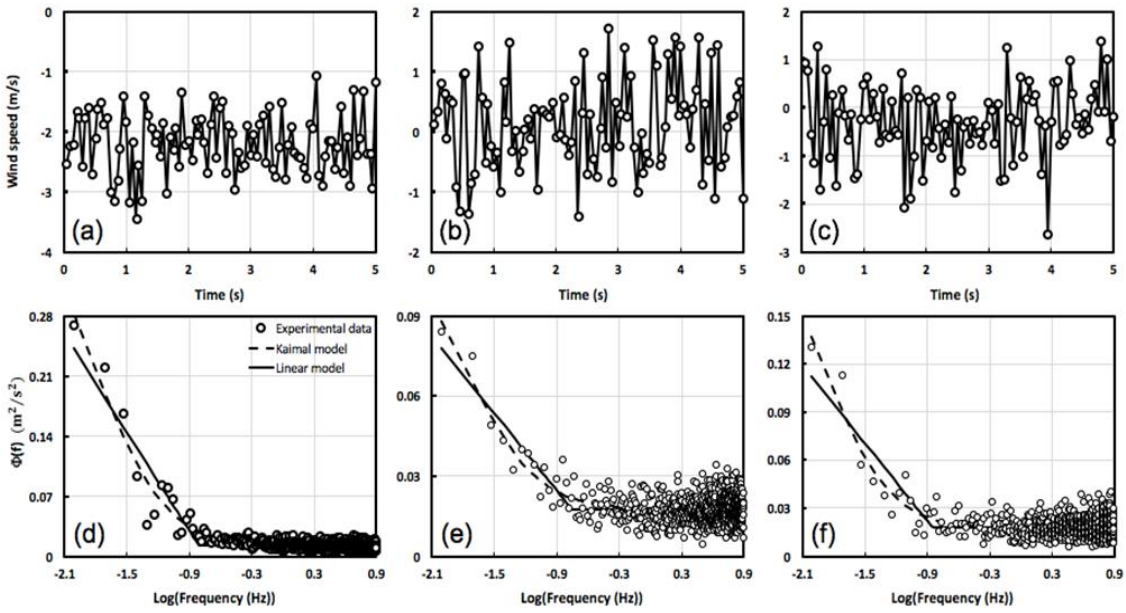

Fig. 6-8. Examples of directional wind speed time series ((a): x-direction, (b): y-direction, and (c): z direction) and corresponding experimental wind speed power spectra ((d): x-direction, (e): y-direction, and (f): z-direction) for wind condition 6.

The individual power spectrum corresponding to each of the three wind directions exhibit a very similar shape where the spectral density ($Log_{10}(f)$) decreases rapidly with

increasing $Log_{10}(f)$, for $Log_{10}(f)$ less than approximately -0.75 (corresponding to 0.18 Hz) but remains approximately constant for $Log_{10}(f)$ above this value. This means that on a relative basis, most of the energy in the wind applied during wind condition 6, is associated with wind speed fluctuations with frequencies below 0.18 Hz. The power spectra corresponding to the remaining wind conditions (except wind condition 0 where no wind was applied) exhibited similar shape characteristics with the main difference between wind conditions being the magnitudes of the corresponding spectral densities.

Table 6-3. Wind speed characteristics for the 11 wind conditions used in this study in terms of basic wind speed characteristics (average wind speed, V, wind speed standard deviation, s, and Log_{10}(wind speed coefficient of variation, CV), Kaimal wind speed power spectrum model (Eq. (17)) parameters (A_K, B_K, C_K, and $Log_{10}(B_K/A_K)$) and linear wind speed power spectrum model (Eq. (18)) parameters (A_L, B_L, and C_L) in all three wind directions (x, y, z).

Wind	Abs(V_x) ms^{-1}	s_x ms^{-1}	$Log_{10}(CV_x)$ ms^{-1}	$A_{k,x}$ ms^{-1}	$B_{k,x}$ ms^{-1}	$C_{K,x}$	$Log_{10}(A_{K,x}/B_{K,x})$	$A_{L,x}$	$B_{L,x}$	$C_{L,x}$
0	0	0	-	-	-	-	-	-	-	-
1	1.89	0.3	-0.69	0.06	26.	0.01	2.60	0.03	0.03	0.01
2	2.30	0.4	-0.67	0.03	15.	0.01	2.64	0.02	0.00	0.01
3	0.58	0.4	-0.09	0.084	13.9	0.016	2.22	0.045	0.007	0.016
4	1.21	0.55	-0.34	0.137	15.2	0.008	2.05	0.088	0.054	0.008
5	1.72	0.34	-0.70	0.107	52.3	0.007	2.69	0.036	0.018	0.007
6	1.59	0.30	-0.72	0.113	21.0	0.011	2.27	0.061	0.033	0.011
7	2.24	0.45	-0.70	0.475	41.1	0.012	1.94	0.190	0.142	0.012
8	2.76	0.47	-0.77	0.089	25.3	0.013	2.46	0.059	0.043	0.013
9	2.47	0.44	-0.75	0.340	94.1	0.010	2.44	0.064	0.041	0.010
10	2.42	0.39	-0.79	0.654	47.7	0.009	1.86	0.238	0.186	0.010

	Abs(V_y) ms^{-1}	s_y ms^{-1}	$Log_{10}(CV_y)$ ms^{-1}	$A_{K,y}$ ms^{-1}	$B_{K,y}$ ms^{-1}	$C_{K,y}$	$Log_{10}(B_{K,y}/A_{K,y})$	$A_{L,y}$	$B_{L,y}$	$C_{L,y}$
0	0	0		-	-	-	-	-	-	-
1	0.10	0.56	0.74	0.046	23.8	0.014	2.72	0.025	0.004	0.014
2	0.01	0.67	1.71	0.028	36.3	0.018	3.11	0.011	0.012	0.018
3	0.02	0.77	1.54	0.043	16.6	0.026	2.59	0.027	0.008	0.020
	Abs(V_y)	s_y	$Log_{10}(CV_y)$	$A_{K,y}$	$B_{K,y}$	$C_{K,y}$	$Log_{10}(B_{K,y}/A_{K,y})$	$A_{L,y}$	$B_{L,y}$	$C_{L,y}$
4	0.23	0.98	0.63	0.145	20.1	0.024	2.14	0.076	0.026	0.025
5	0.06	0.53	0.97	0.018	10.2	0.015	2.75	0.011	0.009	0.014
6	0.09	0.51	0.77	0.004	9.00	0.018	3.41	0.002	0.015	0.013
7	0.19	0.62	0.52	0.083	14.7	0.008	2.25	0.044	0.018	0.008
8	0.09	0.69	0.87	0.117	36.6	0.018	2.50	0.048	0.019	0.018
9	0.16	0.64	0.61	0.070	19.0	0.016	2.43	0.041	0.013	0.017
10	0.90	0.54	-0.22	0.100	11.9	0.007	2.08	0.059	0.025	0.007
	Abs(V_z) ms^{-1}	s_z ms^{-1}	$Log_{10}(CV_z)$ ms^{-1}	$A_{K,z}$ ms^{-1}	$B_{K,z}$ ms^{-1}	$C_{K,z}$	$Log_{10}(B_{K,z}/A_{K,z})$	$A_{L,z}$	$B_{L,z}$	$C_{L,z}$
0	0	0	0	-	-	-	-	-	-	-
1	0.15	0.61	0.60	0.160	222	0.016	3.14	0.017	0.001	0.016
2	0.30	0.75	0.40	0.065	53.9	0.021	2.92	0.025	0.025	0.021
3	0.36	0.60	0.22	0.054	18.9	0.021	2.54	0.035	0.005	0.016
4	1.06	0.67	-0.20	0.052	10.7	0.018	2.31	0.050	0.020	0.018
5	0.05	0.47	0.10	0.062	108	0.013	3.24	0.009	0.007	0.012
6	0.02	0.43	1.27	0.003	9.00	0.013	3.48	0.002	0.010	0.012
7	0.31	0.61	0.30	0.197	120	0.015	2.78	0.034	0.016	0.017
8	0.53	0.64	0.08	0.249	56.4	0.017	2.36	0.081	0.051	0.018
9	0.46	0.59	0.11	0.056	18.1	0.014	2.51	0.032	0.008	0.016
10	0.83	0.59	-0.15	0.150	43.5	0.015	2.46	0.053	0.025	0.016

Values of A_K, B_K, C_K, $Log_{10}(B_K/A_K)$, A_L, B_L and C_L fitted (using Eq. (17) and (18), respectively) from the experimental power spectra for each wind condition (except wind condition 0) are given in Table 6-3 for each of the three wind directions. Examples of fitted Eqs. (17) and (18) to the directional, experimental wind speed power spectra for wind condition 6 are shown in Fig. 6-8d – e. The t0wo models were generally able to fit all 30 directional power spectra well as is also indicated by Fig. 6-8.

6.4 Comparison of Experimental Approaches for Measuring Wind-Induced Gas Transport

Values of D_w for fraction 5, at wind conditions 2.1, 8.1 and 9 for both experiments A and B are shown in Fig. 6-9 where the D_w–z relations follow similar patterns for both types of experiments. There is a large D_w zone near the wind-exposed surface below which D_w decreases quite rapidly with depth to approximately zero. Maximum values of D_w are of the same order of magnitude in both types of experiments, however, the range of observed values is 3.5 times larger for experiment B than experiment A. For experiment A, the zone of large D_w values extends about 30% deeper on average than in experiment B (see Fig. 6-9).

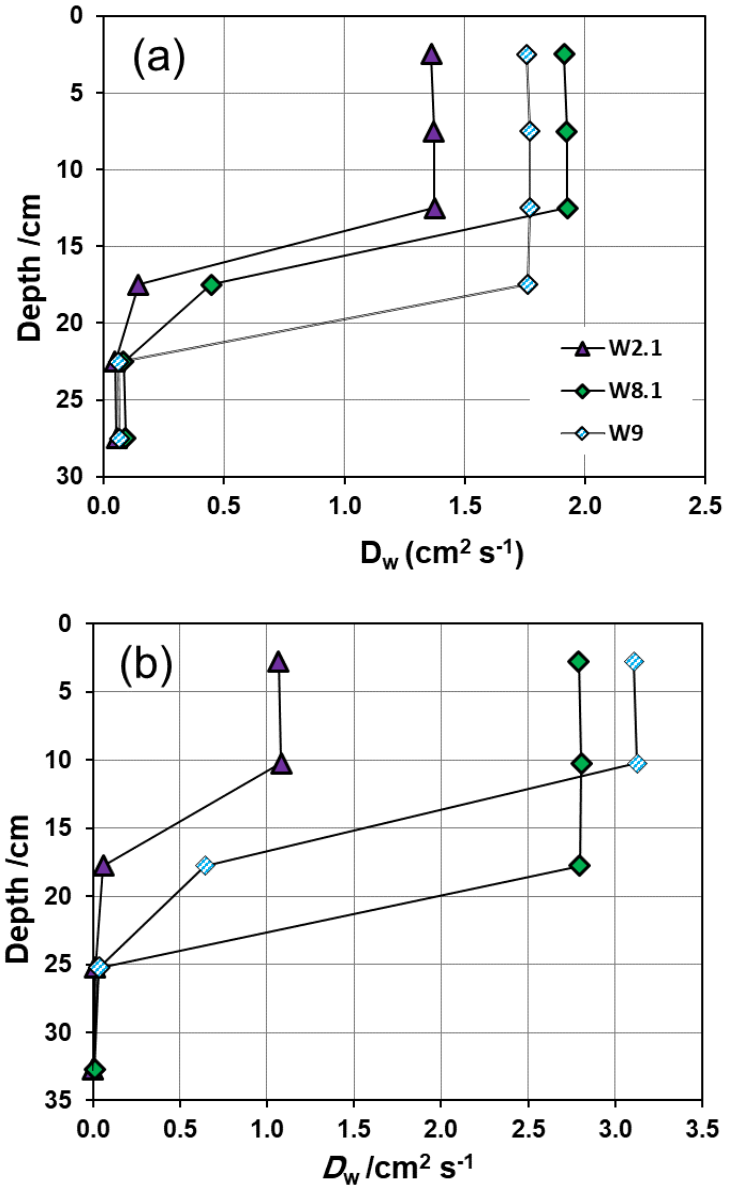

Fig. 6-9. Wind-induced dispersion coefficients (D_w) as a function of depth at wind conditions W2.1, W8.1 and W9 for: (a) Experiments type A and (b) Experiments type B.

These observations indicate that there is a difference between the two methods of measurement to represent wind-induced gas exchange. This is probably because the assumption that both the wind-induced gas transport and the value of D_w for a given

depth are independent of sample thickness is not completely correct, especially for samples that are less than approximately 10-cm thick for the material used in this study. A possible explanation is that for thin samples the effects of wind turbulence can penetrate through the sample and into the gas-filled space below. This means that the gas breakthrough curves measured at different depths during experiment A do not represent the transport conditions that would exist inside a continuous porous medium and fitted D_w values based on such data would therefore be incorrect. When D_w is measured close to the surface exposed to wind, we recommend that the samples used should be of sufficient thickness. The sensor should be installed at the desired location inside the sample (such as in experiment B) rather than use thinner samples with the sensor located at the bottom (such as in experiment A). Wind turbulence penetration is likely to be proportional to air permeability of the porous medium, K_a (Fukuda 1955), therefore values of D_w in porous materials with values of K_a smaller than those used here can probably be measured with thinner samples than we used without any loss of accuracy. For the experiments for fraction 2 to 5, method B is applied.

6.5 Relation between Wind-Induced Gas Transport and Distance to the Surface Exposed to Wind

Values of D_w as a function of depth measured during experiment B for wind conditions 1–10 are shown in Fig. 6-10. The average coefficient of variation (standard deviation divided by mean of the three replicates) across all data points in Fig. 6-10 is 1.24.

The D_w–z relations for all wind conditions show similar patterns; D_w is almost constant for z less than approximately10–15 cm. For $15 < z < 25$cm. values of D_w decrease relatively rapidly to near zero where they remain at larger depths. This is different from the results of earlier theoretical modelling studies (Fukuda 1955; Massmann *et al*. 1997; Poulsen *et al.* 2001; Poulsen *et al.*, 2011) that assumed an exponentially decreasing D_w–z relation. The results in Fig. 6-10 suggest, therefore, that assuming an exponential D_w–z relation when modelling wind-induced gas transport in porous media is possibly not completely correct. This is probably because earlier studies have assumed that wind velocities within the porous medium are one-dimensional and occur perpendicular to the surface exposed to wind only. Although net dispersive gas flux might still be represented as being one-dimensional, wind velocities are in reality likely to be multi-dimensional resulting in more complex D_w–z relations. Observed values of D_w in the upper 10–15 cm of the sample is between approximately 20 (for wind conditions 1–4) and 70 (for wind condition 10) times larger than D_m, which indicates that wind turbulence-induced gas transport in porous media under certain conditions can be more important than molecular diffusion.

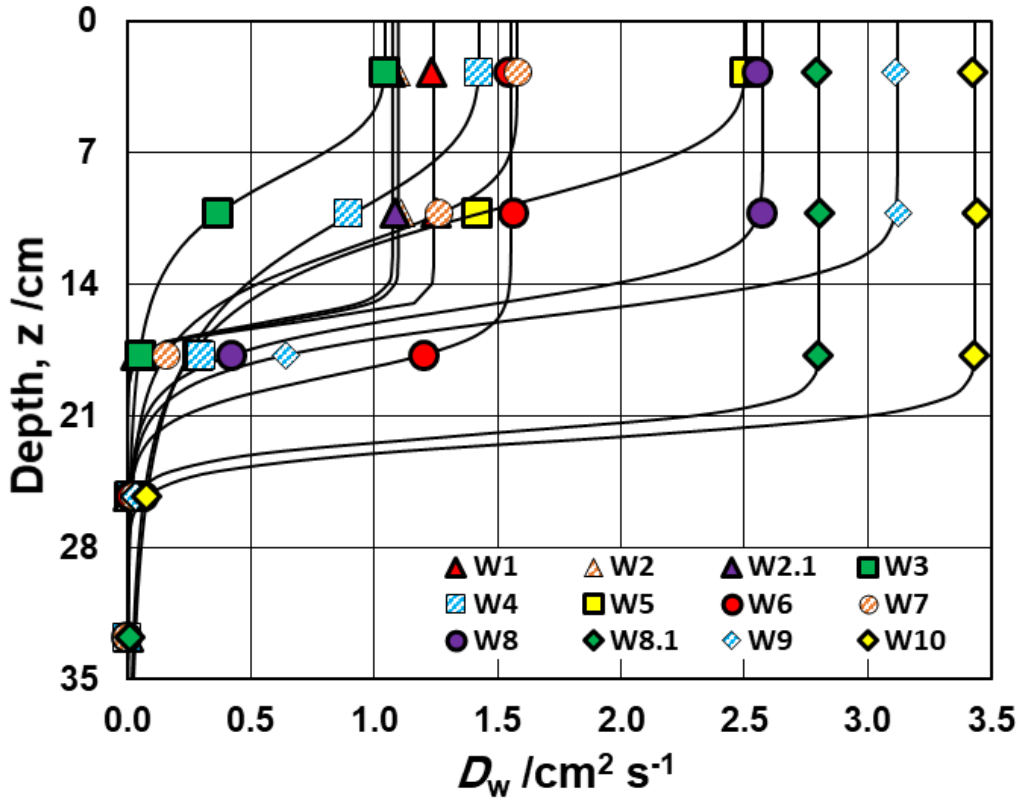

Fig. 6-10. Wind-induced dispersion coefficient, D_w, as a function of depth for wind conditions W1–W10. Symbols indicate D_w values measured during experiment B and curves are those that fitted best from model to the measured data.

Fig. 6-10 further indicates that there is a tendency for D_w to increase with increasing values of vertical, horizontal and total wind velocity together and wind turbulence (standard deviations are an indicator of the intensity of wind turbulence) although the tendency is not fully consistent.

Fig. 6-11 indicates that the relations between D_w and z follow the same general pattern regardless of wind condition. To model relations with this pattern, Poulsen *et al*. (2006) suggested an expression based on the van Genutchen (1980) expression for soil-water retention. With the D_w–z relation, this model takes the form:

$$\frac{D_w}{D_{w0}} = \frac{1}{\left(1+(\alpha z)^{\beta}\right)^{\left(1-\frac{1}{\beta}\right)}}, \tag{26}$$

where D_{w0} is the value of D_w at the surface of the porous medium and α and β are empirical constants. Best fitting curves for Eq. (26) to the D_w–z and the D_w/D_{w0}–z relations using the fitting approach described above with D_{w0}, α and β as fitting parameters are shown in Fig. 6-10 and Fig. 6-11, respectively. Measured values plotted against fitted values of D_w (with Eq. (26)) are shown in Fig. 6-12. Resulting values of D_{w0}, α and β are given in Table 6-4.

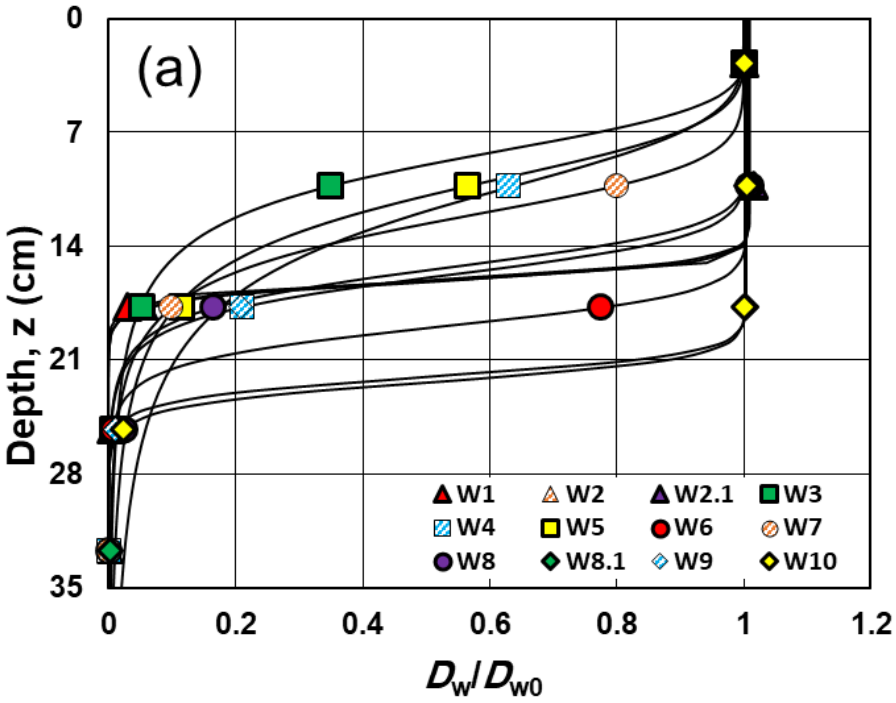

Fig. 6-11. D_w/D_{w0} as a function of depth for wind conditions 1–12. Symbols indicate experimental values and curves are fitted by Eq. (26) to the data

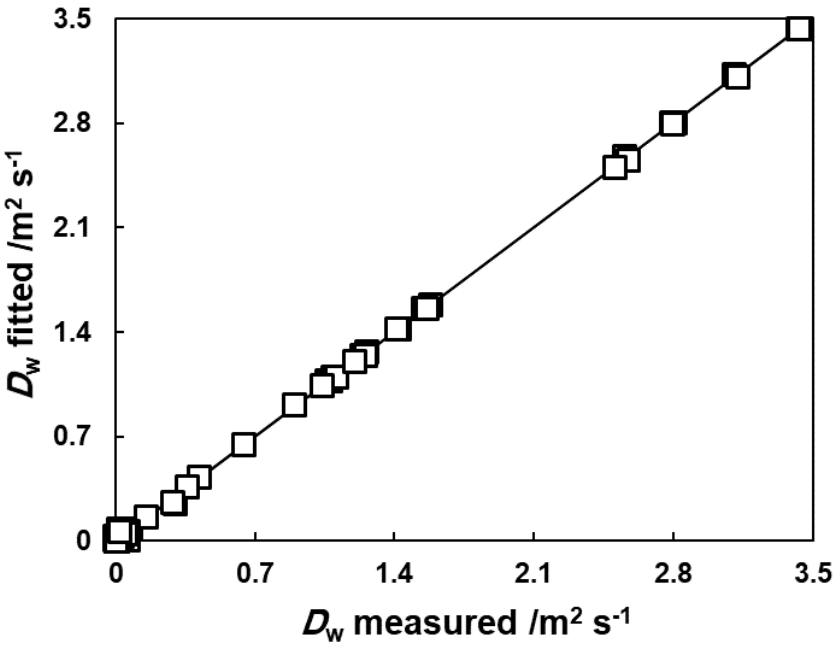

Fig. 6-12. Experimental values plotted against fitted values of D_w for wind conditions 1–10 for material 1.

Fig.s 6-11 and 6-12 show that Eq. 26 can fit the experimental D_w values closely, which indicates that it could potentially be used to represent the D_w–z relation for modelling wind-induced gas transport in porous media. The amount of experimental data used here is relatively small and is based on a single porous medium; therefore, more data from a larger set of porous media with a wider range of physical properties are needed to verify the applicability of Equation (26).

Table 6-4. Wind conditions used in the experiments in this study. V_z, V_x and V are near-surface vertical, horizontal and total wind speeds, respectively (average wind speed out and standard deviations in parentheses). The fitted values of D_{w0}, α and β from Equation (26) are also given.

Wind condition	D_{w0} /m^2 s^{-1}	α	β
W0	-	-	-
W1	1.24(0.01)	0.06	34.24
W2	1.10(0.05)	0.06	23.77
W2.1	1.07(0.01)	0.06	23.98
W3	1.04(0.02)	0.12	5.01
W4	1.42(0.03)	0.09	4.36
W5	2.51(0.04)	0.10	4.98
W6	1.55(0.01)	0.05	18.16
W7	1.58(0.07)	0.08	6.99
W8	2.57(0.06)	0.07	12.10
W8.1	2.80(0.07)	0.05	32.51
W9	3.12(0.12)	0.06	12.75
W10	3.43(0.03)	0.04	31.26

Fig. 6-13 shows the relations between α and V_z (Fig. 6-13a) and also α and β (Fig. 6-13b). V_z is average near-surface vertical wind speed. There is a weak inverse relation between α and V_z, which indicates that, α depends to some degree on wind conditions. Relations between α and other wind characteristics did not show any strong trends. There is a relatively strong inverse relation between α and β, which suggests further that β also depends on wind conditions. A direct correlation between β and wind

characteristics, however, did not reveal any strong trends, which suggests that this relation is possibly more complex.

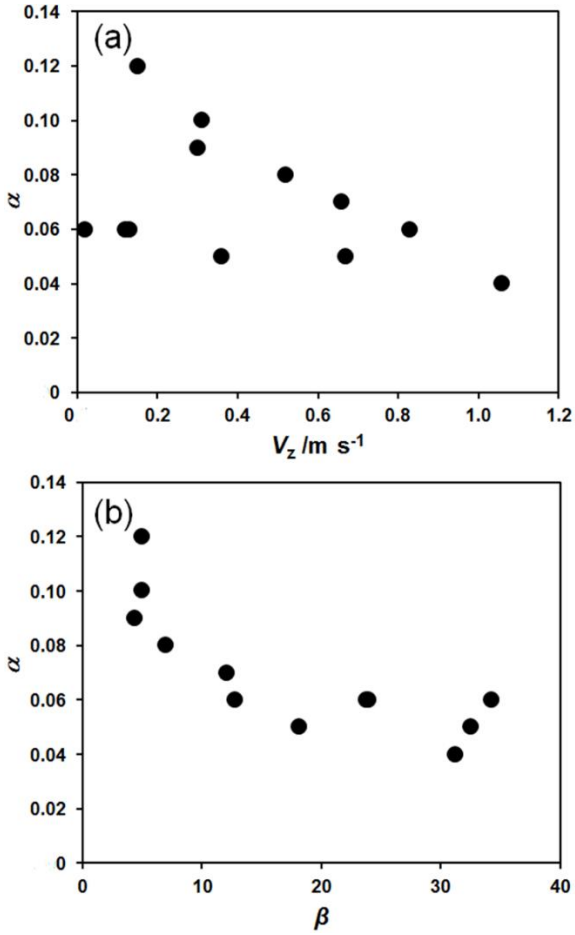

Fig. 6-13. (a) Relation between vertical component of wind (V_z) and empirical constant α and (b) relation between empirical constants α and β.

6.6 Relating pressure variations to wind speed and fluctuation

It was tried to relate wind-induced pressure variation to wind speed and hence to gas transport. A differential pressure sensor was used, having one end at the porous media surface, which is exposed to the wind, and one end at the calm state. The results show no connection between pressure variation and wind speed and turbulences. The reason

could be the very sensitive variation in pressure by any wind speed which caused in no-difference in the pressures for different wind speeds. To the knowledge of the author, there are other researches trying to find the relation between pressure variation and gas transport due to wind which encounter the same problem. Table 6-5 represents result of average pressure and standard deviation of the pressure for all the 11 wind speeds as below:

Table 6-5. Average measured differential pressure at the surface of porous media exposed to wind and the standard deviation, in order of increasing vertical wind.

Wind speed condition	Average measured pressure (Pa)	Standard deviation of pressure
W0	2.223222	1.066115
W1	3.147597	0.48153
W2	2.993649	0.14498
W3	2.925801	0.081859
W4	3.151974	0.123689
W5	3.230343	0.190957
W6	2.99387	0.100087
W7	3.159565	0.377638
W8	3.169223	0.337303
W9	3.151974	0.123689
W10	2.944346	0.100313

Fig. 6-14 shows how the variation of pressure and standard deviation of pressure is random and it cannot be related to a specific wind condition. The wind condition numbering is in order of increasing the wind speed and wind speed vertical component.

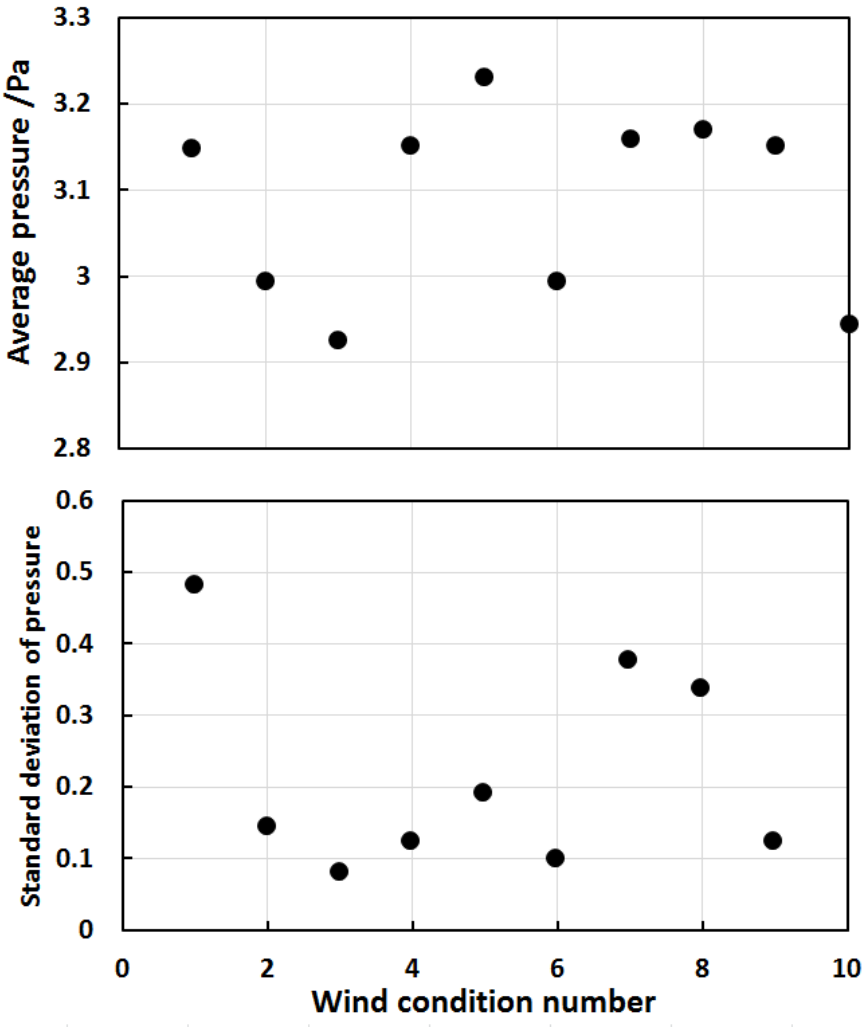

Fig. 6-14. Relation between wind condition and Average differential pressure (a) and standard deviation of pressure (b)

6.7 Linking Breakthrough Time with Basic Wind Speed Characteristics

Results for the statistical analyses of the correlation between $Log_{10}(t_{50})$ and parameters *V*, s and Log_{10}(CV) in the X, Y and Z directions showed that significant correlations (at

the 95% confidence level) existed for V_z, s_x, and $Log_{10}(CV_z)$ at almost all depths in the five materials. Correlations between $Log_{10}(t_{50})$ and V, s or $Log_{10}(CV)$ in the remaining directions (although present) were generally not significant. Results in terms of P-values for the statistical analyses based on the F – test, are presented in terms of relationships between $Log_{10}(t_{50})$ and wind speed characteristics V_z, s_x, and $Log_{10}(CV_z)$ in Table 6-7. r^2 are values for the correlations in parentheses which is known as the coefficient of determination as shows how data are close to the fitted regression line. (Closer value of r-squared to 1, means better fit of data).

Table 6-6. Results of statistical analyses in terms of p-value for assessment of the significance of correlations between Log_{10}(breakthrough time, t_{50}) and basic wind speed characteristics. Only wind speed characteristics for which correlations were generally significant at the 95% confidence level are included. Lines indicate best fit linear relationships to the data.

Medium	V_z ms^{-1}	s_x ms^{-1}	$Log_{10}(CV_z)$ -
1 (5.5 cm)	NS (0.04)	NS (0.05)	NS (0.02)
1 (13.0 cm)	<0.001 (0.78)	0.024 (0.49)	<0.001 (0.87)
1 (20.0 cm)	<0.001 (0.81)	0.005 (0.65)	<0.001 (0.77)
1 (28.0 cm)	<0.001 (0.86)	0.008 (0.61)	<0.001 (0.82)
1 (35.5 cm)	<0.001 (0.84)	0.007 (0.62)	<0.001 (0.80)
2 (4.0 cm)	NS (0.16)	0.014 (0.55)	NS (0.29)
2 (9.5 cm)	NS (0.33)	NS (0.13)	NS (0.34)
2 (15.0 cm)	0.005 (0.64)	0.007 (0.62)	0.001 (0.76)
2 (20.0 cm)	0.002 (0.73)	0.006 (0.64)	<0.001 (0.86)
2 (25.5 cm)	<0.001 (0.82)	0.004 (0.66)	<0.001 (0.81)
3 (3.1 cm)	0.010 (0.59)	0.006 (0.63)	<0.001 (0.80)
3 (7.3 cm)	0.003 (0.66)	0.042 (0.42)	0.002 (0.73)

Medium	V_z	s_x	$Log_{10}(CV_z)$
	ms^{-1}	ms^{-1}	-
3 (20.0 cm)	<0.001 (0.81)	0.006 (0.64)	<0.001 (0.84)
4 (3.1 cm)	NS (0.37)	NS (0.00)	NS (0.37)
4 (7.3 cm)	0.003 (0.69)	NS (0.37)	0.003 (0.69)
4 (11.5 cm)	0.008 (0.61)	0.011 (0.58)	0.004 (0.66)
4 (15.5 cm)	<0.001 (0.80)	0.002 (0.73)	<0.001 (0.79)
4 (20 cm)	<0.001 (0.94)	0.010 (0.59)	0.001 (0.76)

NS: Not significant, r^2 values for the correlations in parentheses.

The relationship between $Log_{10}(t_{50})$ and s_x appears somewhat weaker (higher p-values) compared to the remaining relationships in Table 6-6. That indicates when it comes to the basic wind speed characteristics (V, s and $Log_{10}(CV)$), the vertical (z) direction characteristics are perhaps the most important ones. Table 9 shows that two parameters in the z direction, V_z, and $Log_{10}(CV_z)$, exhibited significant correlation with $Log_{10}(t_{50})$ while only one parameter in the x direction (s_x) and none in the y direction). Because V_z, and $Log_{10}(CV_z)$ are also correlated, it is not possible, based on the data in Table 6-6, to explain which of the two parameters is the better descriptor of the physical mechanisms behind the wind induced gas exchange. The findings in Table 6-6, however, are in agreement with earlier findings of Poulsen and Sharma (2011).

Relationships between $Log_{10}(t_{50})$ and parameters V_z, s_x, and $Log_{10}(CV_z)$ are shown for material 3 in Fig. 6-15(a, b, c), respectively. The Fig. 6-15 shows that $Log_{10}(t_{50})$ decreases with increasing V_z and s_x, (Fig. 6-15a and 6-15b), indicating that, gas exchange tends to increase with increasing average wind speed and wind speed fluctuation magnitude. Fig. 6-14c shows $Log_{10}(t_{50})$ increases with $Log_{10}(CV_z)$ which

seems somewhat counter-intuitive (greater coefficient of variation means larger fluctuation magnitude). The reason here is that the largest values of $Log_{10}(CV_z)$ are observed for smaller values of V_z which means comparably less wind action which in turn results in longer breakthrough time. The above discussion of the vertical wind speed relationships also applied to most of the corresponding relationships for the x, y and z directions for the remaining materials including those relationships that were not significant (although for those relationships correlations were weaker).

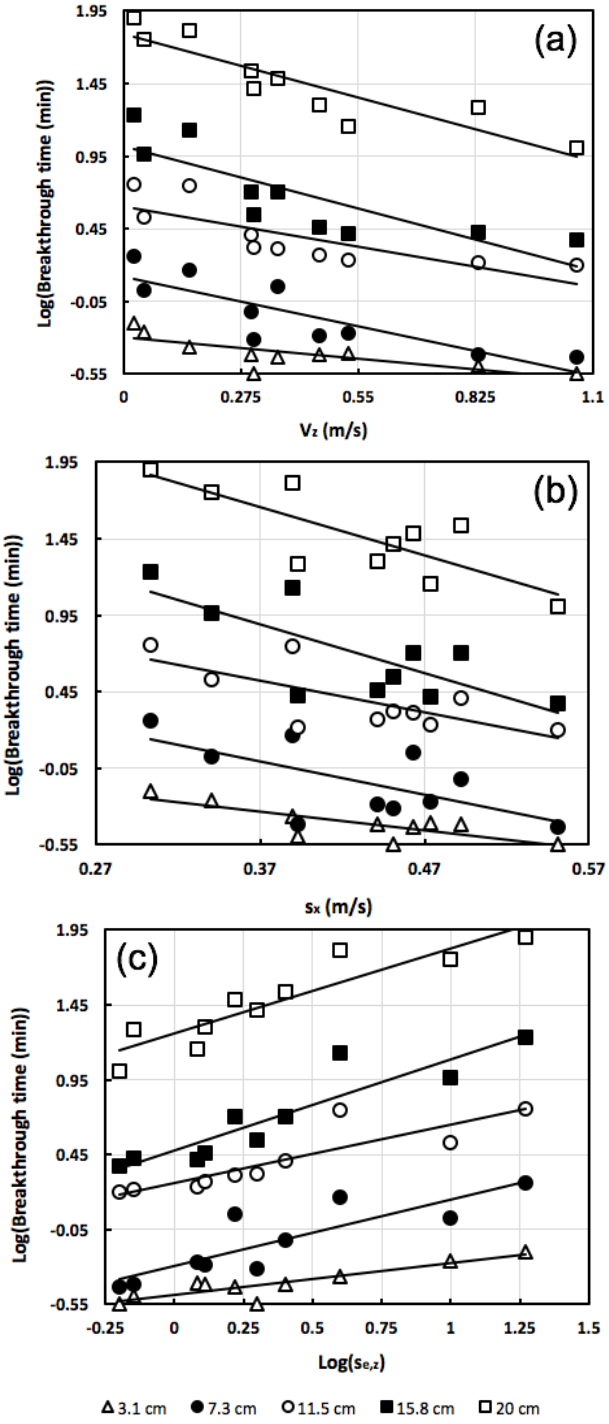

Fig. 6-15. Relationships between $\mathrm{Log}_{10}(t_{50})$ and basic wind speed characteristics: (a) average vertical wind speed V_z, (b) longitudinal, horizontal wind speed standard deviation s_x, and (c) Log_{10}(vertical wind speed coefficient of variation, CV_z) for different depths in material 3

6.8 Linking Breakthrough Time with Kaimal Power Spectrum Model Parameters

The statistical analyses for the correlation between $\text{Log}_{10}(t_{50})$ and the Kaimal model (Eq. (17)) parameters A_K, B_K, C_K, and $\text{Log}_{10}(B_K/A_K)$ showed that the correlation was statistically significant (at the 95% confidence level) at most depths in the four porous materials for parameters $A_{K,y}$, $\text{Log}_{10}(B_{K,y}/A_{K,y})$ and $\text{Log}_{10}(B_{K,z}/A_{K,z})$. The correlation with $\text{Log}_{10}(t_{50})$ for the remaining parameters and directions (although present) was generally not significant or only significant at very few depths. Specific results in terms of p-values for those relationships that were found generally significant are given in Table 6-7. The correlation between $\text{Log}_{10}(t_{50})$ and parameters $A_{K,y}$, $\text{Log}_{10}(B_{K,y}/A_{K,y})$ were generally somewhat weaker (higher p-values) compared to $\text{Log}_{10}(B_{K,z}/A_{K,z})$, indicating once more that z direction wind speed characteristics are perhaps the most important in controlling t_{50}.

Table 6-7. Results of statistical analyses in terms of p-value for assessment of the significance of correlations between Log_{10}(breakthrough time, t_{50}) and Kaimal wind speed power spectrum parameters. Only parameters for which correlations were generally significant at the 95% confidence level are included. Lines indicate best-fit linear relationships to the data.

Medium	$A_{K,y}$	$\text{Log}_{10}(A_{K,y}/B_{K,y})$	$\text{Log}_{10}(A_{K,z}/B_{K,z})$
1 (5.5 cm)	NS (0.13)	NS (0.02)	NS (0.03)
1 (13.0 cm)	0.002 (0.70)	0.005 (0.65)	<0.001 (0.91)
1 (20.0 cm)	<0.001 (0.83)	0.025 (0.49)	<0.001 (0.81)
1 (28.0 cm)	<0.001 (0.83)	0.018 (0.49)	<0.001 (0.87)
1 (35.5 cm)	<0.001 (0.84)	0.018 (0.52)	<0.001 (0.87)
2 (4.0 cm)	NS (0.28)	NS (0.12)	0.044 (0.42)

Medium	$A_{K,y}$	$\text{Log}_{10}(A_{K,y}/B_{K,y})$	$\text{Log}_{10}(A_{K,z}/B_{K,z})$
2 (9.5 cm)	NS (0.24)	NS (0.39)	0.035 (0.45)
2 (15.0 cm)	0.009 (0.59)	NS (0.39)	<0.001 (0.90)
2 (20.0 cm)	0.003 (0.68)	0.021 (0.51)	<0.001 (0.92)
2 (25.5 cm)	<0.001 (0.78)	0.027 (0.48)	<0.001 (0.90)
3 (3.1 cm)	0.007 (0.62)	0.003 (0.68)	0.005 (0.65)
3 (7.3 cm)	0.002 (0.73)	0.004 (0.67)	0.003 (0.68)
3 (11.5 cm)	0.010 (0.59)	0.010 (0.58)	<0.001 (0.87)
3 (15.8 cm)	0.002 (0.71)	0.006 (0.63)	<0.001 (0.89)
3 (20.0 cm)	<0.001 (0.85)	0.009 (0.60	<0.001 (0.91)
4 (3.1 cm)	<0.001 (0.83)	0.021 (0.51)	NS (0.28)
4 (7.3 cm)	0.005 (0.66)	NS (0.38)	0.005 (0.64)
4 (11.5 cm)	0.006 (0.63)	0.010 (0.58)	<0.001 (0.77)
4 (15.5 cm)	0.002 (0.72)	0.017 (0.53)	<0.001 (0.84)
4 (20 cm)	<0.001 (0.76)	0.014 (0.55)	0.001 (0.74)

NS: Not significant. r^2 values for the correlations in parentheses.

The parameter C_K represents as mentioned earlier, the energy in the wind speed fluctuations for fluctuation frequency approaching infinity. High frequency fluctuations will penetrate less depth into the porous medium than low-frequency fluctuations for the same energy level. The high-frequency fluctuations observed in this study further contains less energy relative to the low frequency fluctuations ($\text{Log}_{10}(f) < -0.75$). These two characteristics together likely explain the relatively poor relationships between C_K and $\text{Log}_{10}(t_{50})$ where no significant correlation was found in any of the three directions. A_K is only significantly correlated in the x direction and B_K is not significantly correlated for any direction. A possible reason why the individual A_K and B_K values do

not correlate well with $\mathrm{Log}_{10}(t_{50})$ is that the shape of the Kaimal model (Eq. (17)) depends less on the individual values of A_K and B_K values, but instead more on their ratio.

For the wind speed conditions applied in this study, B_K/A_K is especially important for controlling the Kaimal model shape in the low frequency range ($\mathrm{Log}_{10}(f) < -0.75$) as seen in Fig. 6-8d – e, where values of Φ increase rapidly with decreasing $\mathrm{Log}_{10}(f)$ while Φ at higher frequencies is generally controlled by C_K. This means that low frequency wind speed fluctuations in this case contain more energy (highest values of Φ) and therefore, will have a greater impact on gas transport and breakthrough time compared to higher frequency fluctuations.

Relationships between $\mathrm{Log}_{10}(t_{50})$ and parameters $A_{K,y}$ and $\mathrm{Log}_{10}(B_{K,z}/A_{K,z})$ for material 4 are shown in Fig. 6-16a and 6-16b, respectively. $\mathrm{Log}_{10}(t_{50})$ is inversely correlated with $A_{K,y}$, (Fig. 6-16a) but directly proportional to $\mathrm{Log}_{10}(B_{K,z}/A_{K,z})$ (Fig 6-16b).

This was also the case for most of the corresponding relationships for the remaining wind directions and porous materials including those that were not significant (although for those the correlation was weaker). The reason that $\mathrm{Log}_{10}(t_{50})$ to some degree decreases with increasing A_K is likely that for the wind speed conditions used in current study, A_K tends to be somewhat proportional to the magnitude of the spectral density (the energy) in the wind speed fluctuations at low frequencies. The reason why $\mathrm{Log}_{10}(t_{50})$ decreases with increasing $\mathrm{Log}_{10}(B_K/A_K)$ is likely that $\mathrm{Log}_{10}(B_K/A_K)$ for the wind conditions used in this study, is inversely related to the magnitude of the spectral

density in the low frequency range which has a proportionally larger impact on gas exchange.

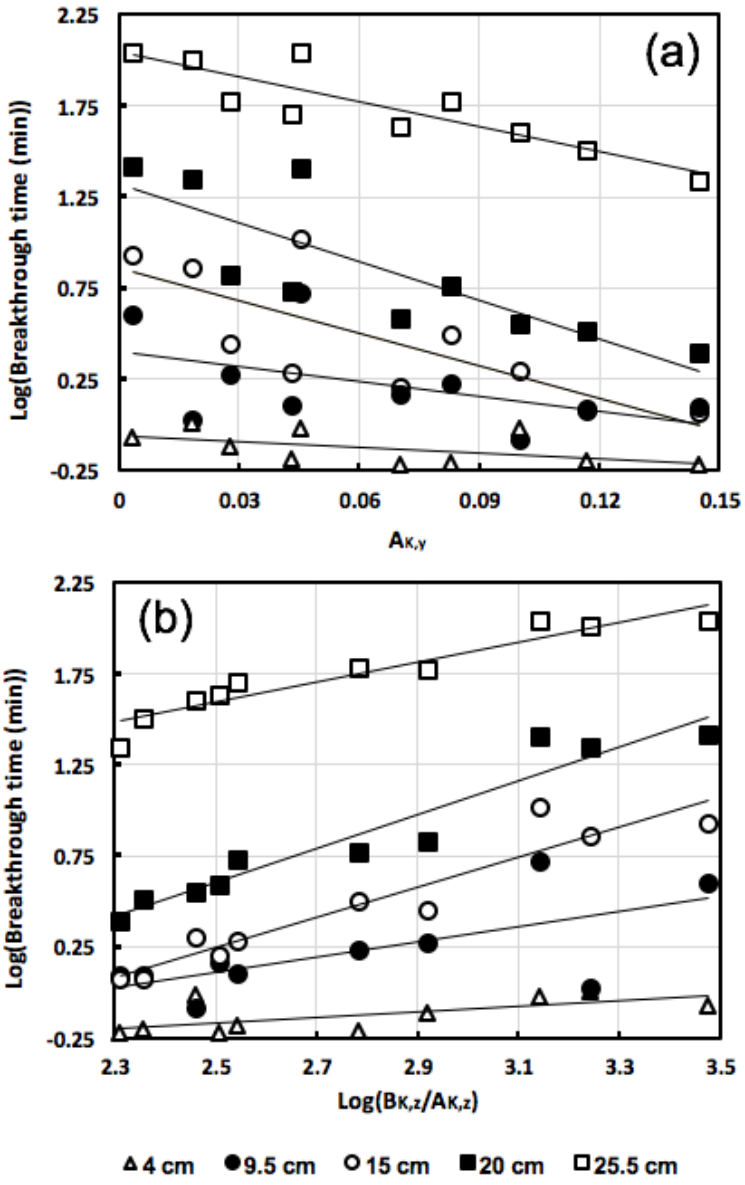

Fig. 6-16. Relationships between $\mathrm{Log}_{10}(t_{50})$ and Kaimal wind speed power spectrum model (Eq. (17)) parameters: (a) $A_{K,y}$, and (b) $\mathrm{Log}_{10}(B_{K,z}/A_{K,z})$ for different depths in material 4.

It is noted that as wind speed characteristics under natural wind conditions may be very different from those used in this study, the specific relationships (inverse or direct)

between the Kaimal power spectrum model parameters and breakthrough time under other wind conditions than used here may be different from what is observed here although correlation with breakthrough time will likely still be significant.

6.9 Linking Breakthrough Time with Linear Power Spectrum Model Parameters

The results of the statistical analyses for the correlation between $Log_{10}(t_{50})$ and the linear power spectrum model (Eq. (18)) parameters A_L, B_L, and C_L, in terms of p-values are shown in Table 6-8. Parameters $A_{L,y}$, $A_{L,z}$, $B_{L,y}$, $B_{L,z}$ and $C_{L,z}$, all showed statistically significant (at the 95% confidence level) correlation with $Log_{10}(t_{50})$ across all depths and porous materials while correlation for the remaining parameters (although present) was generally not significant. As in case of the basic wind speed characteristics (V, and $Log_{10}(CV)$) there was also a tendency for the z direction wind speed characteristics to appear somewhat more important in controlling gas exchange and breakthrough time (All three linear model parameters exhibit significant correlations in the z direction while only 2 parameters in the y direction and none in the x direction.

Table 6-8. Results of statistical analyses in terms of p-value for assessment of the significance of correlations between Log_{10}(breakthrough time, t_{50}) and linear wind speed power spectrum model parameters. Only parameters for which correlations were generally significant at the 95% confidence level are included. Lines indicate best-fit linear relationships to the data. {($A_{L,y}$ $Log_{10}(m^2\ s^{-2})(Log(Hz))^{-1}$, $A_{L,z}$ $Log_{10}(m^2s^{-2})(Log(Hz))^{-1}$}

Medium	$A_{L,y}$	$A_{L,z}$	$B_{L,y}$ $Log_{10}(m^2\ s^{-2})$	$B_{L,z}$ $Log_{10}(m^2\ s^{-2})$	$C_{L,z}$ $Log_{10}(m^2\ s^{-2})$
1 (5.5 cm)	NS (0.07)	NS (0.19)	NS (0.19)	NS (0.23)	NS (0.00)
1 (13.0 cm)	0.002 (0.71)	0.002 (0.74)	0.009 (0.59)	0.017 (0.53)	0.025 (0.49)
1 (20.0 cm)	0.001 (0.75)	0.001 (0.75)	0.001 (0.74)	0.004 (0.67)	0.004 (0.67)

Medium	$A_{L,y}$	$A_{L,z}$	$B_{L,y}$	$B_{L,z}$	$C_{L,z}$
1 (28.0 cm)	<0.001 (0.78)	<0.001 (0.79)	0.003 (0.68)	0.006 (0.63)	0.007 (0.62)
1 (35.5 cm)	<0.001 (0.77)	<0.001 (0.78)	0.004 (0.67)	0.007 (0.61)	0.005 (0.65)
2 (4.0 cm)	NS (0.22)	NS (0.25)	NS (0.15)	NS (0.18)	0.009 (0.59)
2 (9.5 cm)	NS (0.27	NS (0.32)	NS (0.18)	NS (0.20)	NS (0.12)
2 (15.0 cm)	0.014 (0.55)	0.003 (0.70)	0.031 (0.46)	0.015 (0.54)	0.005 (0.64)
2 (20.0 cm)	0.004 (0.66)	0.003 (0.70)	0.007 (0.62)	0.013 (0.56)	0.005 (0.65)
2 (25.5 cm)	0.001 (0.74)	0.002 (0.71)	0.010 (0.59)	0.017 (0.53)	0.002 (0.70)
3 (3.1 cm)	0.003 (0.68)	NS (0.41)	0.002 (0.70)	NS (0.34)	0.013 (0.56)
3 (7.3 cm)	0.001 (0.75)	0.016 (0.54)	<0.001 (0.84)	0.030 (0.47)	0.029 (0.47)
3 (11.5 cm)	0.009 (0.60)	0.006 (0.63)	0.017 (0.53)	0.026 (0.48)	0.019 (0.52)
3 (15.8 cm)	0.003 (0.70)	0.003 (0.69)	0.003 (0.70)	0.013 (0.56)	0.010 (0.59)
3 (20.0 cm)	<0.001 (0.81)	0.001 (0.75)	0.003 (0.68)	0.012 (0.56)	0.003 (0.68)
4 (3.1 cm)	0.039 (0.43)	NS (0.22)	0.038 (0.44)	NS (0.11)	NS (0.01)
4 (7.3 cm)	0.010 (0.58)	<0.001 (0.76)	<0.001 (0.78)	<0.001 (0.80)	NS (0.36)
4 (11.5 cm)	0.004 (0.66)	0.022 (0.50)	NS (0.33)	NS (0.26)	0.016 (0.54)
4 (15.5 cm)	0.001 (0.74)	0.018 (0.52)	0.019 (0.52)	NS (0.34)	<0.001 (0.76)
4 (20 cm)	<0.001 (0.80)	0.202 (0.50)	0.011 (0.58)	NS (0.32)	0.008 (0.61)

NS: Not significant, r^2 values for the correlations in parentheses.

The reason that both A_L and B_L are correlated with $Log_{10}(t_{50})$ in the y and z directions is likely that A_L B_L are mutually correlated for each of the two directions. The B_L – $Log_{10}(t_{50})$ correlations are weaker than for the corresponding A_L – $Log_{10}(t_{50})$ relationships, suggesting that A_L is the more important parameter when it comes to predicting t_{50}.

Fig. 6-17 shows the relationships between $Log_{10}(t_{50})$ and parameters $A_{L,z}$, $B_{L,z}$, $C_{L,z}$ for material 5. $Log_{10}(t_{50})$ generally increases with both $A_{L,z}$ (Fig. 6-17a) and $B_{L,z}$ (Fig. 6-17b) while $Log_{10}(t_{50})$ decreases with $C_{L,z}$ (Fig. 6-17c). This was also observed for most

of the corresponding parameters for the other materials and wind directions including those for whom correlation was not significant (those relationships were weaker). The reason for the positive correlation between Log_{10} (t_{50}) and A_L is that A_L is always negative and larger negative values of A_L are associated with increasing magnitude of the power spectral density in the low wind speed fluctuation frequency range where wind impact on gas transport is greater. The parameter B_L was generally positively correlated with A_L (which explains why $Log_{10}(t_{50})$ and B_L are also positively correlated) but decreases with $C_{L,z}$. The reason is likely that although the magnitude of the high-frequency wind speed fluctuations (represented by C_L) are less important compared to low frequencies, an increase in the energy level for the high frequency wind speed fluctuations will still to some degree increase gas exchange and reduce breakthrough time. The linear power spectrum model parameter $C_{L,z}$ correlations is significant in contrast to the Kaimal power spectrum model (Eq.(18)) where none of the three C parameters had significant correlations. It is likely that C_L is independent of A_L and B_L (C_L is calculated separately as an average of power spectral density at $Log_{10}(f) > -0.75$) while C_K to some degree depends on A_K and B_K as all three Kaimal model parameters are fitted simultaneously.

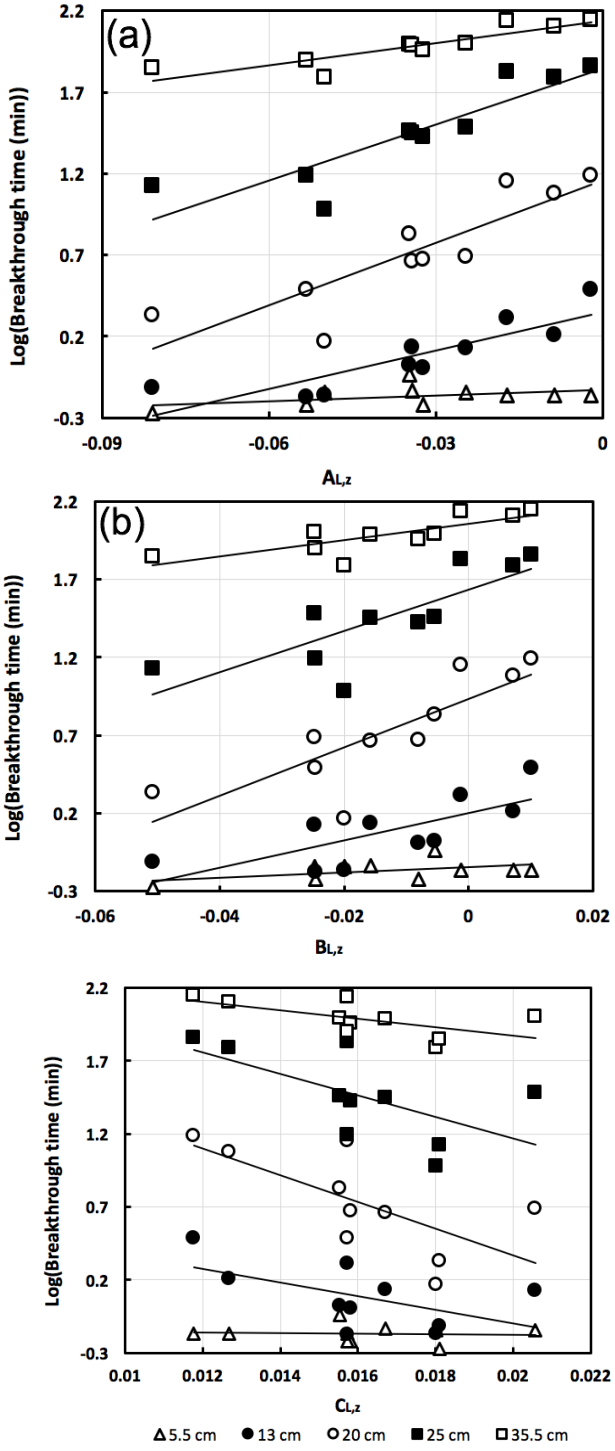

Fig. 6-17. Relationships between $Log_{10}(t_{50})$ and Linear wind speed power spectrum model (Eq. (18)) parameters: (a) $A_{L,z}$, (b) $B_{L,z}$, and (c) $C_{L,z}$ for different depths in material 1.

6.10 Penetration depth and normalized dispersion coefficient slope

The penetration depth (Zp) is defined by

$$Z(x) = \frac{\left(\left(\frac{1}{x}\right)^{\left[\frac{1}{1-\left(\frac{1}{\beta}\right)}\right]} - 1 \right)^{\left[\frac{1}{\beta}\right]}}{\alpha}, \tag{27}$$

where x is the relative D_{w0} fraction. α and β are empirical factors. For Z = Zp, x=0.5.

The relationships between total diffusion-dispersion coefficient (D_{tot}), wind induced dispersion coefficient (D_w), wind induced dispersion coefficient at the wind exposed surface (D_{w0}), depth (Z), and penetration depth (Z_p) are illustrated in Fig. 6-18.

It is observed that the penetration depth is decreasing with reduced grain size, hence fraction 1 has the highest average penetration depth equal to 16.55 cm and fraction 5 has the lowest one, equal to 7.03cm.

The depth of penetration for all porous media is shown in Table 6-9. It was observed by reducing the grain size of the sample, depth of penetration of wind is also decreased. For the 5th fraction, which is the finest sample, the lowest depth of penetration has been achieved. This is compatible with the results where the wind induced dispersion coefficient is almost zero. The same relation holds between the grain size of sample and the dispersion coefficient at its surface.

The relative normalized dispersion coefficient slope (S) is defined at the depth of penetration Zp as

$$S = \frac{Z(x = 0.75) - Z(x = 0.25)}{Zp}. \quad (28)$$

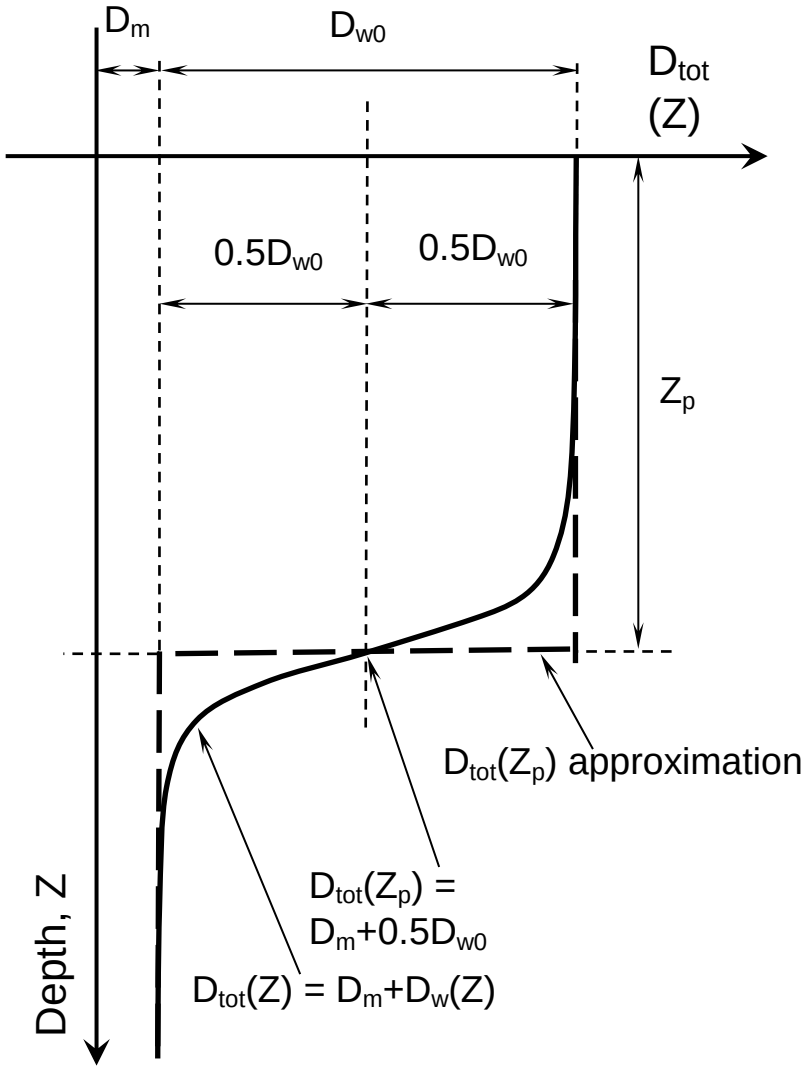

Fig. 6-18. Schematic of the relationships between total diffusion-dispersion coefficient (D_{tot}), wind induced dispersion coefficient (D_w), wind induced dispersion coefficient at the wind exposed surface (D_{w0}), depth (Z), and penetration depth (Z_p)

Table 6-9. Fitted values of model parameters D_{w0}, α and β and calculated penetration depth (Z_{50}, Eq. (27)) for the five porous materials used in this study.

	Medium 1				Medium 2				Medium 3				Medium 4				Medium 5			
	D_{w0} cm^2/s	α	β	Z_{50} cm	D_{w0} cm^2/s	α	β	Z_{50} cm	D_{w0} cm^2/s	α	β	Z_{50} cm	D_{w0} cm^2/s	α	β	Z_{50} cm	D_{w0} cm^2/s	α	β	Z_{50} cm
W1	0.96	0.085	14.2	12.4	0.23	0.068	126	14.9	0.35	0.111	8.51	9.88	0.014	0.142	197	7.07	0	0.10	50.02	10.3
W2	1.42	0.056	60.6	18.1	0.90	0.057	129	17.6	0.61	0.082	13.2	12.9	0.052	0.143	237	7.01	0	0.17	49.68	5.9
W3	1.53	0.057	40.4	17.9	1.14	0.057	54.9	17.8	0.51	0.067	71.5	15.1	0.052	0.145	51	6.99	0	0.15	163.34	6.4
W4	3.24	0.045	60.0	22.5	1.66	0.057	18.4	18.3	1.36	0.060	78.8	16.8	0.150	0.099	99	10.2	0	0.15	163.33	6.4
W5	1.22	0.065	163	15.5	0.24	0.065	401	15.4	0.37	0.079	57.8	12.8	0.016	0.117	119	8.60	0	0.16	163.33	6.4
W6	0.80	0.075	27.9	13.7	0.27	0.072	69.6	14.0	0.29	0.110	11.8	9.69	0.010	0.118	186	8.51	0	0.15	163.33	6.4
W7	1.60	0.056	54.3	18.1	0.80	0.057	212	17.6	0.67	0.068	48.3	14.9	0.049	0.112	165	8.97	0	0.15	163.33	6.4
W8	2.69	0.060	14.4	17.6	1.70	0.067	13.5	15.8	1.15	0.061	88.2	16.5	0.070	0.132	13.0	8.03	0	0.15	163.33	6.4
W9	1.73	0.064	17.8	16.3	1.34	0.054	258	18.6	0.78	0.067	31.5	15.3	0.046	0.113	17.9	9.22	0	0.15	163.33	6.4
W10	2.56	0.060	16.9	17.4	1.12	0.054	67.1	18.7	1.40	0.115	6.18	9.94	0.146	0.146	60.6	6.93	0	0.15	163.33	6.4

In Eq. 26 both part, like any other equation needs to have same dimensions. Since the left side of the equation is dimensionless, and in the right side, depth with dimension of length exist, therefore, right side needs to be investigated for determining dimensions of experimental parameters α and β.

The penetration depth and the relative normalized dispersion coefficient slope at penetration depth are plotted as a function of $1/\alpha$ and $1/\beta$ in Figs. 6-18a, b. The results in Fig. 6-18a represent a linear relation between the penetration depth and the inverse of α for all the fractions which means that the penetration depth is mainly based on parameter α, whereas no relation can be found in Fig. 6-18b, between penetration depth and β. The relation between the relative normalized dispersion coefficients at penetration depth is found to be the opposite. It can be seen that there is no specific relation between S at Zp and $1/\alpha$, however a linear relation with $1/\beta$ can be observed in Figs. 6-19c, d.

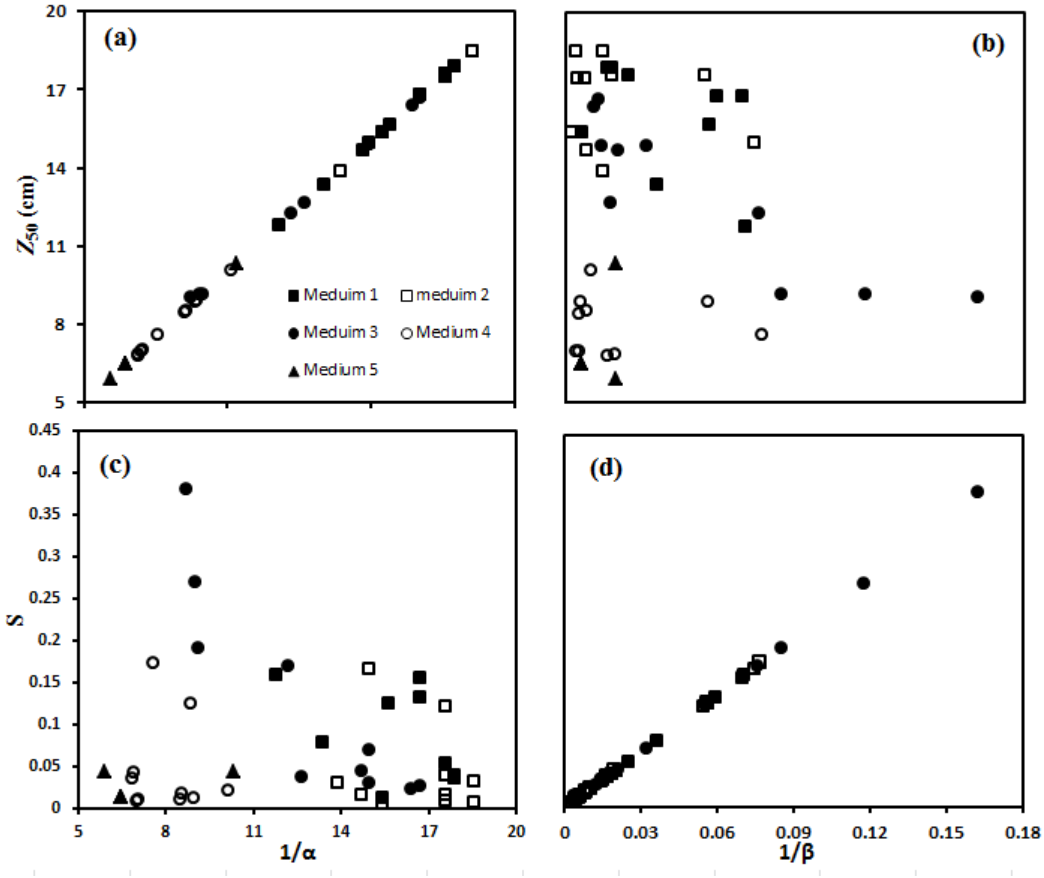

Fig. 6-19. Penetration depth (Z_{50}) as a function of 1/α and 1/β (a, b) and relative normalized dispersion coefficient slope (S) at Z_p as a function of 1/α and 1/β (c, d).

The results of Fig. 6-19 show that α has the dimension of inverse of length (L^{-1}) and β is dimensionless. The results match well with the equation 26 and can make left side of that equation dimensionless, similar to the left side and satisfy the dimension analysis. These results suggest, that α may be regarded as the inverse of the depth of penetration for wind action, while for constant α (and z_p) β controls the slope of the $D_w(z)$ relationship at $z = z_p$.

6.11 Linking model parameters with wind speed characteristics and particle properties

The relation between calculated values of model parameters and wind speed characteristics is being investigated. It includes simple wind speed characteristics and power spectrum values of wind by Kaimal model and linear model. Fig. 6-20a shows the relation between the mean value of the vertical component of wind, V_z, and D_{w0}. Fig. 6-20b,c shows the relation between two horizontal wind components V_x & V_y and D_{w0}. It is evident that the vertical wind speed has a direct impact on the wind induced dispersion coefficient at the surface of media 1, 2 and 3, however the effect is diminished for medium 4, whereas for medium 5 is negligible. That's becasue of the very fine particle size and narrower paths for the air to pass through it. Although the effect of horizontal wind components for two fine fractions is also very low, unlike V_z, there is no direct relation between them and D_{w0}. Wind characteristics could affect the gas transport speed and penetration depth inside porous media for particle sizes above 1mm. For finer porous media, the effect of wind was found to be low. At particle size below 0.5 mm

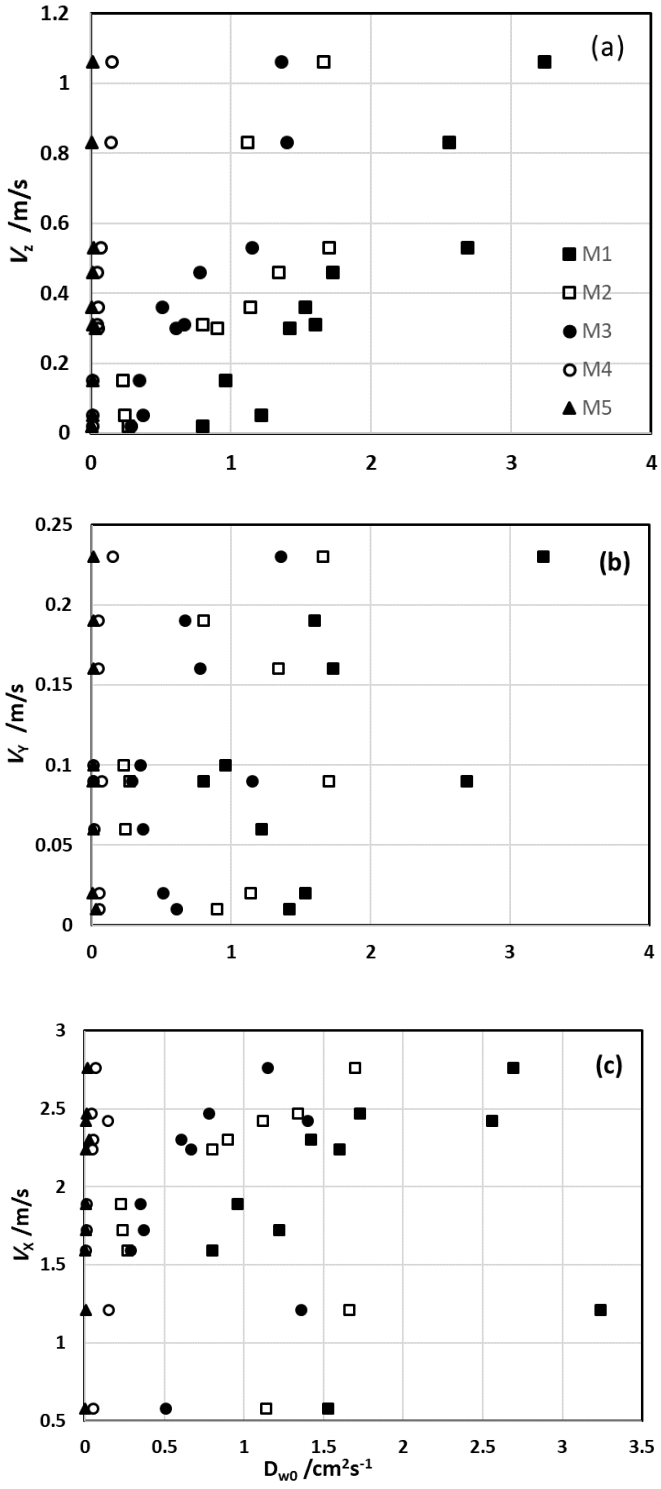

Fig. 6-20. (a) Relation between Vertical component of wind speed (u), (b) Horizontal components (v, w) and dispersion coefficient at surface of porous media (D_{w0})

The relation between the vertical wind speed and its standard deviation which is indicative of the wind fluctuations in that direction, and the depth of penetration, Dp. The relation between the standard deviation of the vertical wind and wind induced dispersion coefficient cannot be proven for any of the porous media fractions. Results can be seen in Fig. 6-21a, b

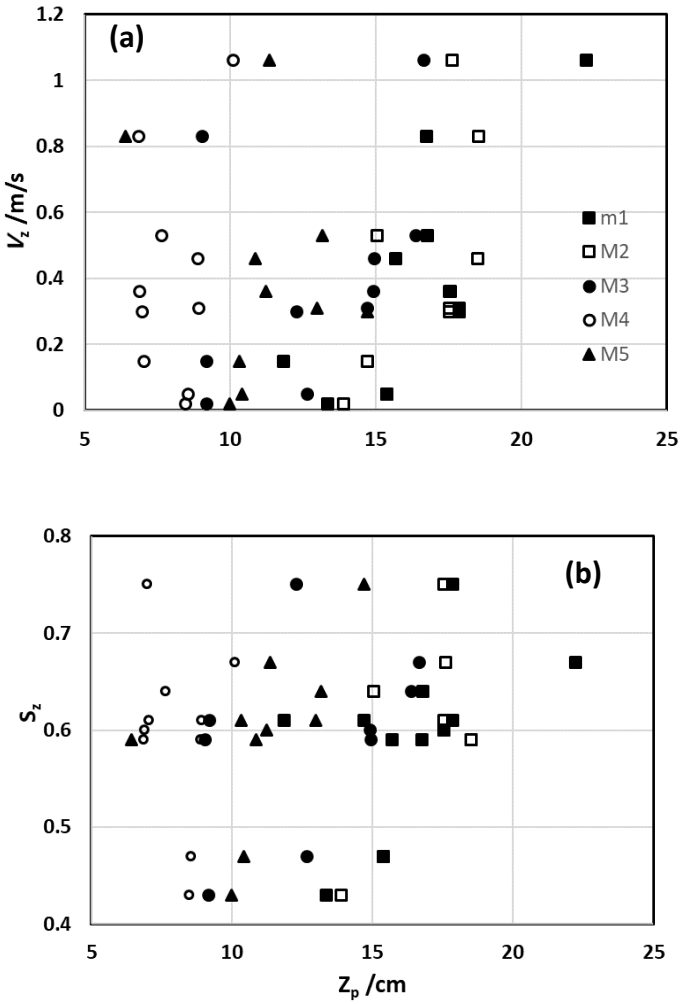

Fig. 6-21. (a) Relation between penetration depth and vertical wind speed and (b) its standard deviation.

The model parameters α and β have shown some significant correlations with different wind speed characteristics. For example, the correlation between α and S_x, S_y, V_z, log (S_z/V_z) and $\log(B_{k,z}/A_{k,z})$ for medium 1 is significant and there was no other significant correlation between α and other wind characteristics. The number of significant correlations between α and various wind characteristics is reduced with decreasing grain size of the porous medium. For media 4 and 5 there is no correlation between α and any wind characteristics. On the other hand, the number of significant correlations between β and wind characteristics, which is zero for media 1 and 2, is increasing to one significant relation in medium 3, two in medium 4 and one for medium 5. The behaviour of Zp is similar to α where the number of significant correlations between penetration depth and different wind characteristics is decreasing by reducing the grain size of the medium.

The depth of penetration for wind induced dispersion z_s is introduced and then D_{ws} is defined as an effective, constant, near-surface wind-induced dispersion coefficient valid for $z \leq z_s$.

Relationship between wind-induced dispersion model parameters and power spectrum wind speed characteristics is also investigated. Relationships between dispersion model parameters, D_{w0}, α, β, D_{ws} and z_s and wind speed characteristics, V, s, T, A_K, B_K, C_K, Log(A_K/B_K), A_L, B_L, C_L, in all three spatial directions (x, y, z) for all four porous media, were generally best described by linear functions. Statistical significance of the slope being different from zero (p) and regression coefficient (r^2), were determined for all 600 combinations of dispersion model parameter, wind speed characteristic, spatial direction

and porous medium. Values of p and r^2 for the combinations of dispersion model parameter, wind speed characteristic and spatial direction, that were significant at the 98% level ($p \leq 0.02$) for all four porous media, or at the 99% level ($p \leq 0.01$) for at least three out of the four porous media are summarized in Table 6-10. Selected relationships from Table 6-10 are plotted in Fig. 6-22.

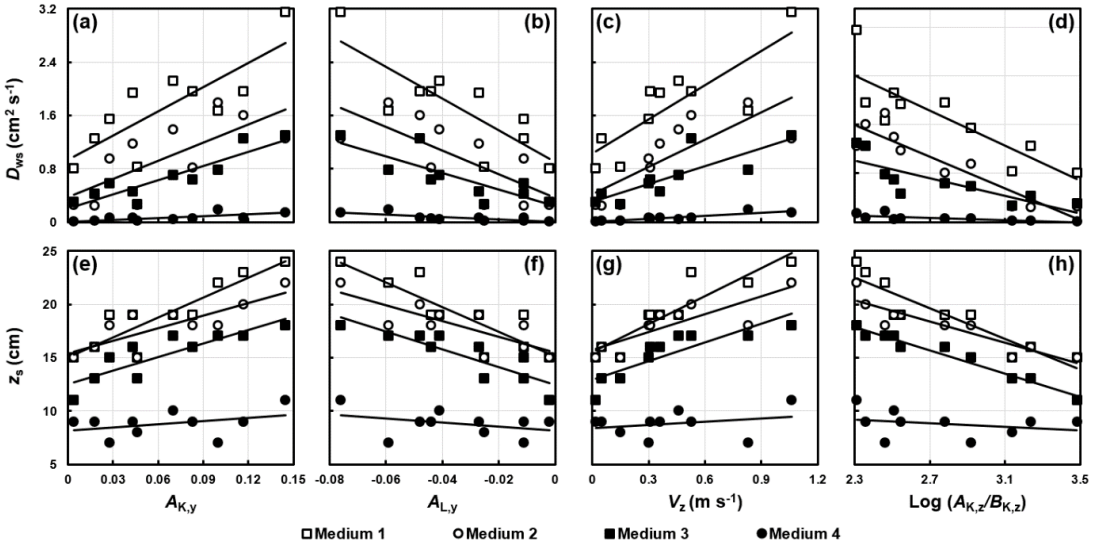

6-22. Selected relationships between model parameters (D_{w0}, D_{ws} and z_s) and wind speed characteristics across the four porous materials. Symbols indicate experimental data and lines are best fit linear relationships to the data.

Table 6-10. . Strength of linear correlation between model parameters (D_{w0}, D_{ws} and z_s) and wind speed characteristics. Only parameter combinations that exhibited significant correlation at the 98 % level for all four materials or at the 99% level for at least three materials are included. For each parameter combination, the first row of values represent the significance level p (in %) and the second row represent r^2.

Parameter	D_{w0}				D_{ws}				z_s			
Medium	1	2	3	4	1	2	3	4	1	2	3	4
$A_{k,y}$	<0.1	0.4	<0.1	0.4	0.5	<0.1	1.7	1.4	<0.1	0.4	0.2	29
	0.88	0.72	0.80	0.68	0.65	0.53	0.82	0.55	0.81	0.66	0.73	0.14
$A_{L,y}$	<0.1	0.9	<0.1	0.1	0.4	0.4	1.7	0.5	0.1	0.7	0.1	29
	0.82	0.74	0.79	0.75	0.66	0.53	0.67	0.64	0.73	0.61	0.74	0.14
$B_{L,y}$	0.5	2.4	0.1	0.8								
	0.65	0.62	0.72	0.62								
V_z	<0.1	0.4	<0.1	<0.1	0.3	0.3	0.6	0.1	<0.1	0.3	0.1	45
	0.89	0.90	0.89	0.84	0.69	0.63	0.69	0.94	0.82	0.70	0.73	0.07
$\mathrm{Log}_{10}(B_{k,z}/A_{k,z})$	0.1	<0.1	0.2	1.8	0.2	0.4	<0.1	0.9	<0.1	<0.1	<0.1	45
	0.76	0.84	0.70	0.60	0.71	0.84	0.70	0.60	0.84	0.82	0.96	0.07
$A_{L,z}$	0.1	0.1	0.2	4.6					<0.1	1.0	0.3	78
	0.74	0.71	0.70	0.46					0.81	0.59	0.68	0.11

Dispersion model parameters did generally not show any significant (95% level) correlation with wind speed characteristics in the *x*-direction. It may be speculated, that a larger sample dimension in the *x* direction may increase the importance of the *x*-direction wind speed characteristics, however, additional experiments are needed to verify if this is the case. Experimental parameters α and β did generally not correlate significantly (95% level) with any of the wind speed characteristics except in a few cases for material 1. Remaining dispersion model parameters D_{w0}, D_{ws} and z_s, correlated best with wind speed power spectrum characteristics (Table 6-10), although strong correlation was also found with V_z. Correlations were generally strongest for material 1 and weakest for material 4, likely because the slopes of the relationships were lowest for material 4 (Fig. 6-22).

Results of statistical analysis of correlation between D_{w0} and most of wind characteristics, including basic wind characteristics like V_y, Kaimal wind characteristics such as $A_{k,y}$ and Linear wind characteristics such as $B_{l,z}$ showed that significant correlations (at the 95% confidence level) existed for all medium size fractions. Results in terms of p-values for statistical analysis for relation between some of wind speed characteristics including basic, Kaimal and linear characteristics and empirical parameters α, β, D_{w0} and Z_p are presented in Table 6-11.

Table 6-11. Resulting p-values for significance of correlation between model parameters (D_{w0}, α, β and Z_{50}) and wind speed characteristics. Only parameters where at least one combination exhibited significant correlation at the 95% level are included in the table. Values are in percentages.

Parameter	Medium 1			Medium 2			Medium 3			Medium 4		Medium 5
	D_{w0} cm^2/s	α	z_{50} cm	D_{w0} cm^2/s	α	z_{50} cm	D_{w0} cm^2/s	α	β	z_{50}	D_{w0} cm^2/s	β	β
s_x	3.3	1.2	0.3	0.6	-	4.0	-	2.3	-	0.9	-	-	-
V_y	-	-	-	-	-	-	3.9	-	-	-	2.6	-	-
S_y	3.5	1.7	0.2	1.8	-	-	-	2.8	4.1	1.1	-	-	3.4
$A_{k,y}$	<0.1	-	2.3	0.4	-	-	<0.1	-	-	-	0.4	-	-
$Log_{10}(B_{k,x}/A_{k,x})$	<0.1	-	-	-	4.7	2.8	1.2	-	-	-	1.8	-	-
$A_{L,y}$	<0.1	-	2.5	0.9	-	4.8	<0.1	-	-	-	0.1	-	-
$B_{L,y}$	0.5	-	-	2.4	-	4.0	0.1	-	-	-	0.8	-	-
V_z	<0.1	2.9	0.6	0.4	-	2.1	<0.1	-	-	-	<0.1	-	-
$Log_{10}(S_z/V_z)$	0.8	3.5	3.0	3.3	3.0	1.8	1.4	-	-	-	2.0	-	-
$Log_{10}(B_{k,z}/A_{k,z})$	0.1	2.6	1.4	<0.1	3.4	0.9	0.2	-	-	2.9	0.9	1.9	-
$A_{L,z}$	0.1	-	-	0.1	-	-	0.2	-	-	-	3.0	4.0	-
$B_{L,z}$	1.6	-	-	1.0	-	-	1.4	-	-	-	-	-	-

Fig. 6-20 and 6-21 showed the relation between wind characteristics and model parameters for five fractions of materials, therefore it is shown how changing in particle size affects the relations. For example, in Fig. 6-23(a) it can be seen how the decrease in particle size, decrease the impact of wind on gas transport for a specific wind speed. It was tried to find relation between other particle parameters roughness and roundness, particle size with model parameters. That can be seen in Fig. 6-23. The relation between average values of D_{w0} for 5 fractions is plotted versus average amount of roughness, roundness, gas permeability and particle size.

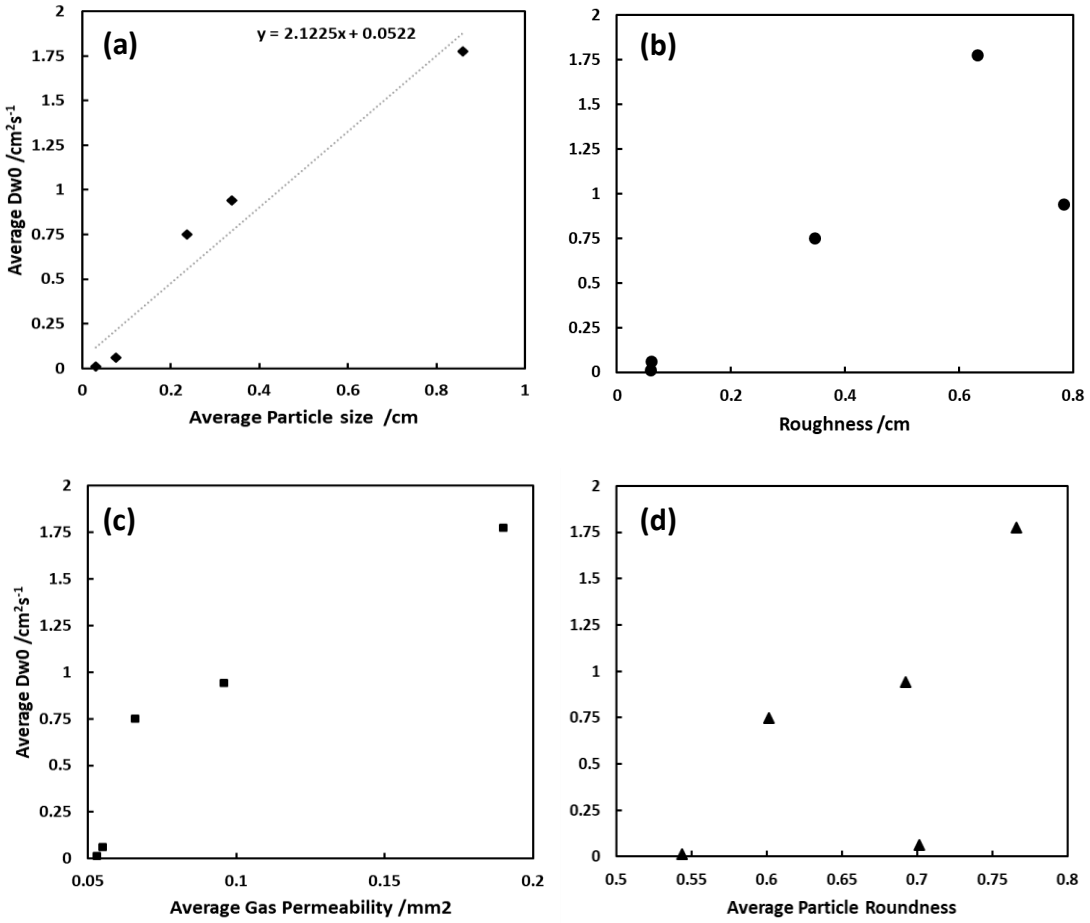

Fig. 6-23. Relating average D_{w0} for each fraction with particle properties, consist of (a) average particle size, (b) roughness, (c) gas permeability and (d) particle roundness.

The only relation that could be found was between average D_{W0} and average particle size of the fraction. (Fig. 6-23 a) According to that, there is a linear relation which shows how by increasing average size of particle, average value of D_{W0} increases

6.12 Comparison of accuracy of two analyses approaches

The described approach was to calculate the wind induced dispersion coefficient at each of the depths that an oxygen sensor is placed. This was done by fitting experimental and modelled data of oxygen concentration. Subsequently, the three parameters of Eq. 26 (α, β and D_{w0}) were calculated using the obtained dispersion coefficients. In addition to that, in this research the empirical parameters were calculated by incorporating them directly in the model and obtaining them by fitting the measured and modelling values of oxygen concentration. To compare the efficiency and accuracy of each approach, the value of SSE and RMSE was calculated using Eq.s 19 and 23 respectively, for each of the fraction wind condition. The average value of RMSE for the previously used approach is equal to 0.074 (dimensionless), whereas for the direct-fitting approach is equal to 0.007. This indicates that the new approach of direct fitting is more accurate due to the reduction of the RMSE value by an order of magnitude.

Indirect fitting approach is the one that fitting between modelled data of oxygen concentration and measured one is done by changing the five D_w values at location of five sensors in the model. Later, Eq. 26 is used for fitting the experimental parameters, α, β and D_{w0}. The direct approach fits the modelled and measured values by directly changing the experimental parameters.

CONCLUSIONS

Primary aim of this research was to measure effect of wind turbulences on the variation in gas concentration of the porous medium at different depths from the surface exposed to wind, and to use these measurements for determining D_w as a function of distance to the surface exposed to wind. This research also aimed to investigate the links between wind-induced gas transport inside porous media, wind speed characteristics (average wind speed, wind speed variability, wind direction) and porous medium physical properties (particle size, air permeability, hydraulic conductivity, porosity, etc.). Investigations were based on measurements made by experimental study in laboratory which then were fitted to the modelled data, calculated by finite difference method. Main conclusions of the research are listed below:

- The results of numerical and experimental showed that wind turbulence can potentially have a considerable effect on gas dispersion in the porous medium and on gas exchange between the medium and the atmosphere. For the wind conditions considered in this study, gas dispersion was 20–100 times greater than for calm conditions (molecular diffusion only) near the surface of the porous medium exposed to wind. In addition, it was observed that although wind turbulence affects gas dispersion close to the surface exposed to wind only (in this case 20 cm into the medium), it can have effects on the variation in gas concentration at higher depths.
- The results indicated further that measurements with thicker samples and with multiple gas sensors placed inside the sample are more reliable than for a series

of thinner samples with the gas sensor placed at the bottom. Measurements with deeper samples equipped with multiple gas sensors are also much more rapid to carry out, therefore, it is suggested that, this approach should be adopted for the measurement of wind turbulence-induced gas transport.

- Analysis of a large set of experimental gas transport data across different wind conditions and five different porous media showed that wind induced gas exchange between porous media and the atmosphere at the medium surface is strongly dependent on the wind speed characteristics and also particle size and properties of the porous media. Gas exchange, as quantified by the tracer gas breakthrough time corresponding to 50% of the maximum steady state surface tracer gas concentration at different depths inside the porous media, was significantly correlated with basic wind speed characteristics such as mean wind speed and wind speed coefficient of variation. The breakthrough time further correlated well with several wind speed power spectra related characteristics especially those controlling the shape of the power spectra in the low-frequency wind speed fluctuation range. The vertical (Z) wind speed characteristics generally appeared more related to breakthrough time than the wind speed characteristics in the horizontal (X and Y) directions.
- The vertical component of the wind had a direct effect on the gas transport whereas the standard deviation couldn’t represent a directly effective factor in gas transport through porous media. Calculating the empirical factors and wind induced dispersion coefficient of porous media at the surface could be more

accurate by calculating them directly in fitting procedure of modelled and measured data. Other wind characteristics including Kaimal and Linear wind characteristics based on power spectra were calculated and their relation to gas transport in porous media is determined.

- An experimental equation was derived and verified by experiments on different fractions. The equation (Eq. 26) includes two experimental parameters (α & β). One of the experimental parameters, α may be regarded as the inverse of the depth of penetration for wind action, while for constant α (and z_p) β controls the slope of the $D_w(z)$ relationship at $z = z_p$.
- The penetration depth (Z_{50}) and the relative normalized dispersion coefficient slope (S) were introduced. Linear relation between penetration depth Z_{50} and $1/\alpha$ in one hand and between S and $1/\beta$ in other hand exist. This showed the empirical factors are meaningful and linearly related to experiments parameters. Wind characteristics could affect the gas transport speed and penetration depth inside porous media for particle sizes above 1mm. For finer porous media, the effect of wind was found to be low. At particle size below 0.5 mm, the effect of wind on gas transport was found to be negligible. A linear relation between D_{w0} and particle size is concluded.
- Particle parameters such as particle size, roughness and roundness were calculated. A linear relation between average particle size and average D_{w0} was found. Also, it was concluded that a specific wind can penetrate a higher depth

for coarser porous materials. The relations between particle properties and wind-induced gas transport in that materials were gained.

- Two types of fitting between measured data and modelled ones were used. The RMSE value was calculated and used as an indicator of accuracy of each fitting approach. The comparison indicated that the direct fitting approach is more accurate compared to indirect fitting approach.

Overall, the data indicate that wind induced gas dispersion in near-surface porous media is strongly related to both wind speed characteristics and to porous medium properties.

Recommendations for Future work

In this research five fractions of porous materials is used which provides different grain sizes and porosities as the variable factors to investigate how those parameters affects the gas transport through porous media. It is suggested that for more studies in this field, several fractions of material with same grain size distribution be investigated in which the porosity of the material is changing. Different porosities can be achieved by different compaction forces. This can help to discover the effect of grain size on gas transport individually.

In the current research, all materials were dry. Effect of water and different saturation levels can also be interesting to investigate and know.

Pressure fluctuation amplitude, frequency and power spectrum are controlled both by the wind conditions in the un-obstructed atmosphere (well above the ground surface) and by obstacles present on the ground such as buildings, plant cover, rocks etc. Understanding how these obstacles alter the characteristics of the wind flow is necessary for estimating wind conditions at the ground surface. So in further work, a field study for measure and model the effect of ground condition such as the plant cover can be investigated and results would be very useful for environmental study of the subject.

REFERENCES

Acharya, C.L. & Prihar, S.S. 1969. Vapor losses through soil mulch at different wind velocities. Agronomy Journal, 61, 666–668.

Basirat, F., Niemi, A., Perroud, H., Lofi, J., Denchik, N., Lods, G., Pezard, P., Sharma, P. and Fagerlund, F. 2013. Modeling Gas Transport in the Shallow Subsurface in Maguelone Field Experiment. Energy Procedia 40, 37 – 345

Cheung, J.C.K., Melbourne, W.H., 1983. Turbulence effects on some aerodynamic parameters of a circular cylinder at supercritical Reynolds number. Journal of wind engineering and industrial aerodynamics, 14, 399-410.

Costanza-Robinson, M. S., Brusseau, M.L. 2006. Gas-phase dispersion in porous media, transport in porous media. volume 20, 121-132.

Colbeck, S. C. 1981. A simulation of the enrichment of atmospheric pollutants in snow cover runoff. Water Resources Research, 17, 1383–1388.

De Beule, C., Wurm, G., Kelling, T., Kupper, M., Jankowski, T., Tieser, J., 2013. The Martian soil as planetary gas pump, Nature physics, Vol 10.

De Karman, T., and Howarth, L. 1938. On the statistical theory of isotropic turbulence. Proceedings of the Royal Society of London, Series A, Mathematical and Physical Sciences 164, 192-215.

Denny, M.W. 1993. Air and Water: The Biology and Physics of Life's Media. Princeton University Press, Princeton, NJ.

Farrell, D.A., Greacen, E.L. & Gurr, C.G. 1966. Vapor transfer in soil due to air turbulence. Soil Science, 102, 305–313.

Fukuda, H. 1955. Air and vapor movement in soil due to wind gustiness. Soil Science, 79, 249–256.

Goffin, S., Wylock, C., Haut, B., Maier, M., Longdoz, B., and Aubinet, M. 2015. Modeling soil CO_2 production and transport to investigate the intra-day variability of surface efflux and soil CO_2 concentration measurements in a scots pine forest (Pinus Sylvestris, L.). Plant and Soil 390, 195-211.

Haghighi, E. & Or, D. 2015a. Evaporation from wavy porous surfaces into turbulent airflows, Transp Porous Med (2015) 110:225–250.

Haghighi, E., & Or, D. 2015b. Interactions of bluff-body obstacles with turbulent airflows affecting evaporative fluxes from porous surfaces, Journal of Hydrology 530 (2015) 103–116

Hanks, R.J. & Woodruff, N.P. 1958. Influence of wind on water vapor transfer through soil, gravel, and straw mulches. Soil Science, 86, 160–164.

Ishihara, Y., Shimojima, E. & Harada, H. 1992. Water-vapor transfer beneath bare soil where evaporation is influenced by a turbulent surface wind. Journal of Hydrology, 131, 63–104.

Kaimal, J. C, Wyngaard, J. C., Izumi, Y., and Coté, O. R. 1972. Spectral characteristics of surface-layer turbulence. Quarterly Journal of the Royal Meteorological Society, 98, 563-589.

Kaimal, J. C, Wyngaard, J.C, Haugen, D. A., Coté, O. R., Izumy, Y., Caughey, S. J., and Readings, C. J. 1976. Turbulence structure on the convective boundary layer. Journal of the Atmospheric Sciences, 33, 2152-2169.

Kimball, B.A. & Lemon, E.R. 1970. Spectra of air pressure fluctuations at the soil surface. Journal of Geophysical Research, 75, 6771–6777.

Kirkham, D. 1947. Field method for determination of air permeability of soil in its undisturbed state. Soil Science Society America Journal, 11, 93–99.

Maier, M., Schack-Kirchner, H., Aubinet, M., Goffi, S., Longdoz, B. & Parent,F. 2012. Turbulence effect on gas transport in three contrasting forest soils. Soil Science Society of America Journal, 76, 1518–1528.

Massman, W.J. & Frank, J.M. 2006. Advective transport of CO_2 in permeable media induced by atmospheric pressure fluctuations: 2. Observational evidence under snowpacks. Journal of Geophysical Research: Biogeosciences, 111, G3

Massman, W.J., Sommerfeld, R.A., Mosier, A.R., Zeller, K.F., Hehn, T.J. & Rochelle, S.G. 1997. A model investigation of turbulence-driven pressure-pumping effects on the

rate of diffusion of CO_2, N_2O and CH_4 through layered snowpacks. Journal of Geophysical Research, 102, 18 851–18 863.

Millington, R. & Quirk, J.P. 1961. Permeability of porous solids. Transactions of the Faraday Society, 57, 1200–1207.

Mohr, M., Laemmel, T., Maier, M., and Schindler, D. 2016. Analysis of air pressure fluctuations and topsoil gas concentrations within a scots pine forest. Atmosphere 7, 125.

Nazaroff, W. W. 1992. Radon transport from soil to air. Reviews of Geophysics, 30, 137–160.

Novak, M.D., Chen, W., Orchansky, A.L. & Ketler, R. 2000a. Turbulent exchange processes within and above a straw mulch. Part I: Mean wind speed and turbulent statistics. Agricultural and Forest Meteorology, 102, 139–154.

Novak, M.D., Ketler, R., Chen, W. & Orchansky, A.L. 2000b. Turbulent exchange processes within and above a straw mulch. Part II: Thermal and moisture regimes. Agricultural and Forest Meteorology, 102, 155–171.

Oertel, C., Matschullat, J., Zurba, K., Zimmermann, F. & Erasmi, S. 2016. Greenhouse gas emissions from soils—A review. Chemie der Erde – Geochemistry, 76, 327–352.

M.A. Oliver, A.L. Khayrat 2001, A geostatistical investigation of the spatial variation of radon in soil, Computers & Geosciences, 27, 939–957

Penman, H.L. 1940. Gas and vapor movements in the soil. I. The diffusion of vapors through porous solids. Journal of Agricultural Science, 30, 437–462.

Poulsen, T.G., Christophersen, M., Moldrup, P. & Kjeldsen, P. 2001. Modeling lateral gas transport in soil adjacent to old landfill. Journal of Environmental Engineering(ASCE), 127, 145–153.

Poulsen, T.G. & Moldrup, P. 2006. Evaluating effects of wind-induced pressure fluctuations on soil-atmosphere gas exchange at a landfill using stochastic modelling. Waste Management & Research, 24, 473–481.

Poulsen, T.G., Moldrup, P., Yoshikawa, S. & Komatsu, T. 2006. Bimodal probability law model for unified description of water retention, air and water permeability, and gas diffusivity in variably saturated soil. Vadose Zone Journal, 5, 1119–1128.

Poulsen, T.G., Suwarnarat, W., Hostrup, M.K. & Kalluri, P.N.V. 2008. Simple and rapid method for measuring gas dispersion in porous media: Methodology and applications. Soil Science, 173, 169–174.

Poulsen, T.G. & Sharma, P. 2011. Apparent porous media gas dispersion in response to rapid pressure fluctuations. Soil Science, 176, 635–641.

Pourbakhtiar, A., Poulsen, T. G., Wilkinson, S., and Bridge, J. 2017. Impact of wind turbulence on gas transport in porous media: Experimental method and preliminary results. European Journal of Soil Science 68, 48-56.

Redecker, K. R., Baird, A. J., and Teh, Y. A. 2015. Quantifying wind and pressure effects on trace gas fluxes across the soil-atmosphere interface. Biogeosciences, 12 7423-7434.

Riley, W.J., Robinson, A.L., Gadgil, A.J. & Nazaroff, W.W. 1999. Effects of variable wind speed and direction on radon transport from soil into buildings: model development and exploratory results. Atmospheric Environment, 33, 2157–2168.

Russ, J.C. 2007. The Image Processing Handbook, Fifth Edition. CRC, Taylor & Francis Group, Boca Raton, FL.

Saffman, P.G. 1960. Dispersion due to molecular diffusion and macroscopic mixing in flow through a network of capillaries. Journal of Fluid Mechanics, 7, 194–208.

Scotter, D.R. & Raats, P.A.C. 1968. Dispersion in porous mediums due to oscillating flow. Water Resources Research, 4, 1201–1206.

Scotter, D.R. & Raats, P.A.C. 1969. Dispersion of water vapor in soil due to air turbulence. Soil Science, 108, 170–176.

Stevens, A.H., Patel, M.R., Lewis, S.R., 2015. Numerical modelling of the transport of trace gases including methane in the subsurface of Mars. Icarus 250, 587–594.

Smith, S., Lason, L., 1992. Solving large sparse nonlinear programs using GRG. ORSA journal on computing, Vol. 4, No. 1.

Takle, E.S., Brandle, J.R., Schmidt, R.A., Garcia, R., Litvina, I.V., Massman, W.J.et al. 2003. High-frequency pressure variations in the vicinity of a surface CO_2 flux chamber. Agricultural and Forest Meteorology, 114, 245–250.

Takle, E.S., Massman, W.J., Brandle, J.R., Schmidt, R.A., Zhou, X.H., Litvina, I.V.et al. 2004. Influence of high-frequency ambient pressure pumping on carbon dioxide efflux from soil. Agricultural and Forest Meteorology, 124, 193–206.

Thomas, N., Portyankina, G., Hansen, C.J., Pommerol, A., 2011. Sub- surface CO_2 gas flow in Mars' polar regions: Gas transport under constant production rate conditions, GEOPHYSICAL RESEARCH LETTERS, VOL. 38, L08203.

Topp, E. & Pattey, E. 1997. Soils as sources and sinks for atmospheric methane. Canadian Journal of Soil Science, 77, 167–178.

Van Der Hoven, I. 1956. Power spectrum of horizontal wind speed in the frequency range from 0.0007 to 900 cycles per hour. Journal of Meteorology 14, 160-164.

Van Genutchen, M.T. 1980. A closed-form equation for predicting the hydraulic conductivity of unsaturated soils. Soil Science Society of America Journal, 44, 892–898.

Wang, F. & Ward, I.C. 2002. Radon entry, migration and reduction in houses with cellars. Building and Environment, 37, 1153–1165.

APPENDICES

Appendix A. Wind speed diagrams

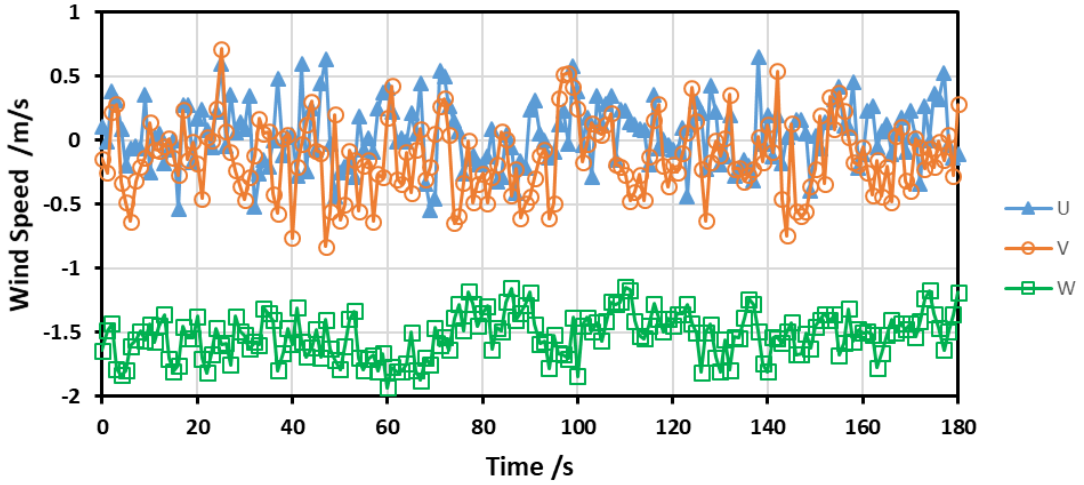

Fig. A1. Measured wind speed of three components of wind condition 1 according to Table 6-4.

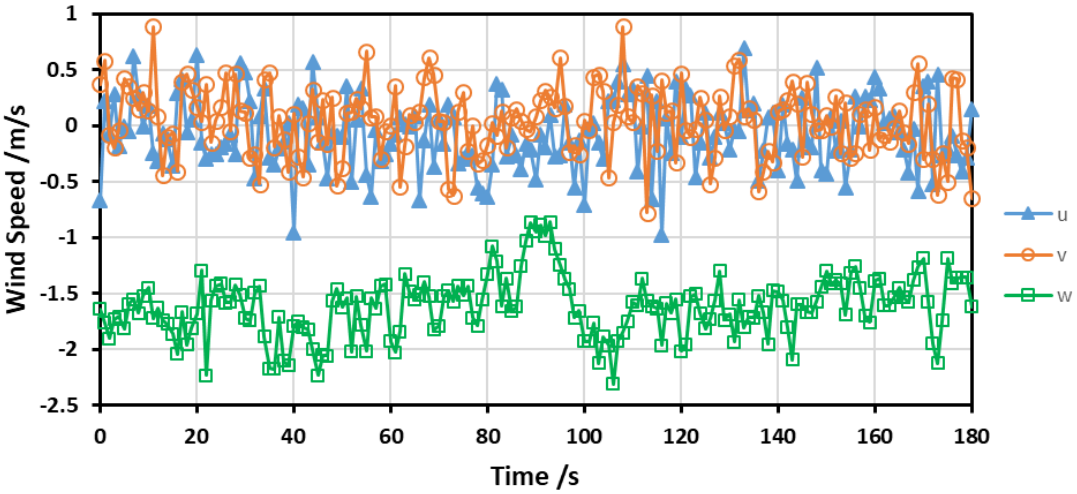

Fig A2. Measured wind speed of three components of wind condition 2 according to Table 6-4.

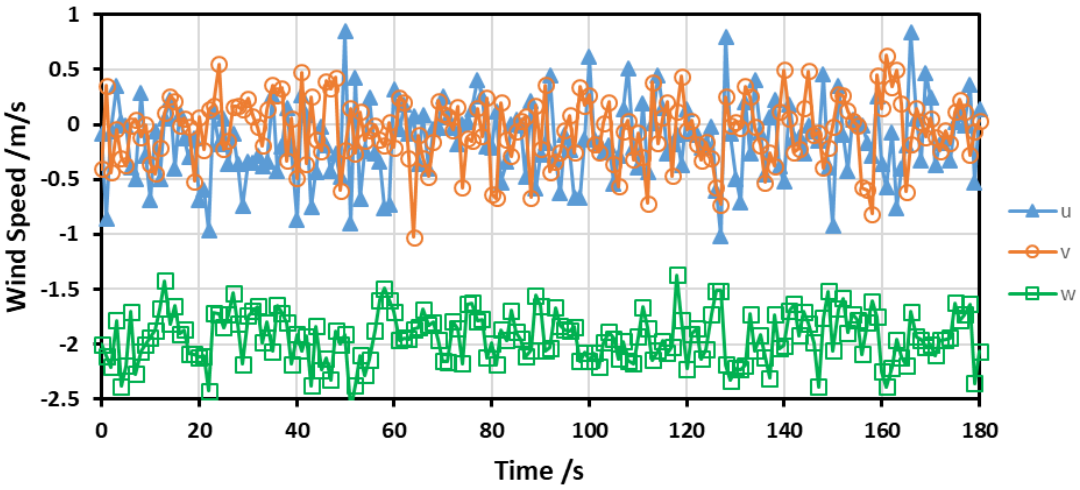

Fig. A3. Measured wind speed of three components of wind condition 3 according to Table 6-4.

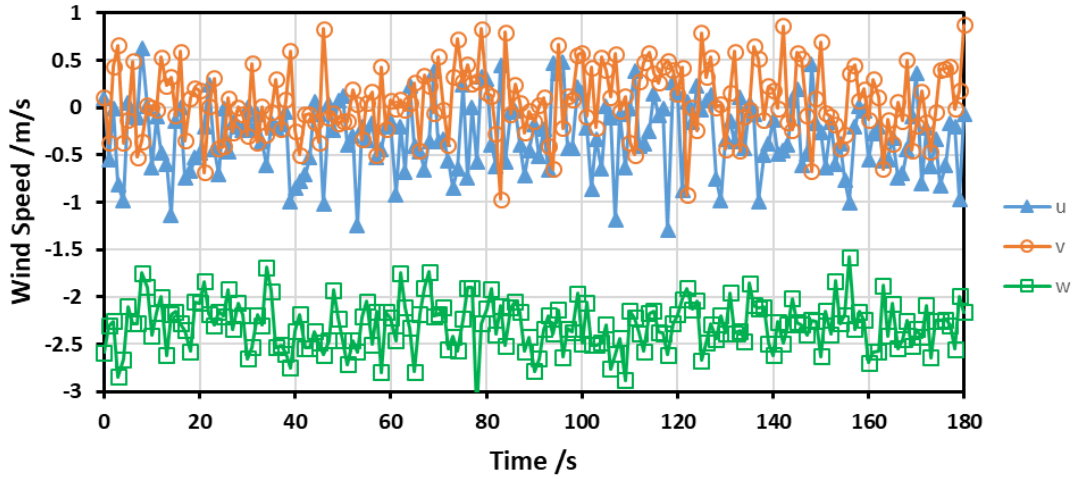

Fig. A4. Measured wind speed of three components of wind condition 4 according to Table 6-4.

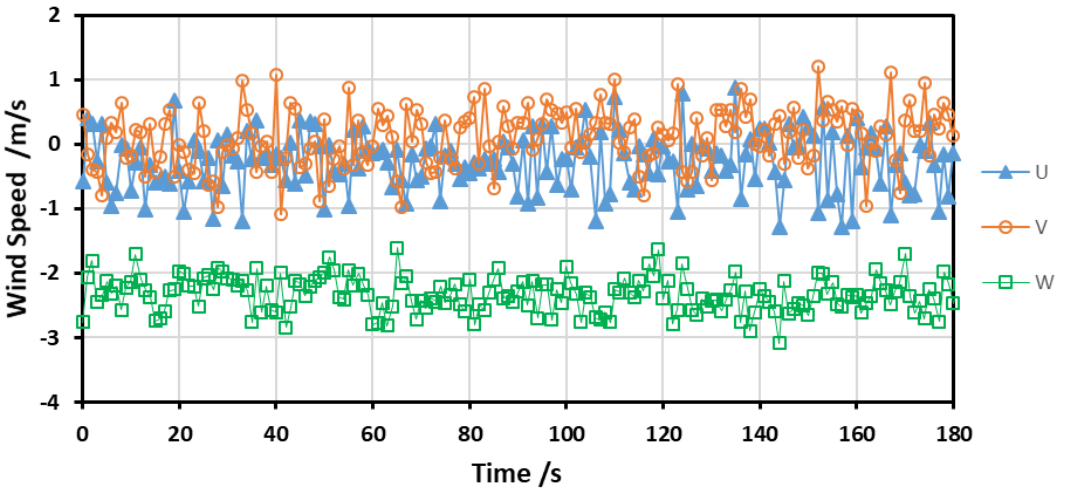

Fig. A5. Measured wind speed of three components of wind condition 5 according to Table 6-4.

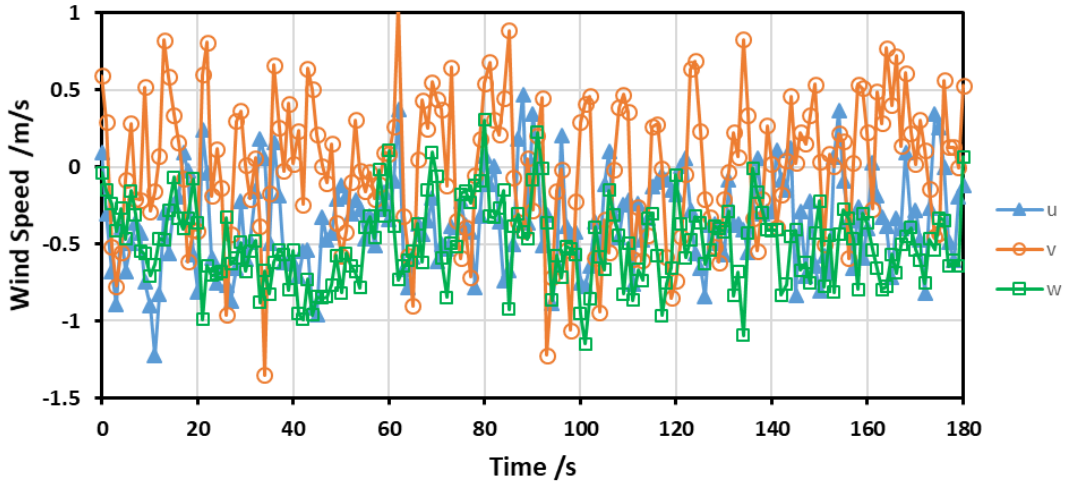

Fig. A6. Measured wind speed of three components of wind condition 6 according to Table 6-4.

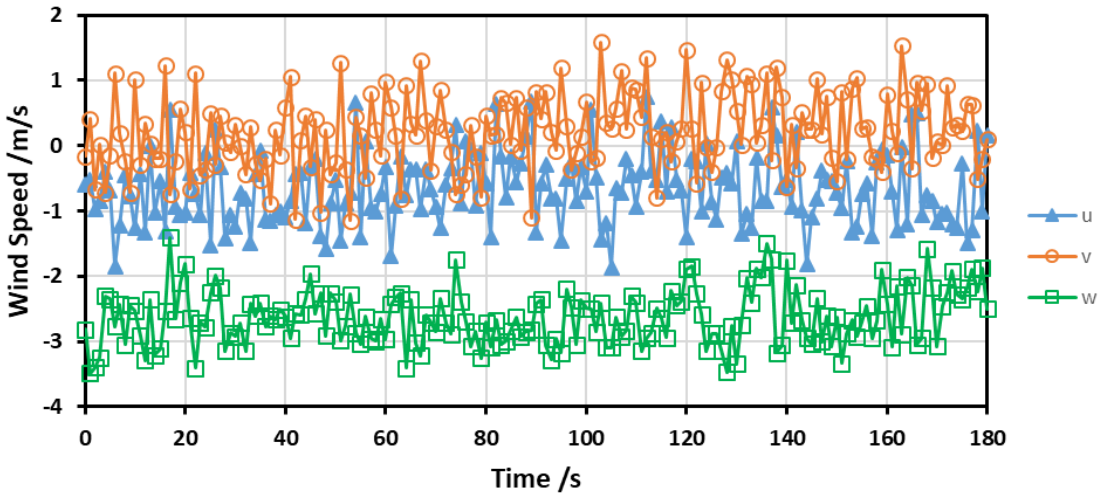

Fig. A7. Measured wind speed of three components of wind condition 7 according to Table 6-4.

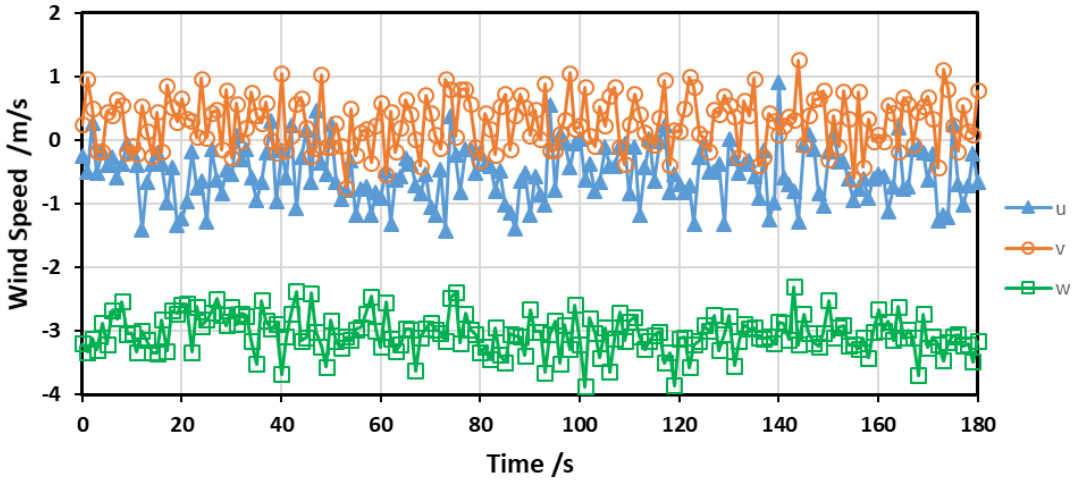

Fig. A8. Measured wind speed of three components of wind condition 8 according to Table 6-4.

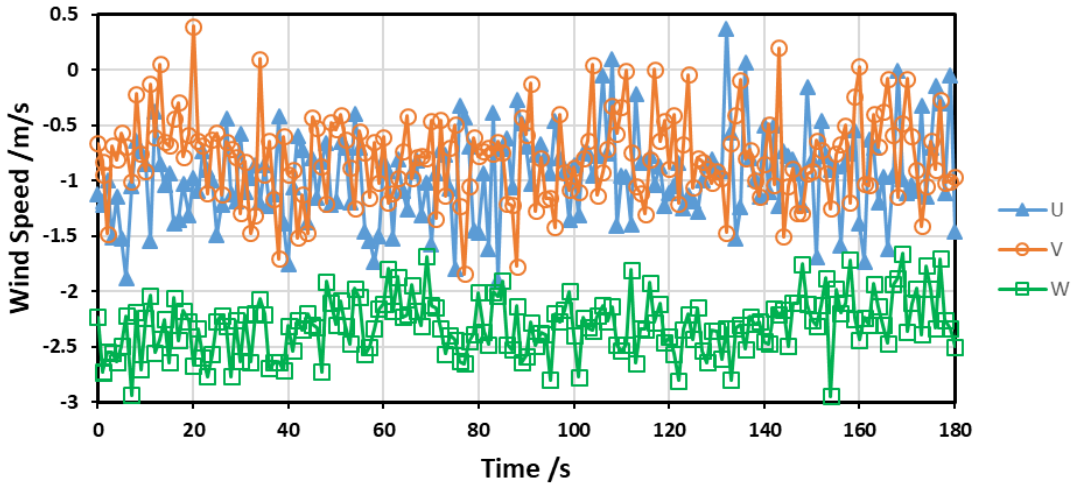

Fig. A9. Measured wind speed of three components of wind condition 9 according to Table 6-4.

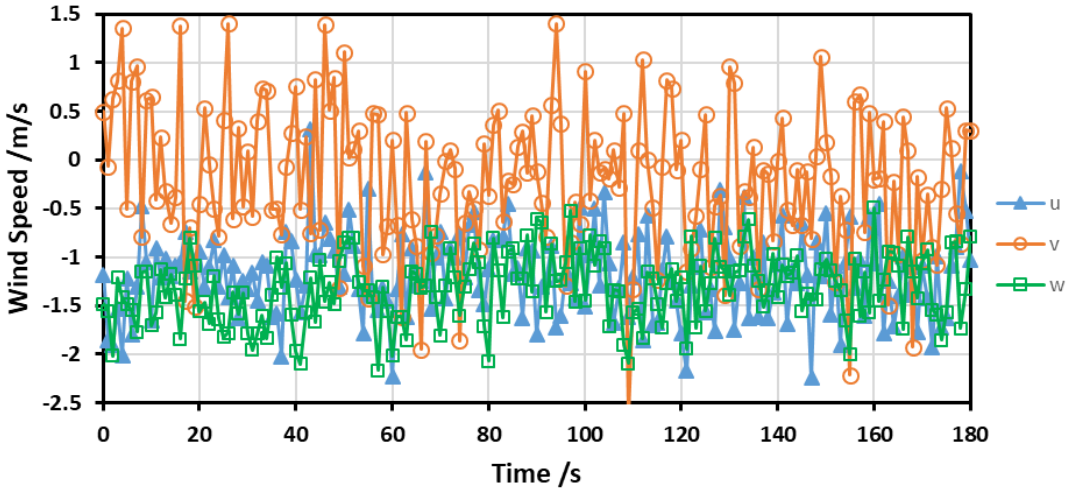

Fig. A10. Measured wind speed of three components of wind condition 10 according to Table 6-4.

Appendix B. Relative oxygen concentration (C/C_{atm}) as a function of time and depth.

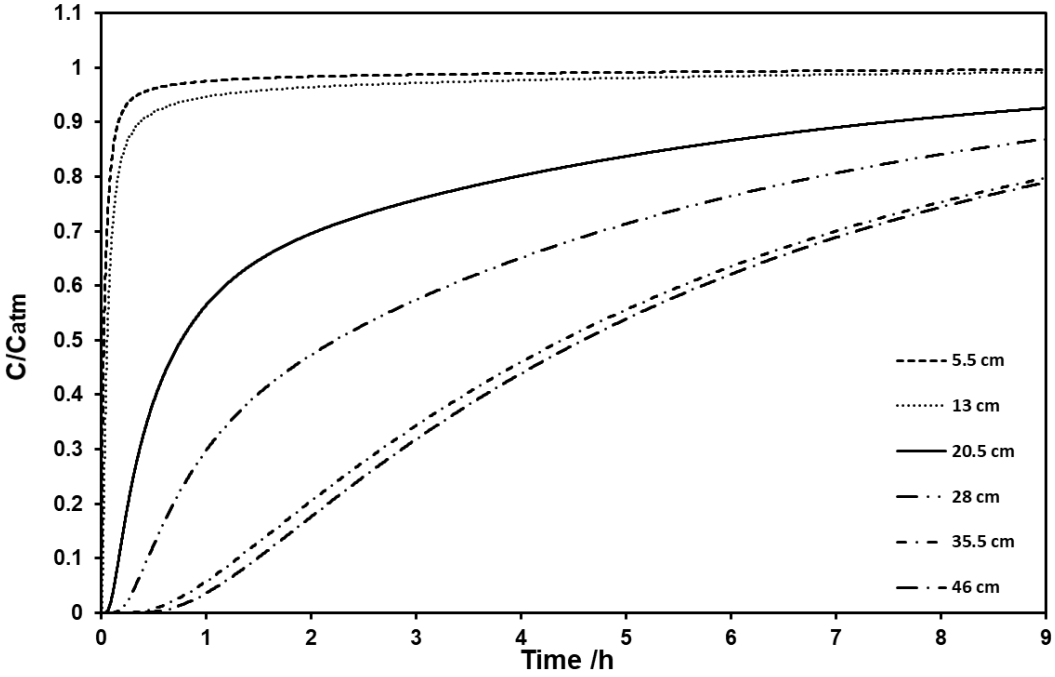

Fig. B1. Relative oxygen concentration (C/C_{atm}), fraction 1, wind condition 1.

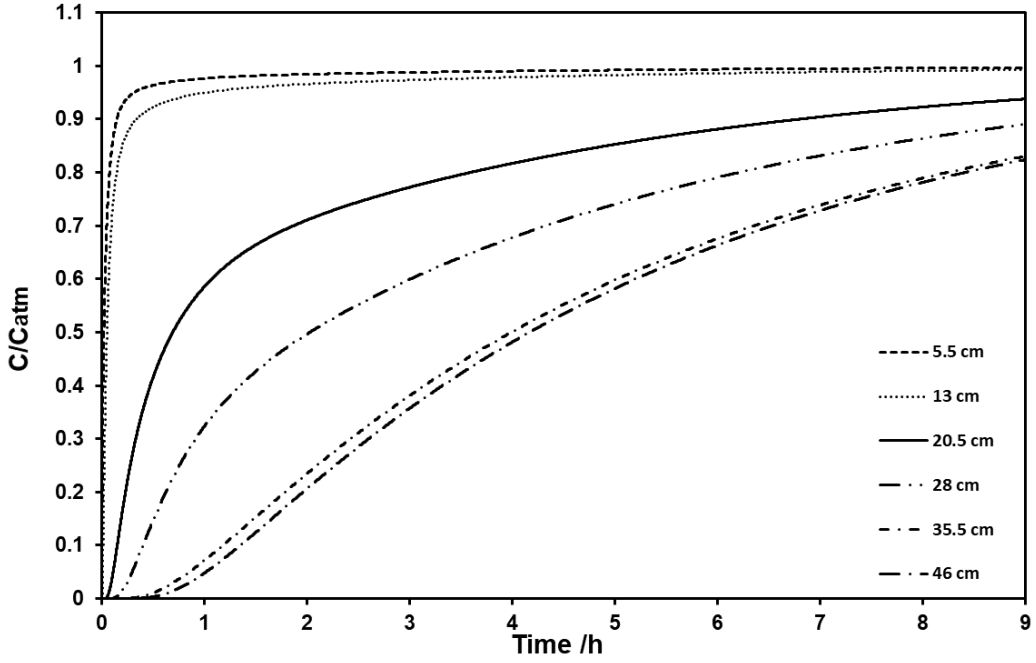

Fig. B2. Relative oxygen concentration (C/C_{atm}), fraction 1, wind condition 2.

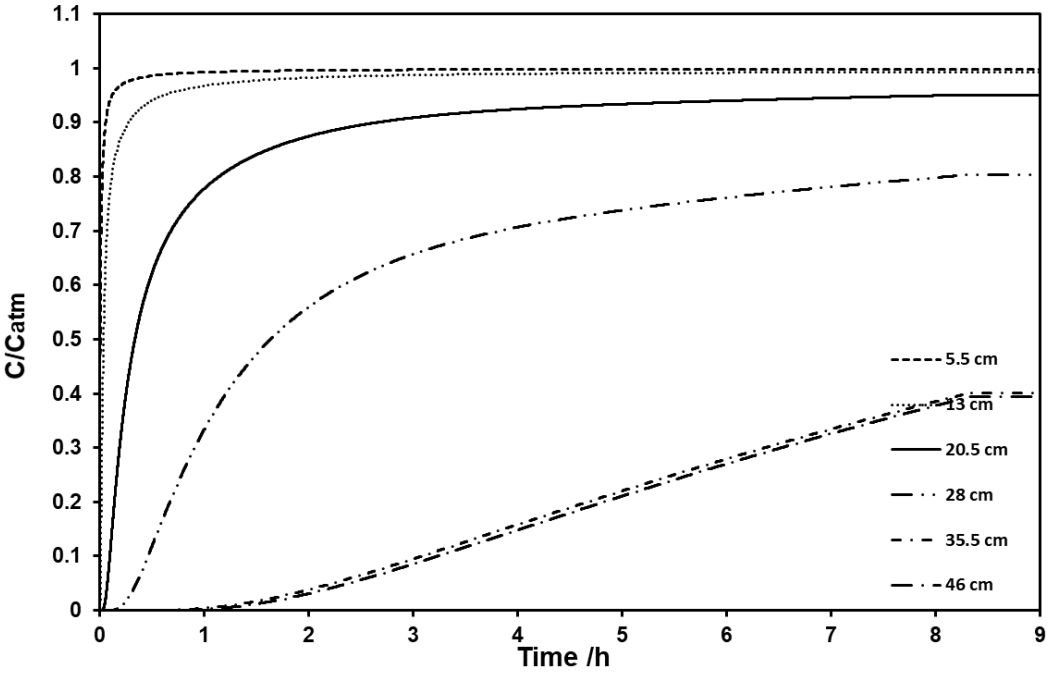

Fig. B3. Relative oxygen concentration (C/C_{atm}), fraction 1, wind condition 3.

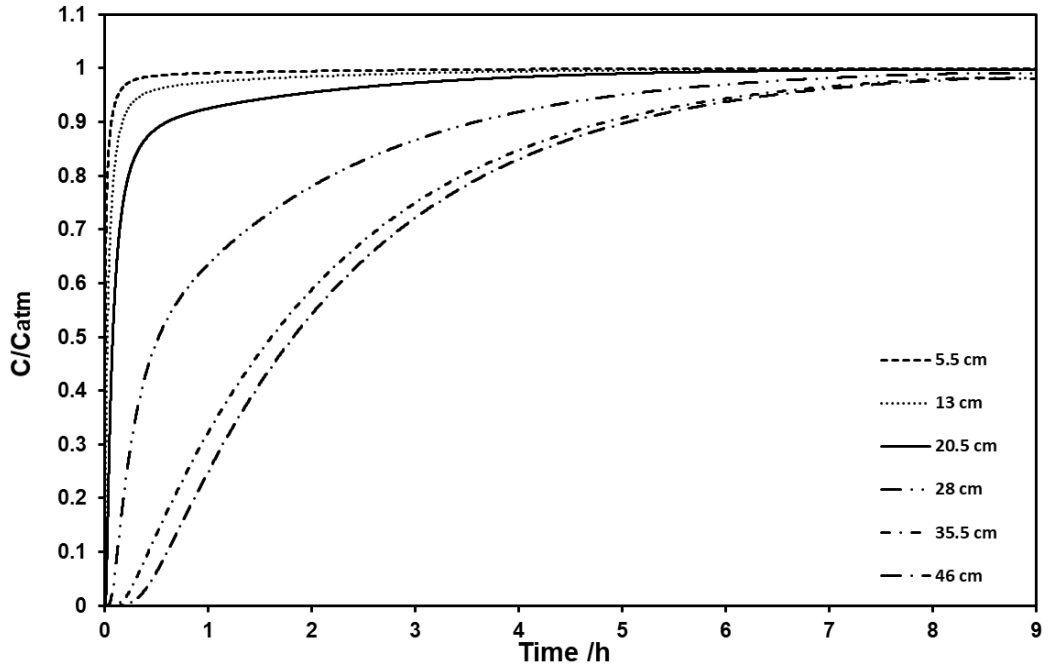

Fig. B4. Relative oxygen concentration (C/C_{atm}), fraction 1, wind condition 4.

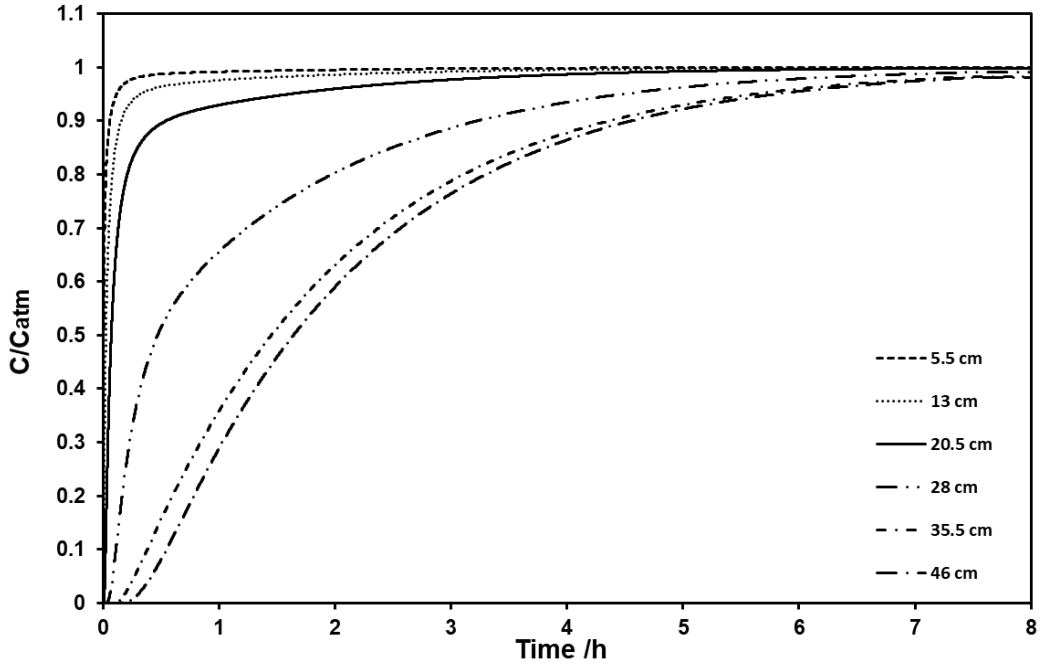

Fig. B5. Relative oxygen concentration (C/C_{atm}), fraction 1, wind condition 5.

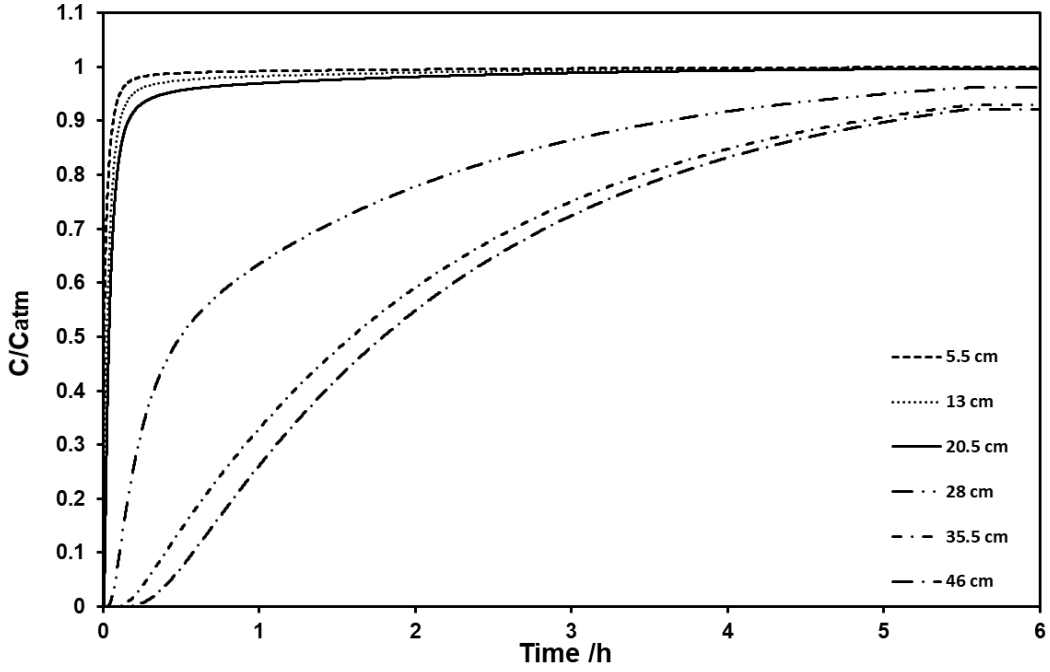

Fig. B6. Relative oxygen concentration (C/C_{atm}), fraction 1, wind condition 6.

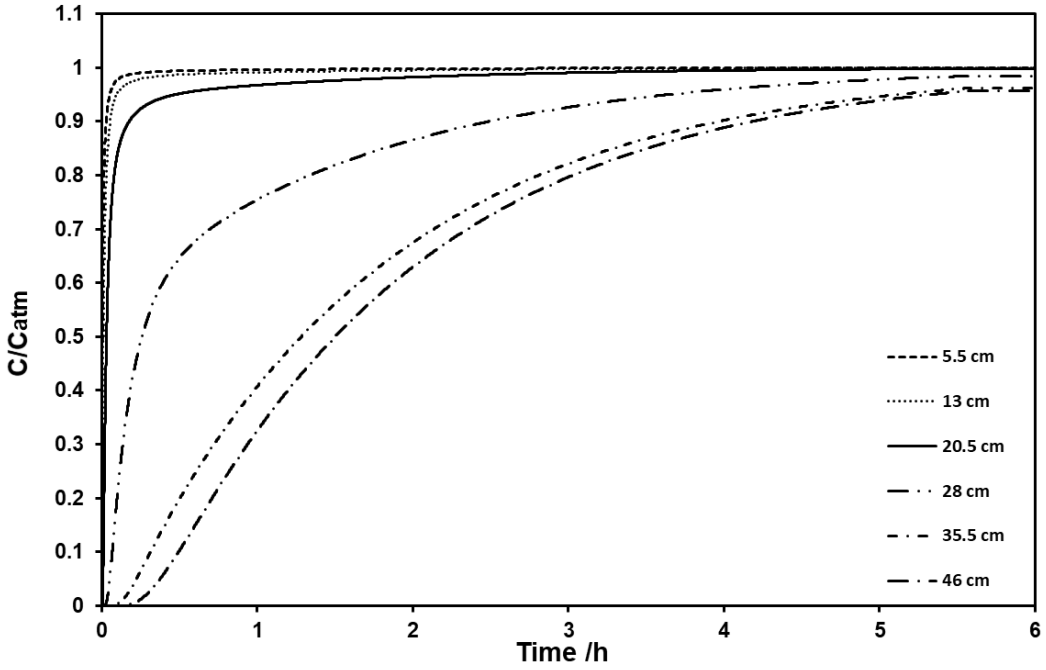

Fig. B7. Relative oxygen concentration (C/C_{atm}), fraction 1, wind condition 7.

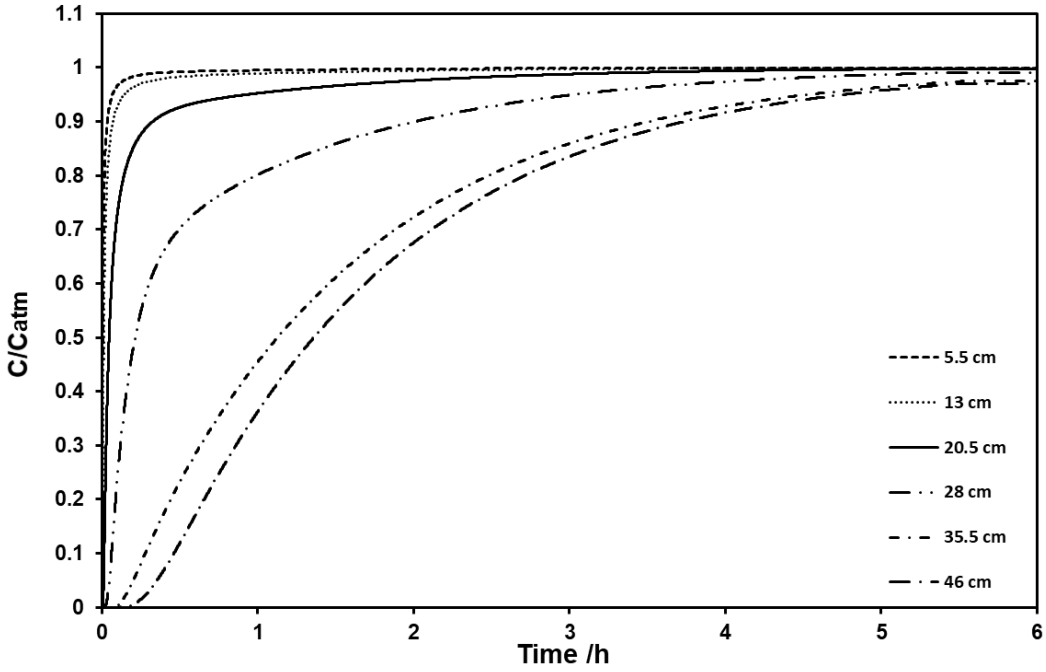

Fig. B8. Relative oxygen concentration (C/C_{atm}), fraction 1, wind condition 8.

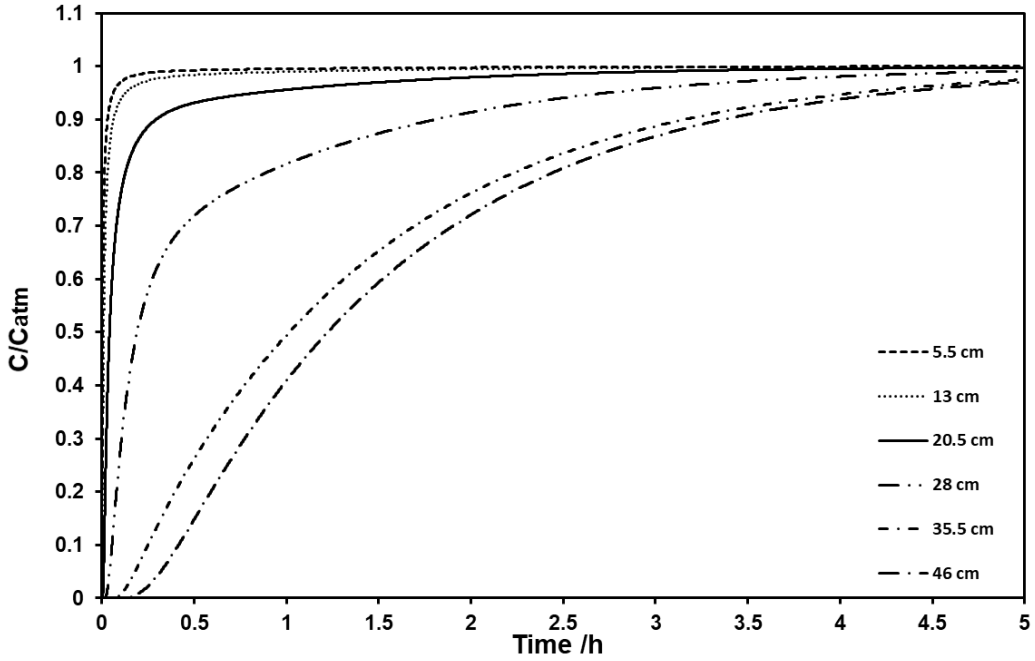

Fig. B9. Relative oxygen concentration (C/C_{atm}), fraction 1, wind condition 9.

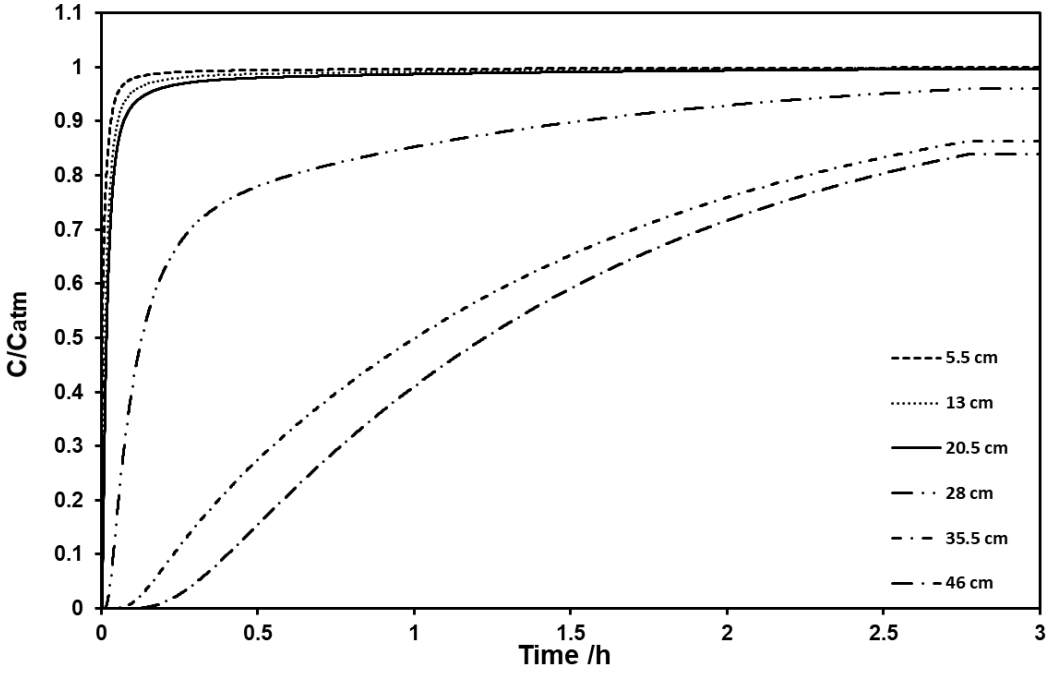

Fig. B10. Relative oxygen concentration (C/C_{atm}), fraction 1, wind condition 10.

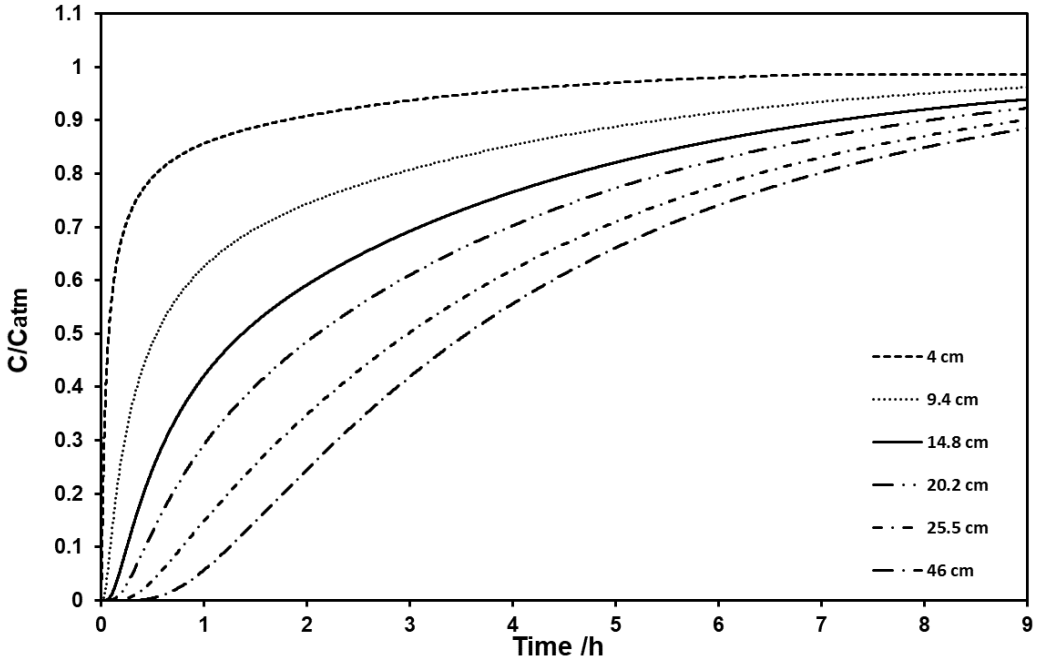

Fig. B11. Relative oxygen concentration (C/C_{atm}), fraction 2, wind condition 1.

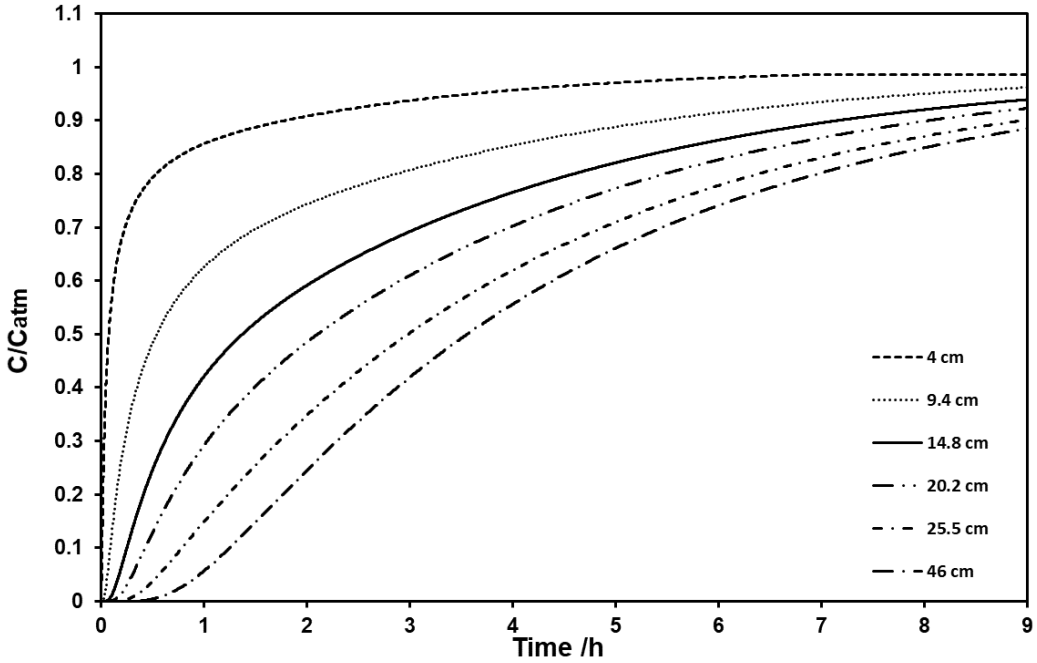

Fig. B12. Relative oxygen concentration (C/C_{atm}), fraction 2, wind condition 2.

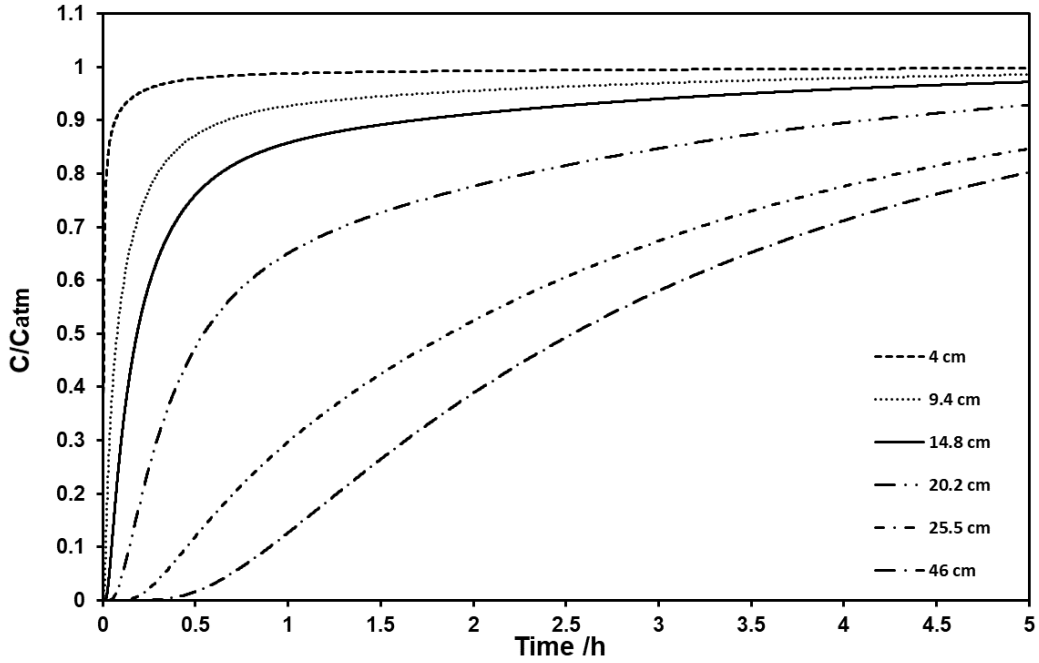

Fig. B13. Relative oxygen concentration (C/C_{atm}), fraction 2, wind condition 3.

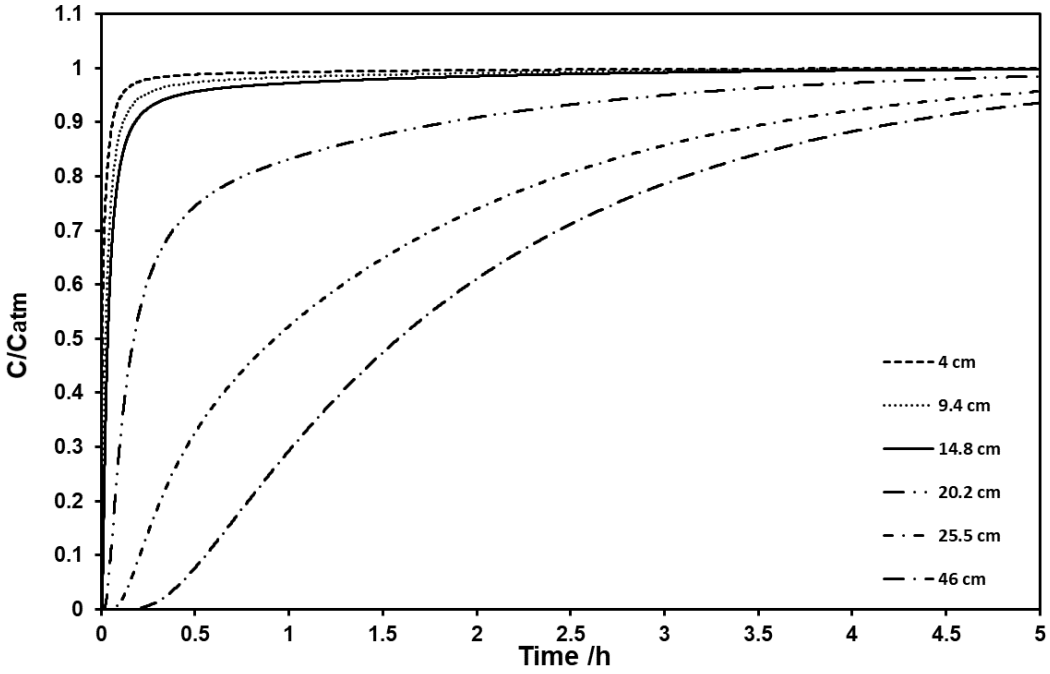

Fig. B14. Relative oxygen concentration (C/C_{atm}), fraction 2, wind condition 4.

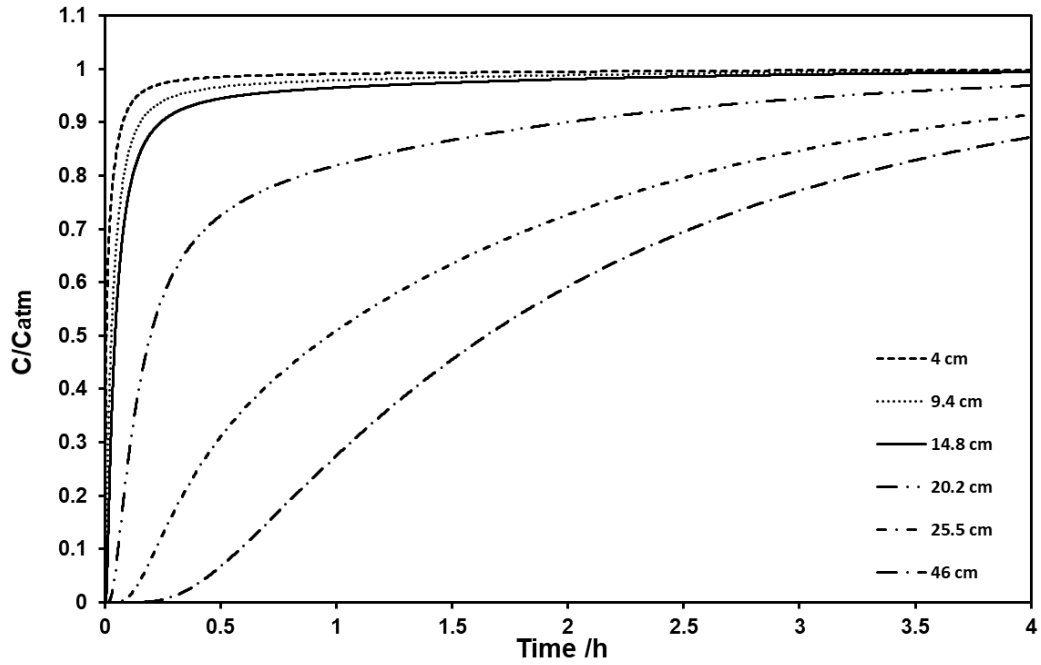

Fig. B15. Relative oxygen concentration (C/C_{atm}), fraction 2, wind condition 5.

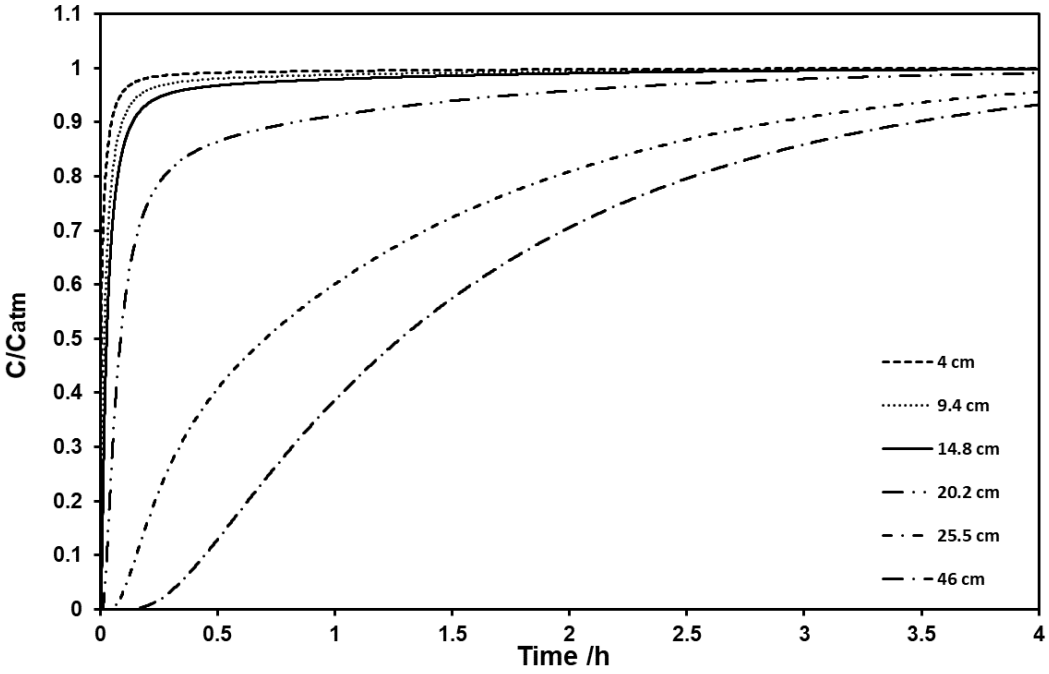

Fig. B16. Relative oxygen concentration (C/C_{atm}), fraction 2, wind condition 6.

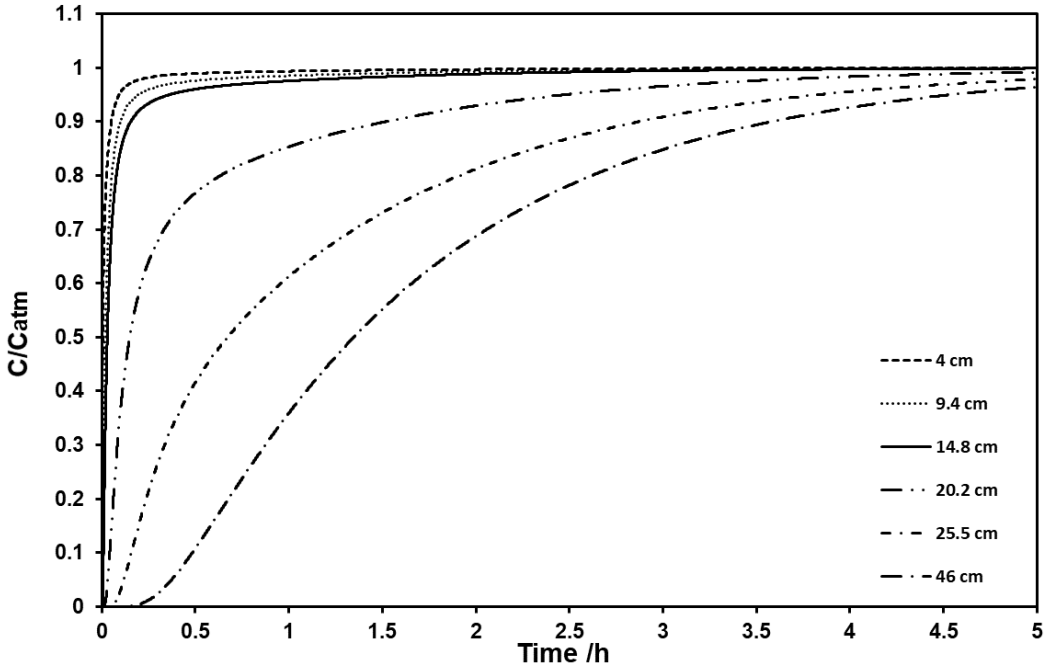

Fig. B17. Relative oxygen concentration (C/C_{atm}), fraction 2, wind condition 7.

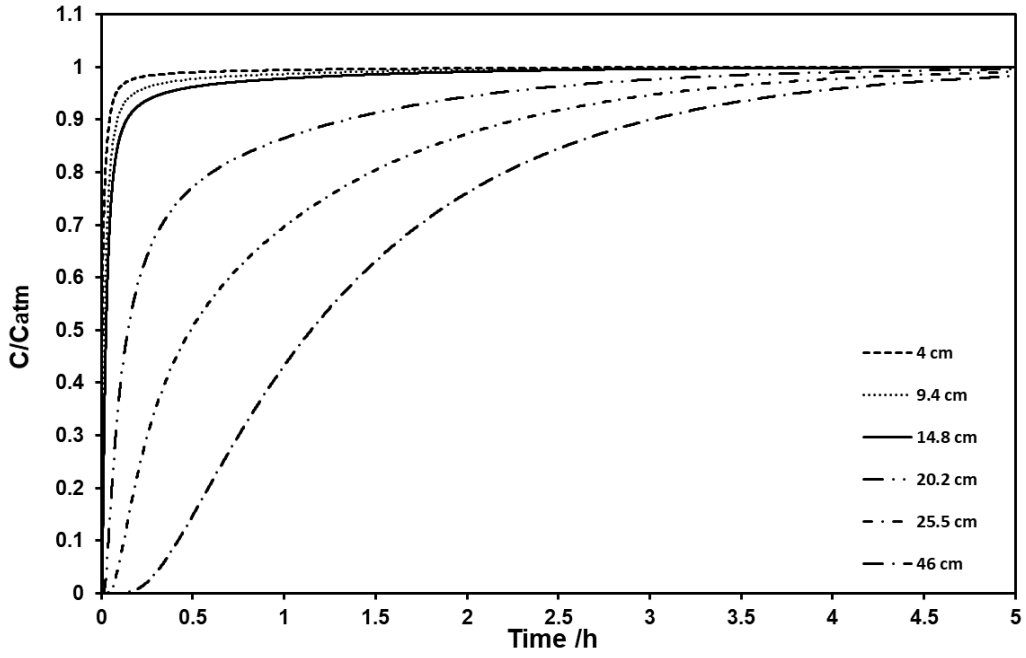

Fig. B18. Relative oxygen concentration (C/C_{atm}), fraction 2, wind condition 8.

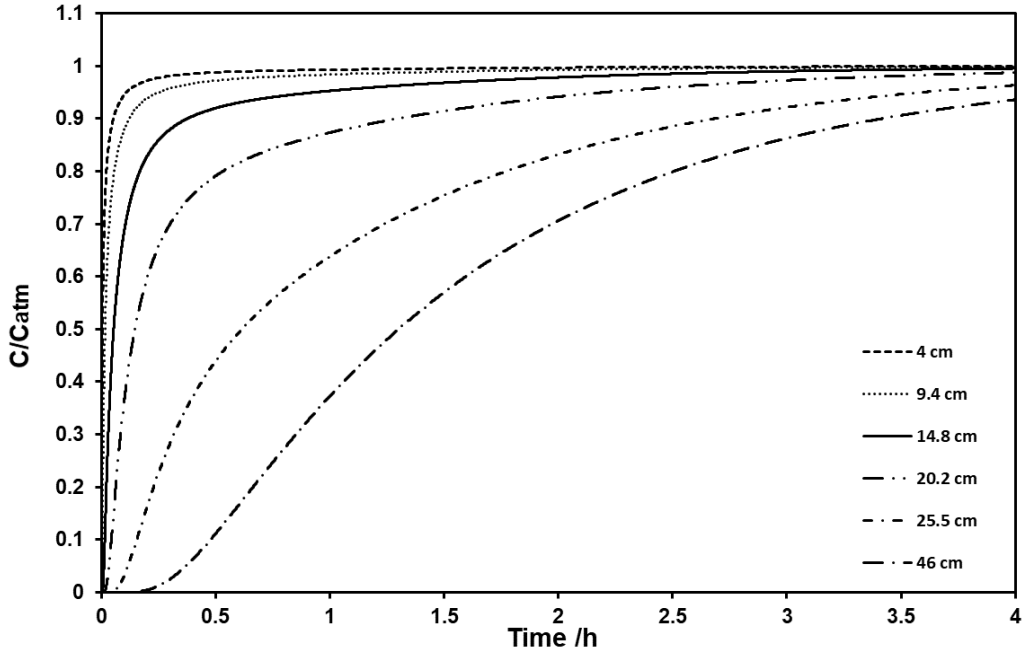

Fig. B19. Relative oxygen concentration (C/C_{atm}), fraction 2, wind condition 9.

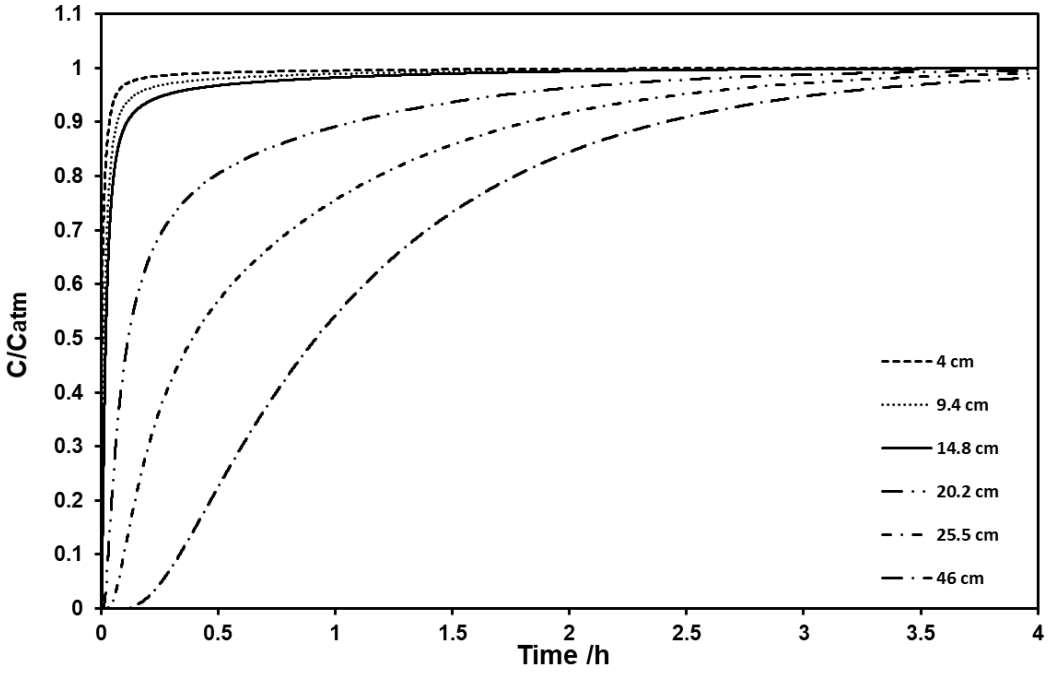

Fig. B20. Relative oxygen concentration (C/C_{atm}), fraction 2, wind condition 10.

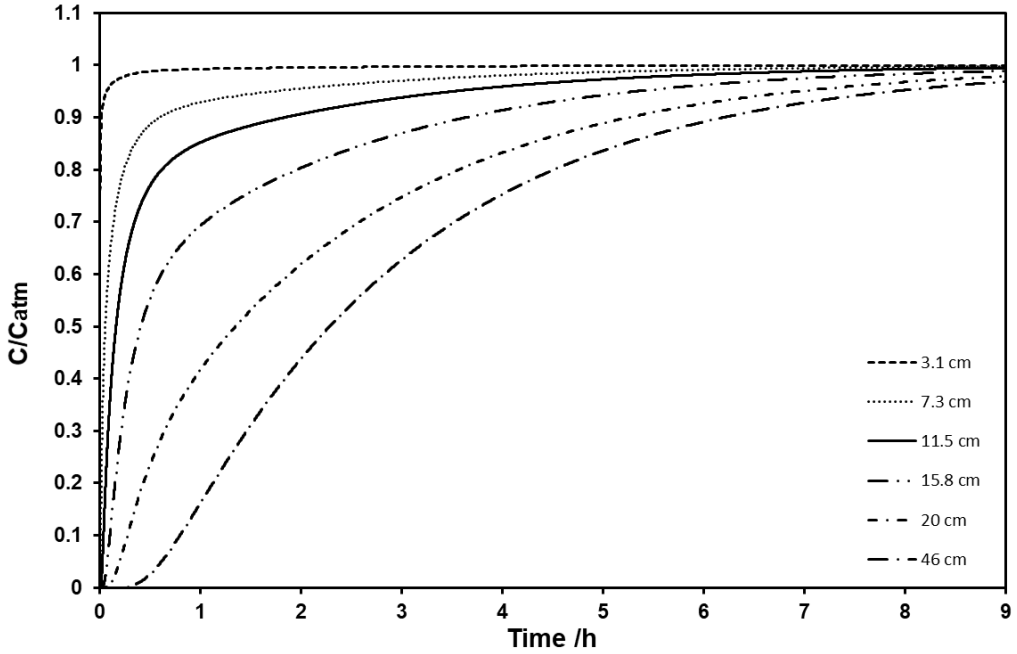

Fig. B21. Relative oxygen concentration (C/C_{atm}), fraction 3, wind condition 1.

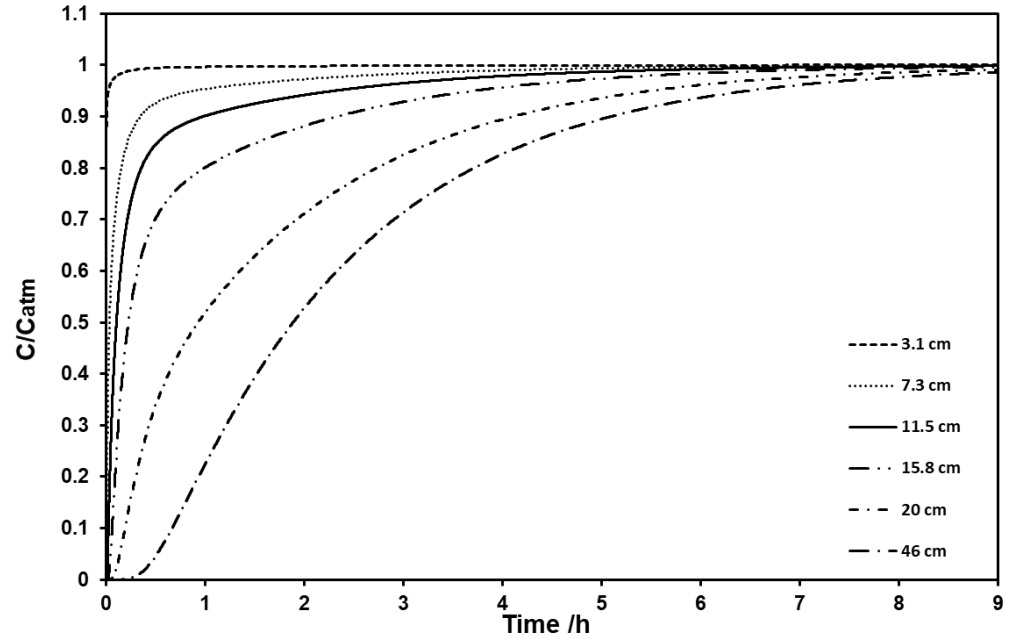

Fig. B22. Relative oxygen concentration (C/C_{atm}), fraction 3, wind condition 2.

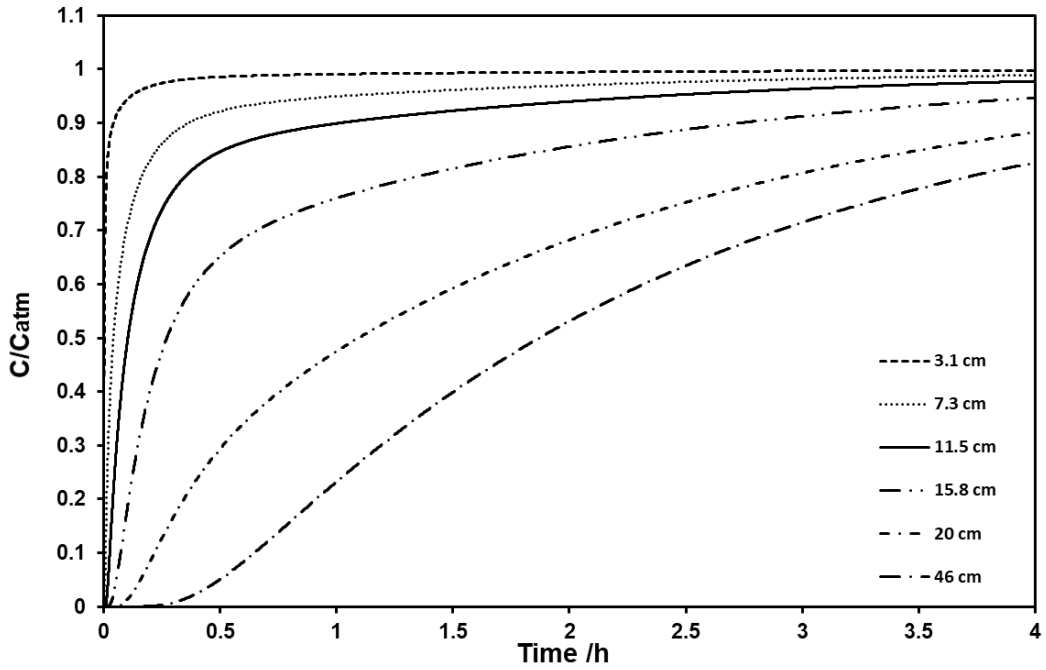

Fig. B23. Relative oxygen concentration (C/C_{atm}), fraction 3, wind condition 3.

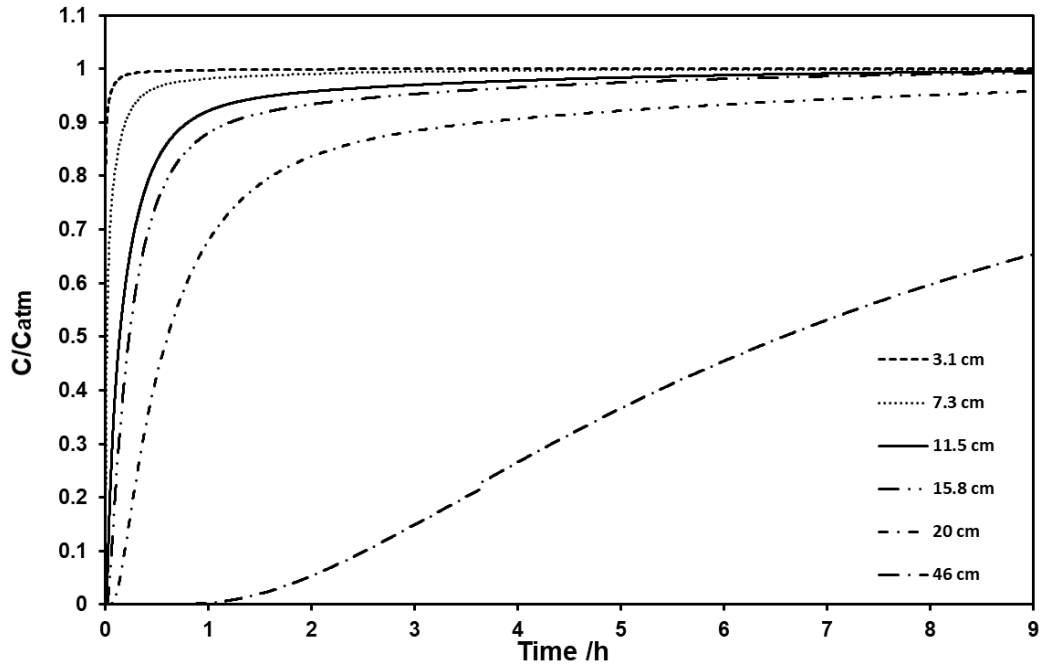

Fig. B24. Relative oxygen concentration (C/C_{atm}), fraction 3, wind condition 4.

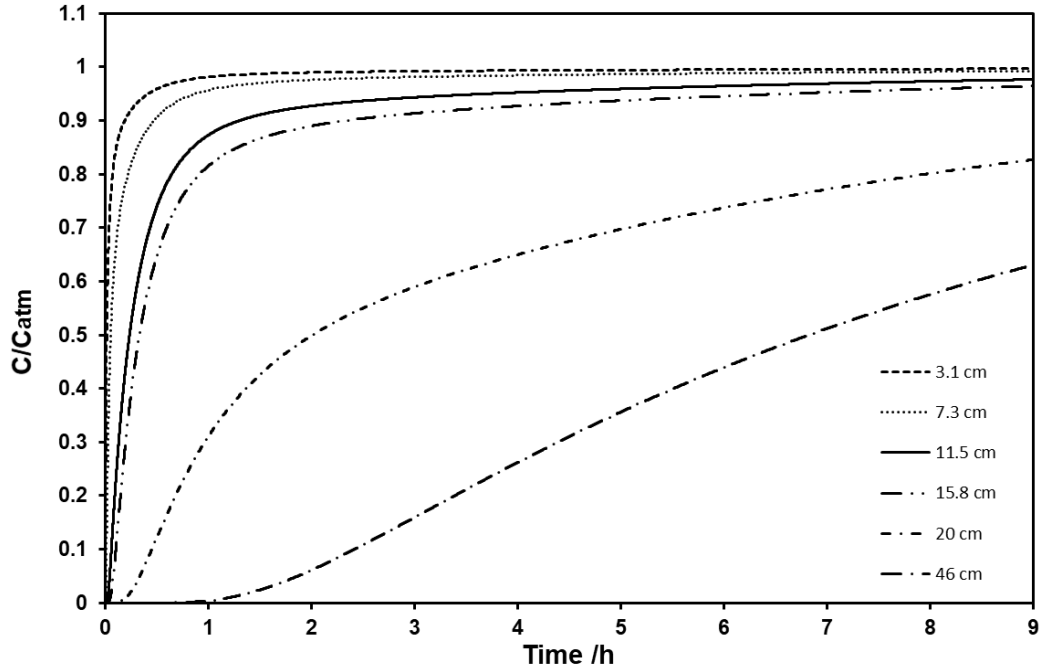

Fig. B25. Relative oxygen concentration (C/C_{atm}), fraction 3, wind condition 5.

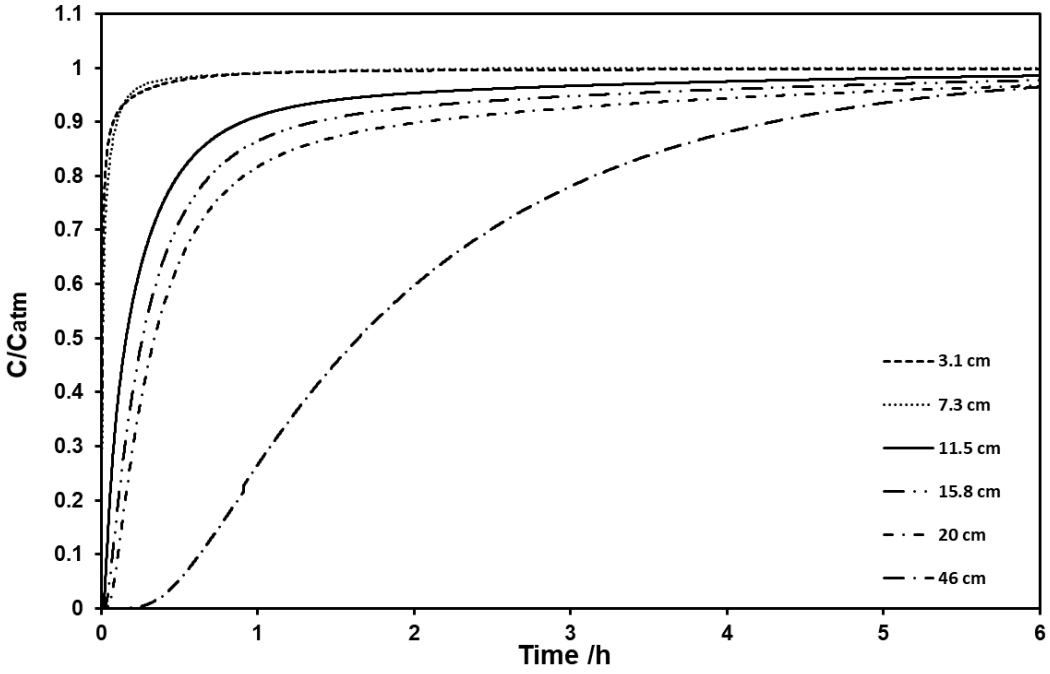

Fig. B26. Relative oxygen concentration (C/C_{atm}), fraction 3, wind condition 6.

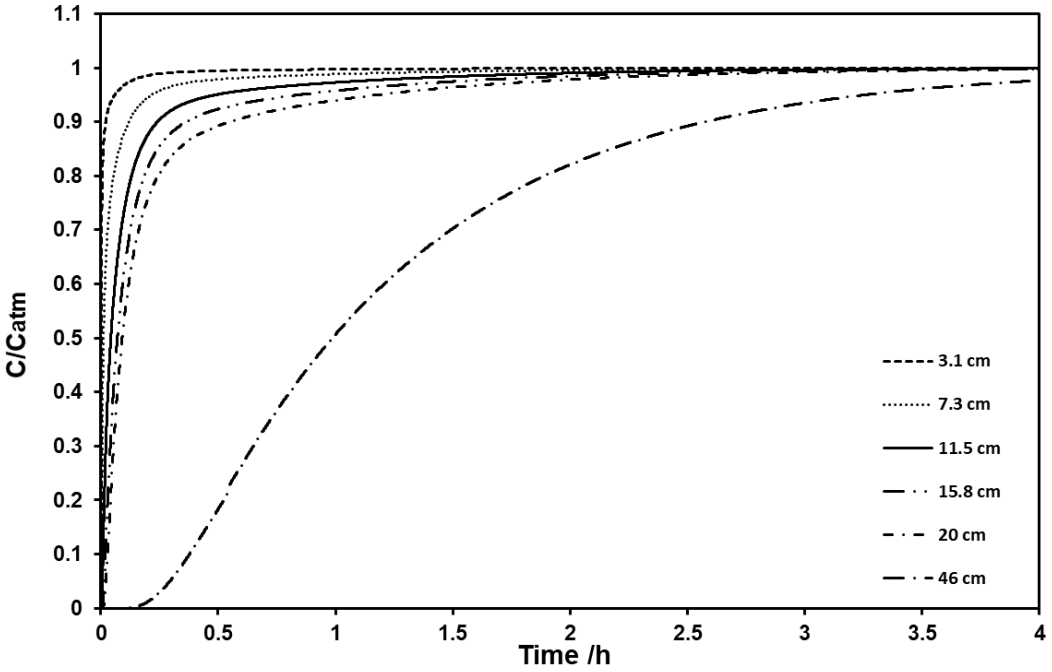

Fig. B27. Relative oxygen concentration (C/C_{atm}), fraction 3, wind condition 7.

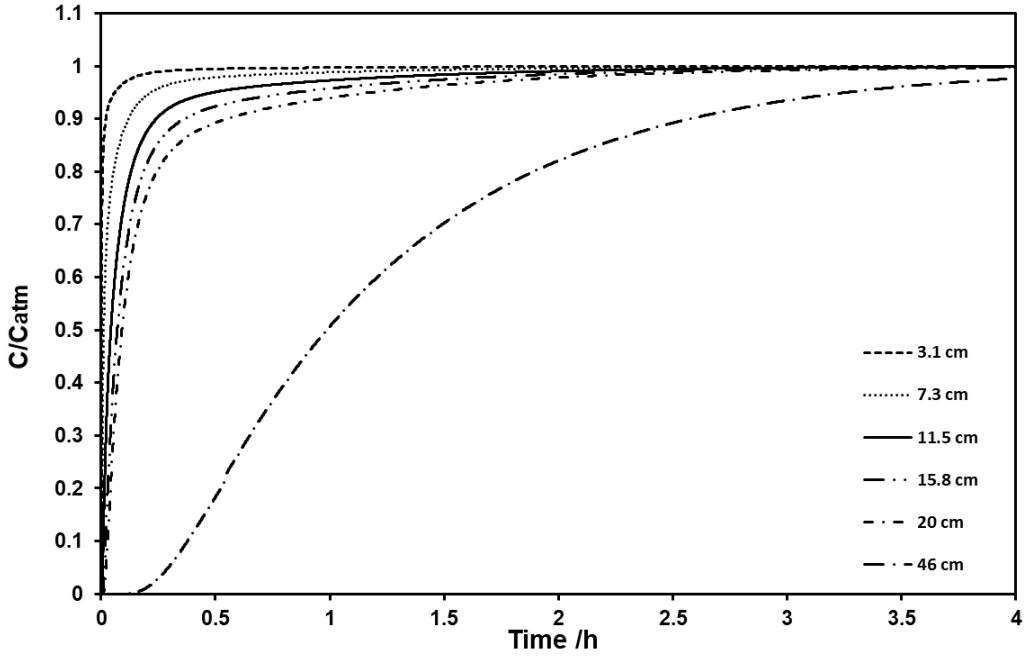

Fig. B28. Relative oxygen concentration (C/C_{atm}), fraction 3, wind condition 8.

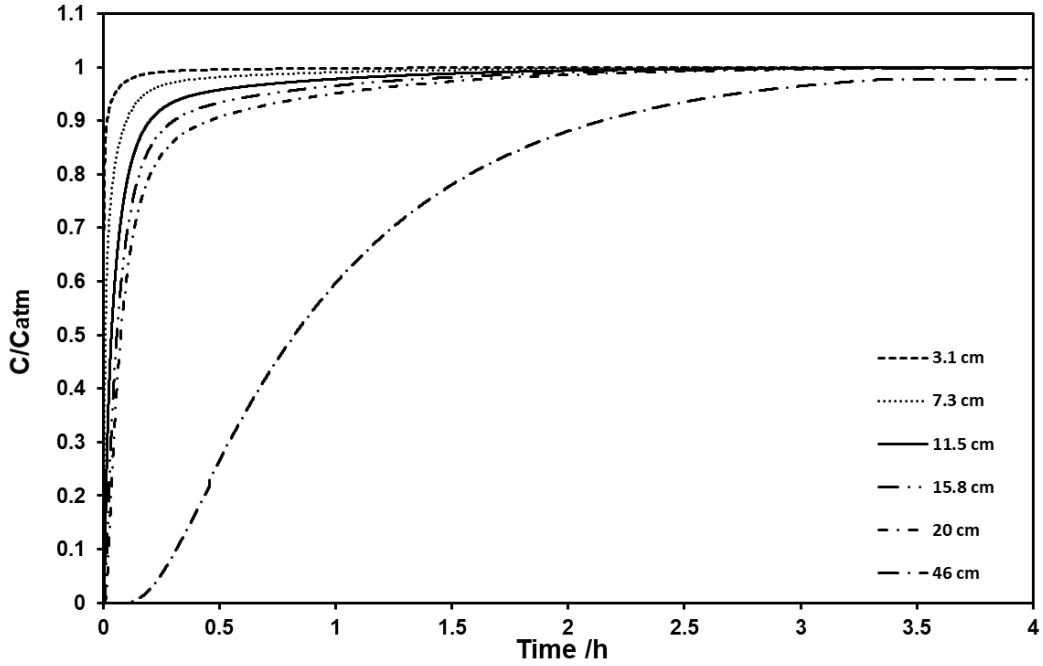

Fig. B29. Relative oxygen concentration (C/C_{atm}), fraction 3, wind condition 9.

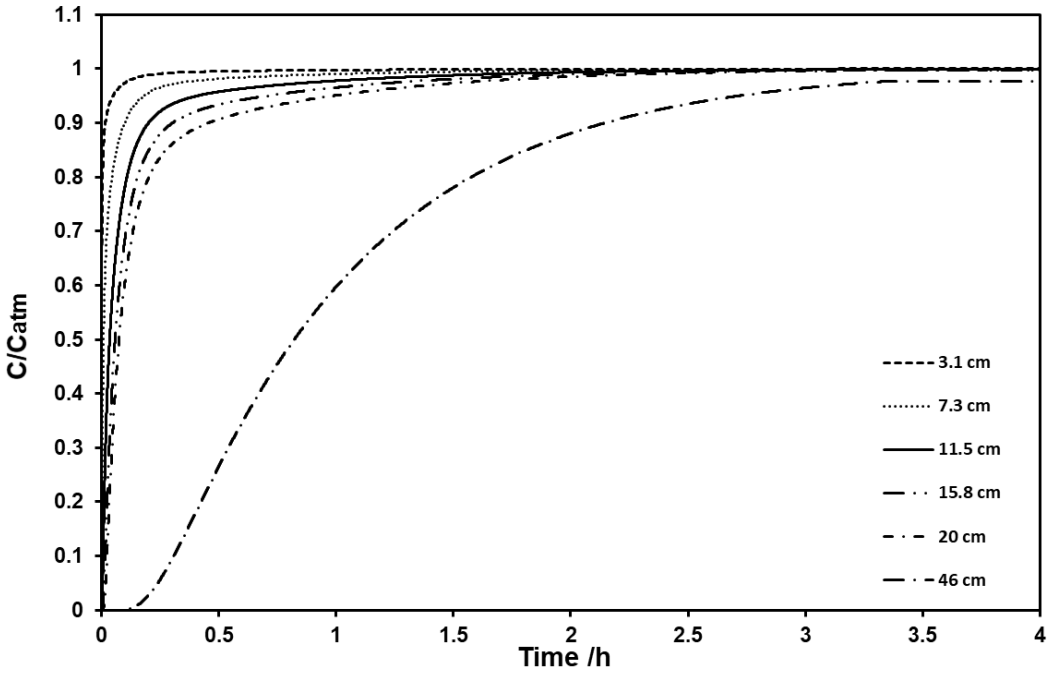

Fig. B30. Relative oxygen concentration (C/C_{atm}), fraction 3, wind condition 10.

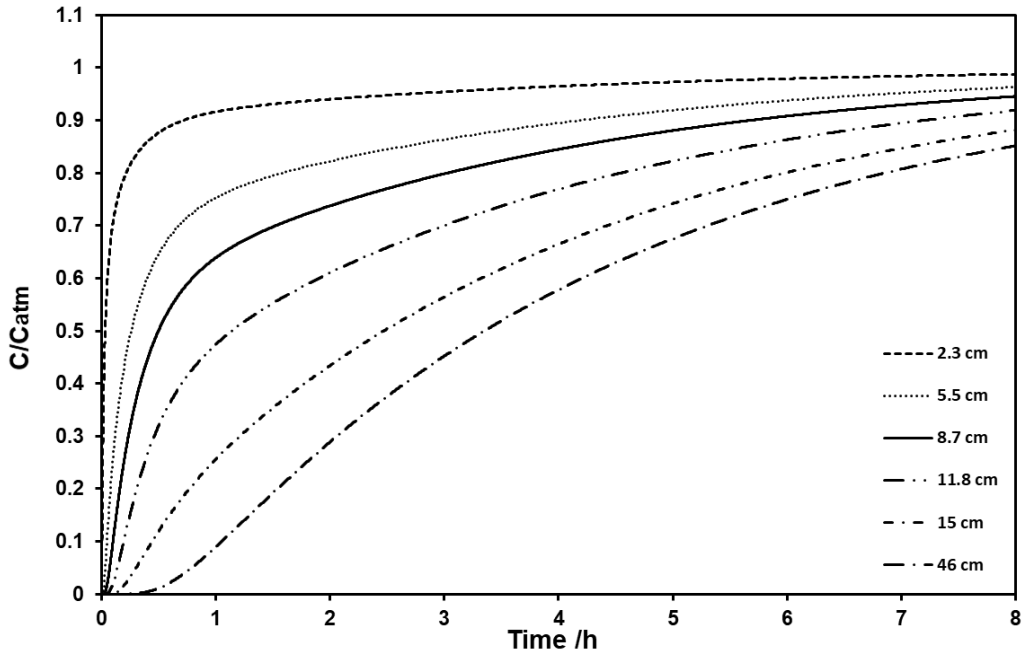

Fig. B31. Relative oxygen concentration (C/C_{atm}), fraction 4, wind condition 1.

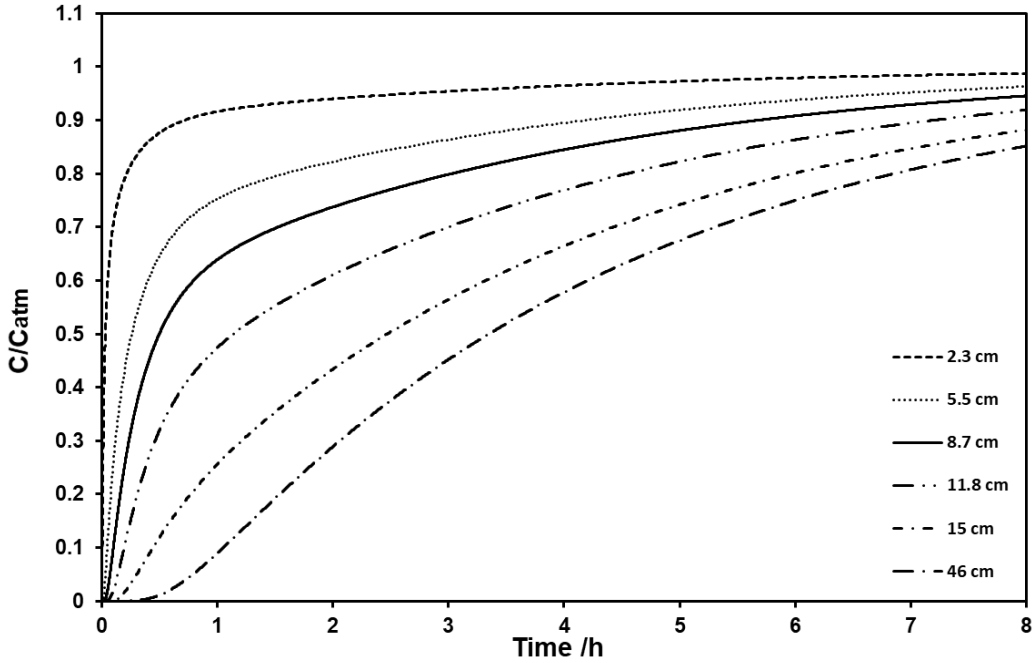

Fig. B32. Relative oxygen concentration (C/C_{atm}), fraction 4, wind condition 2.

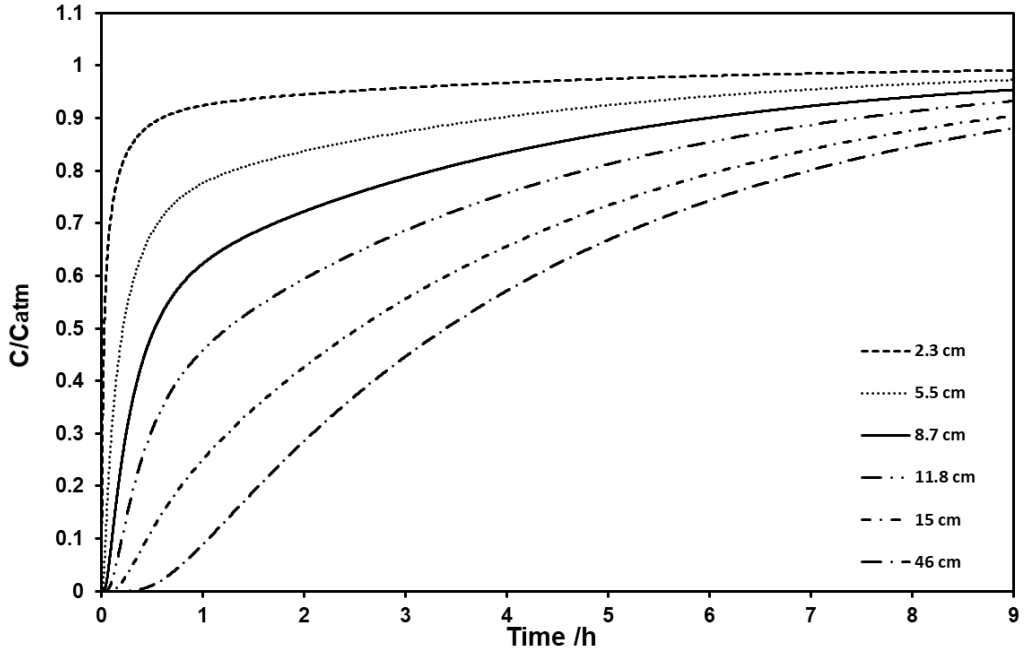

Fig. B33. Relative oxygen concentration (C/C_{atm}), fraction 4, wind condition 3.

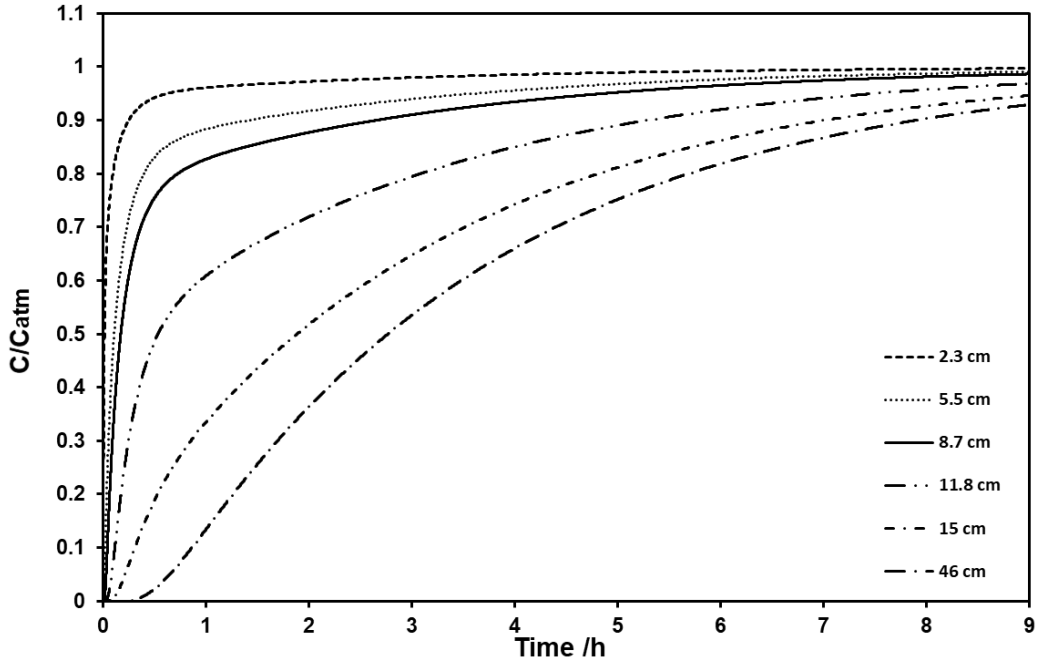

Fig. B34. Relative oxygen concentration (C/C_{atm}), fraction 4, wind condition 4.

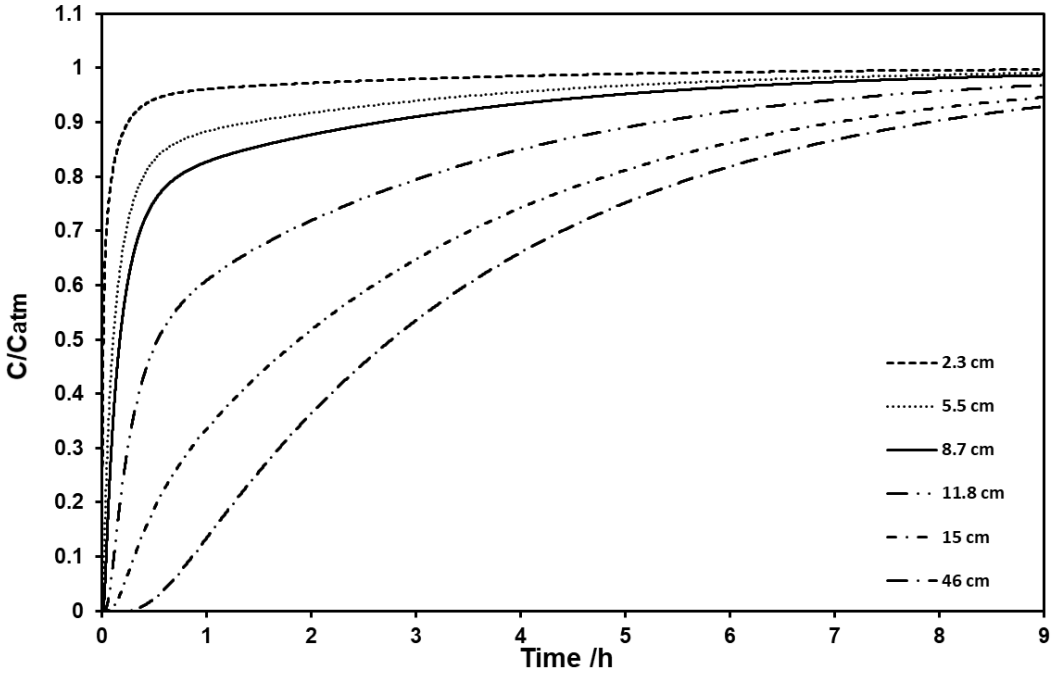

Fig. B35. Relative oxygen concentration (C/C_{atm}), fraction 4, wind condition 5.

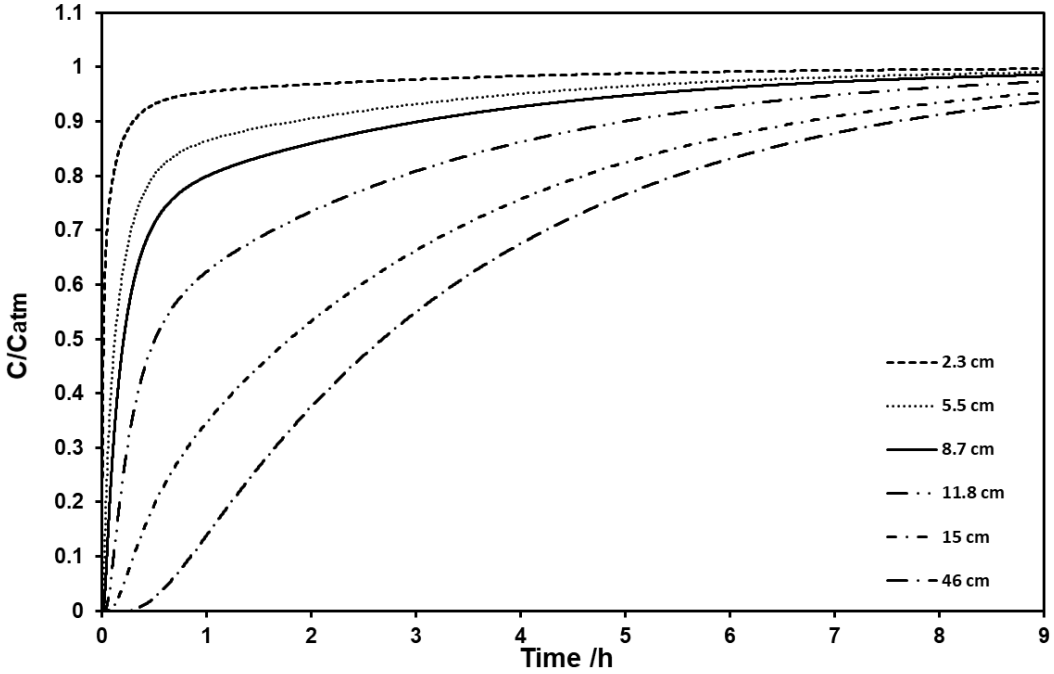

Fig. B36. Relative oxygen concentration (C/C_{atm}), fraction 4, wind condition 6.

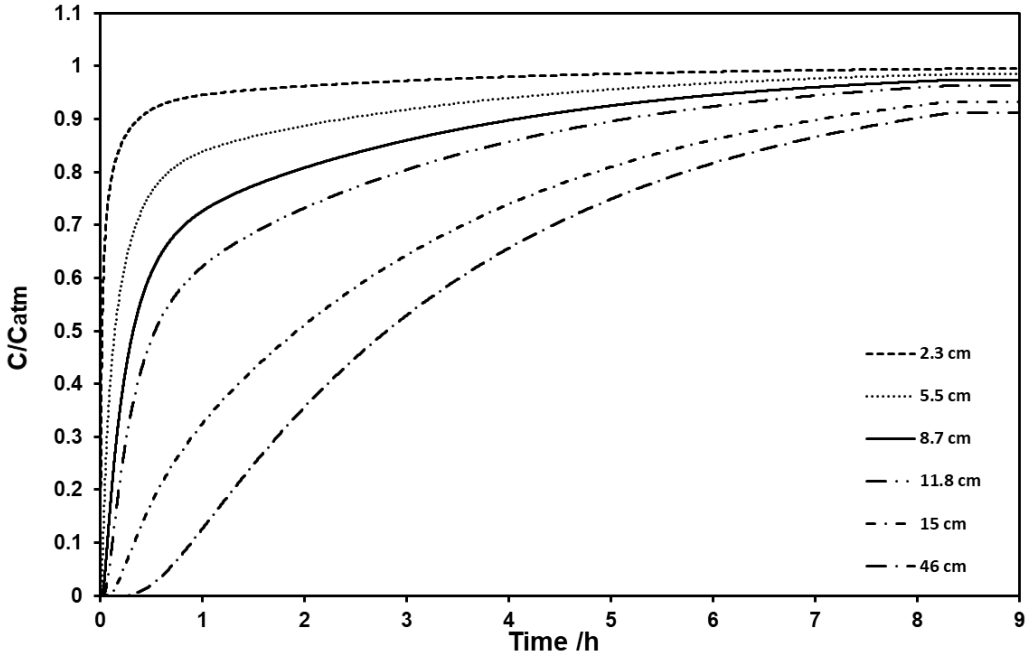

Fig. B37. Relative oxygen concentration (C/C_{atm}), fraction 4, wind condition 7.

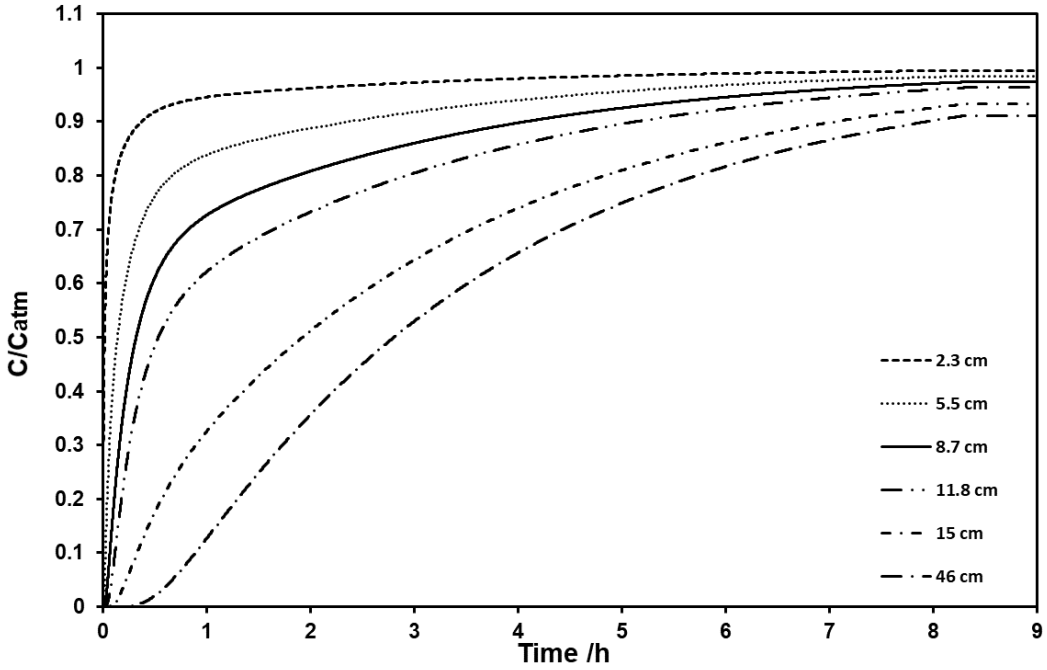

Fig. B38. Relative oxygen concentration (C/C_{atm}), fraction 4, wind condition 8.

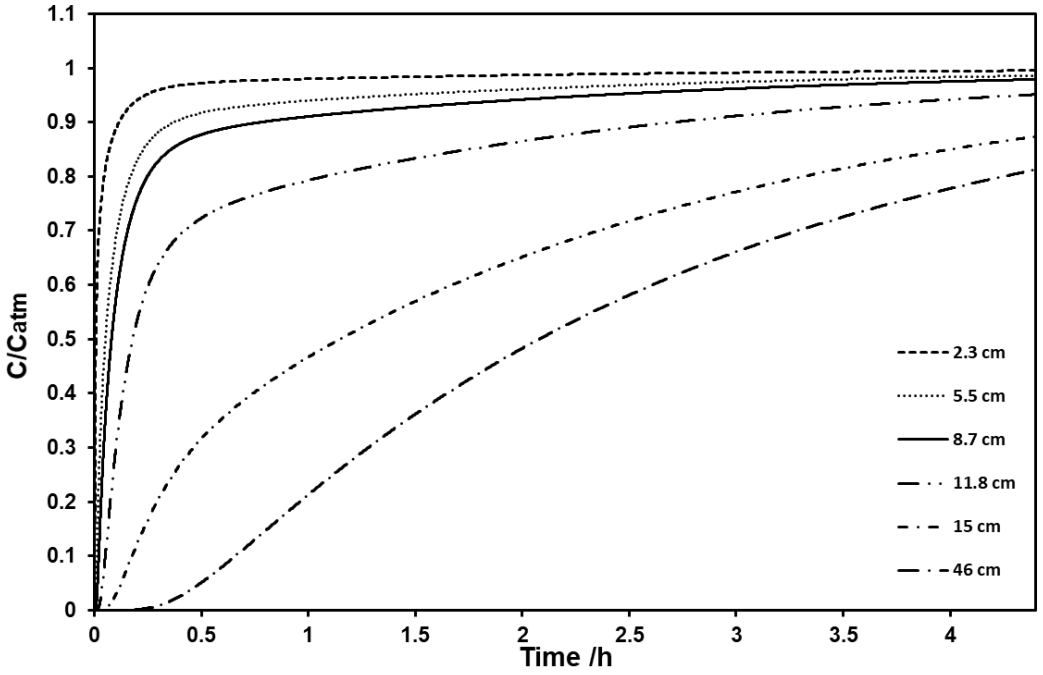

Fig. B39. Relative oxygen concentration (C/C_{atm}), fraction 4, wind condition 9.

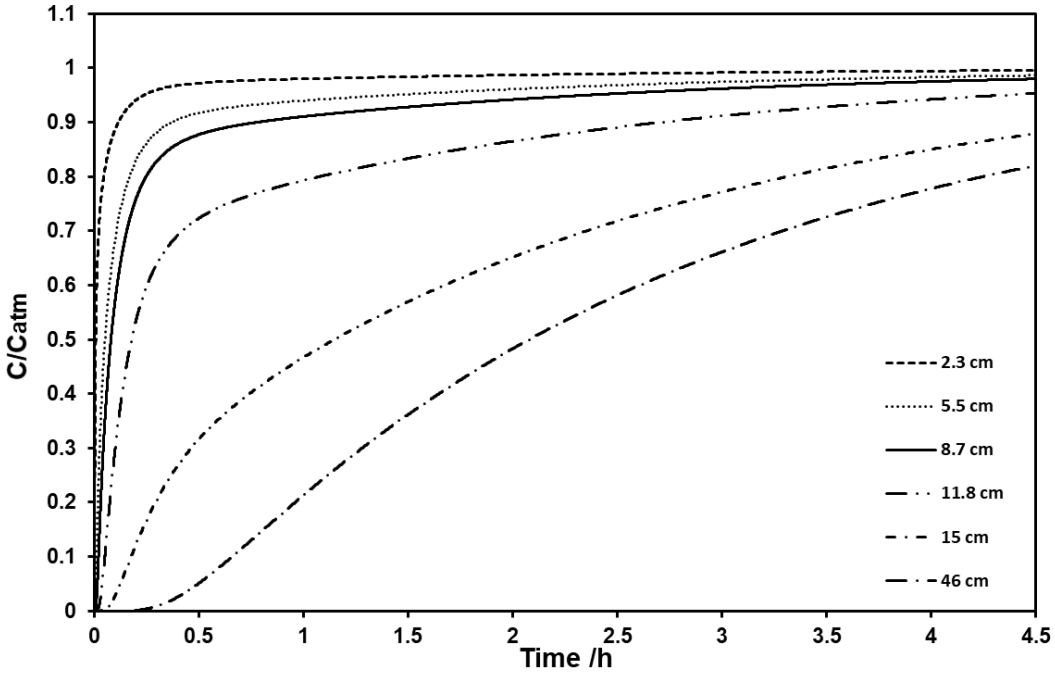

Fig. B40. Relative oxygen concentration (C/C_{atm}), fraction 4, wind condition 10.

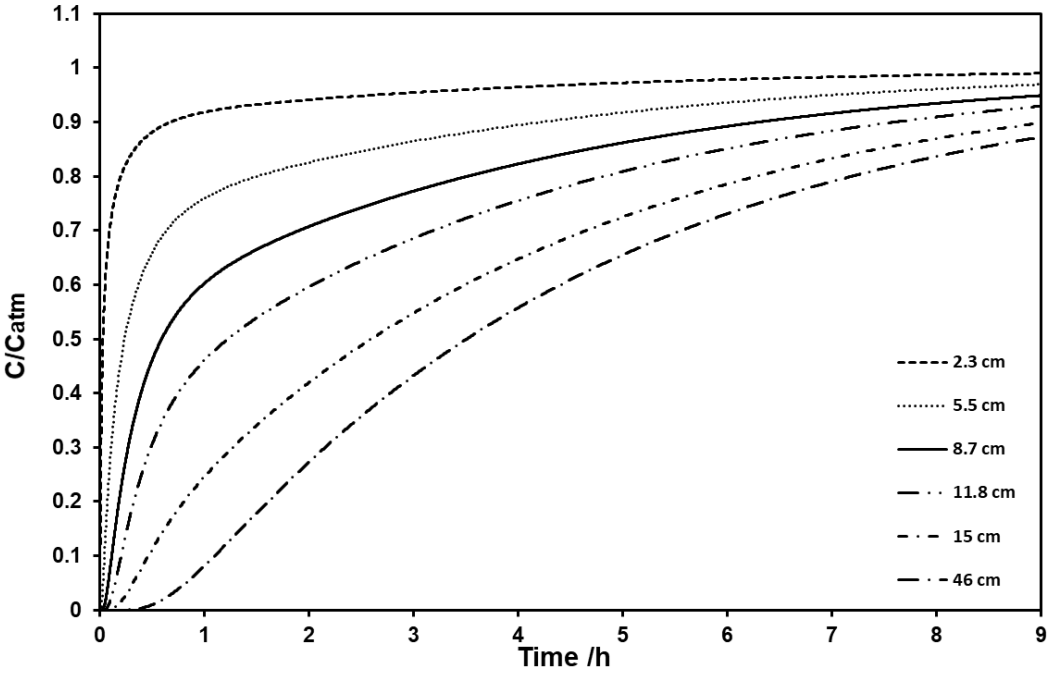

Fig. B41. Relative oxygen concentration (C/C_{atm}), fraction 5, wind condition 1.

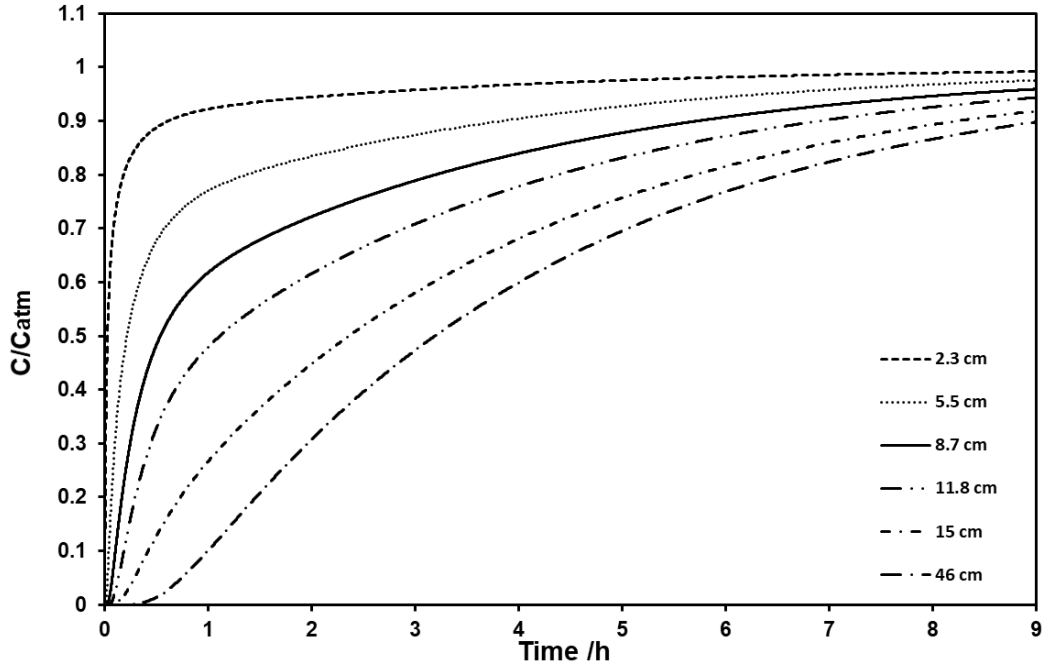

Fig. B42. Relative oxygen concentration (C/C_{atm}), fraction 5, wind condition 2.

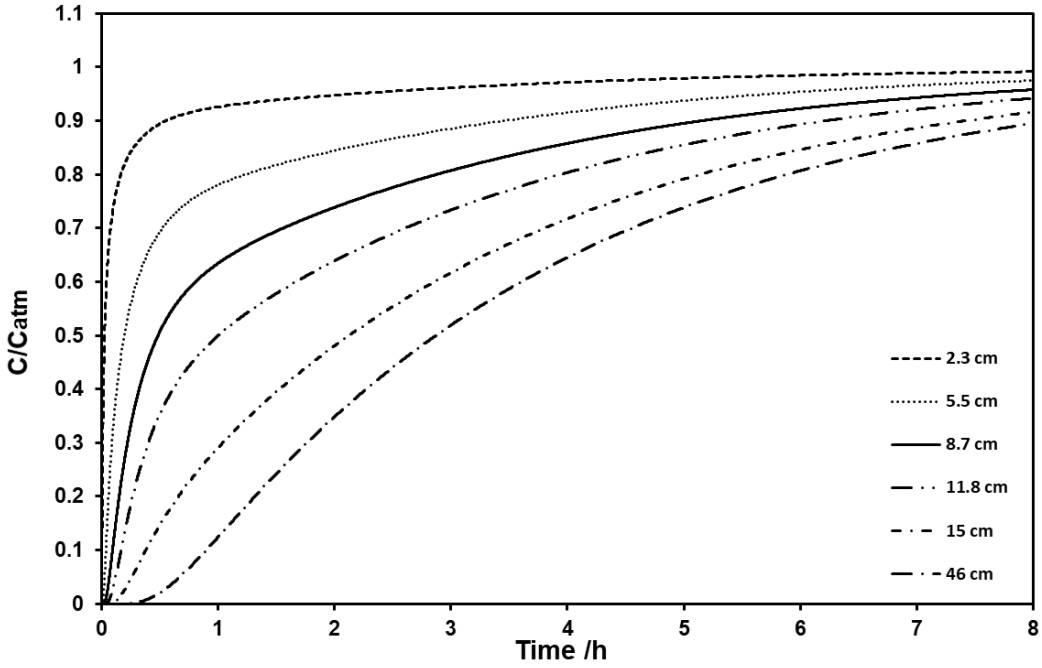

Fig. B43. Relative oxygen concentration (C/C_{atm}), fraction 5, wind condition 3.

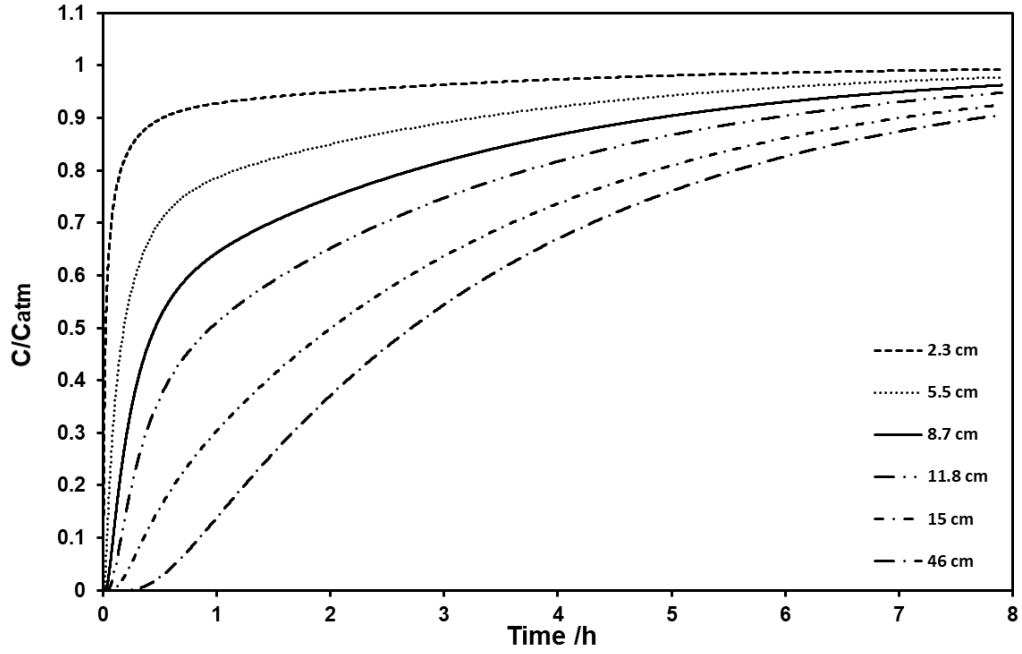

Fig. B44. Relative oxygen concentration (C/C_{atm}), fraction 5, wind condition 4.

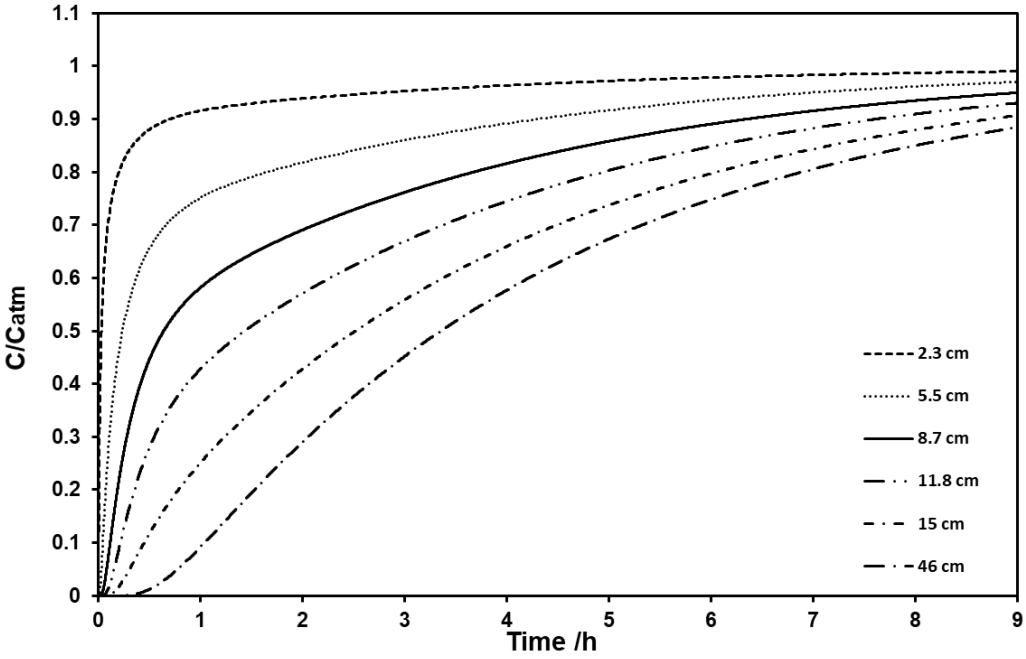

Fig. B45. Relative oxygen concentration (C/C_{atm}), fraction 5, wind condition 5.

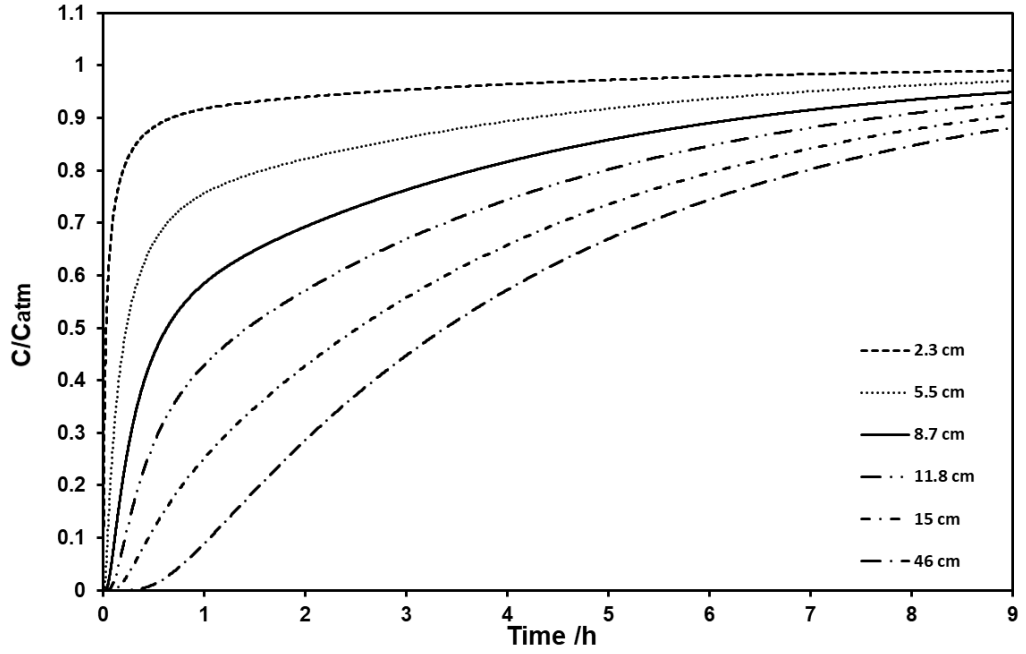

Fig. B46. Relative oxygen concentration (C/C_{atm}), fraction 5, wind condition 6.

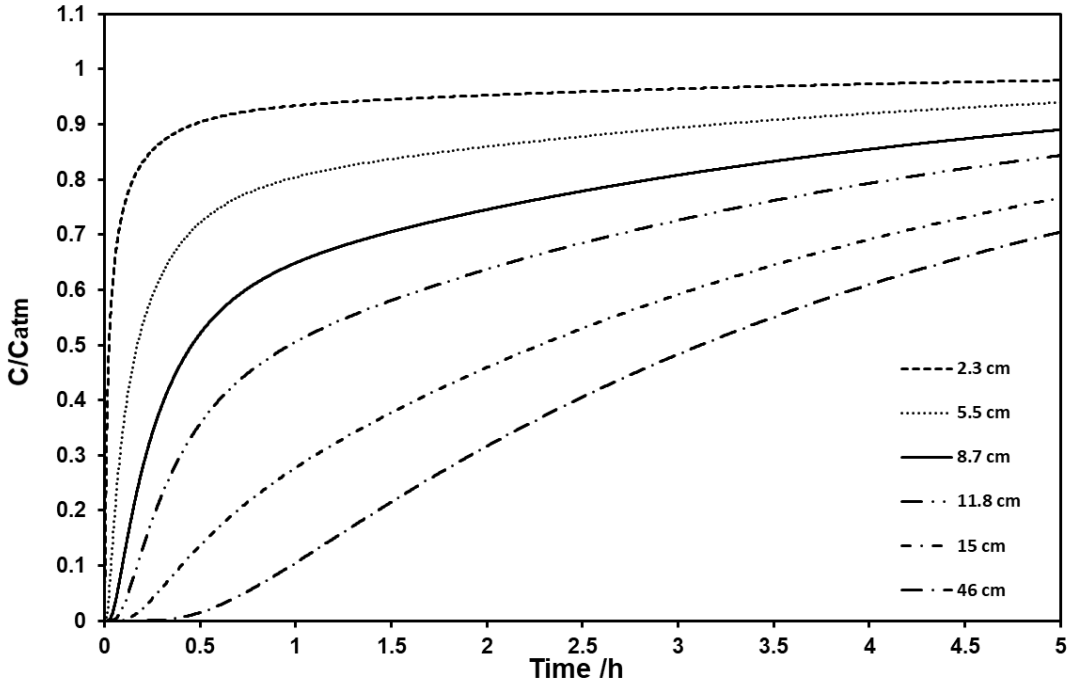

Fig. B47. Relative oxygen concentration (C/C_{atm}), fraction 5, wind condition 7.

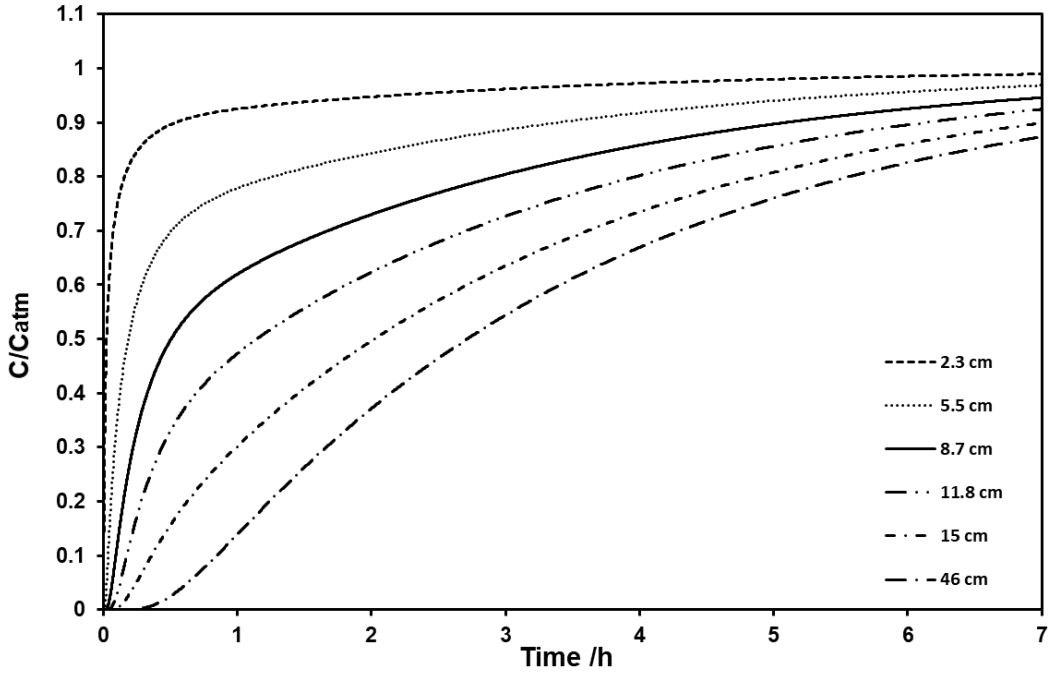

Fig. B48. Relative oxygen concentration (C/C_{atm}), fraction 5, wind condition 8.

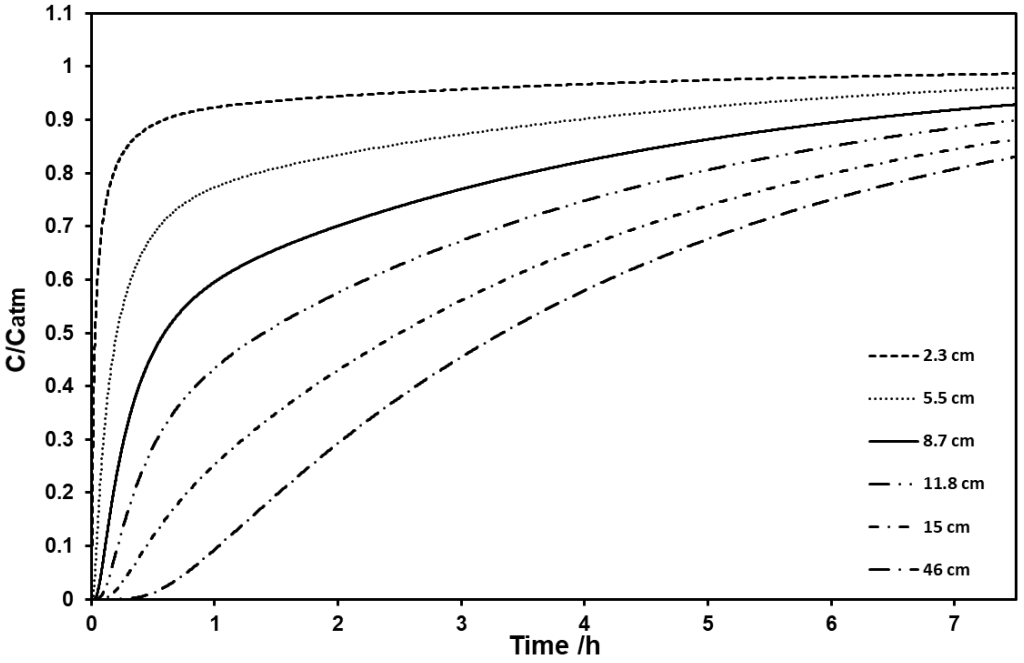

Fig. B49. Relative oxygen concentration (C/C_{atm}), fraction 5, wind condition 9.

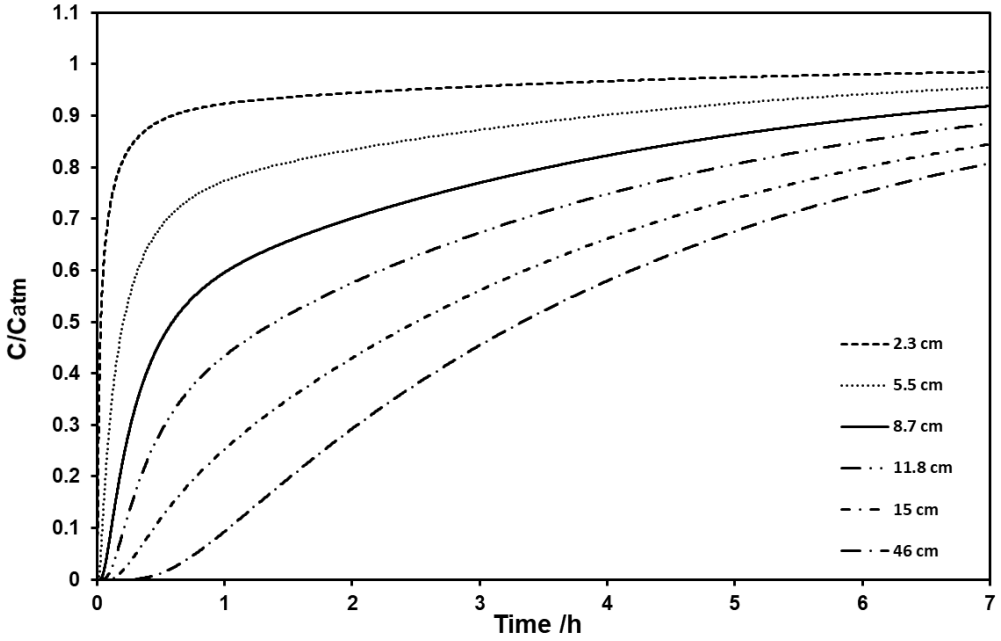

Fig. B50. Relative oxygen concentration (C/C_{atm}), fraction 5, wind condition 10.

Appendix C. Porous Medium Images

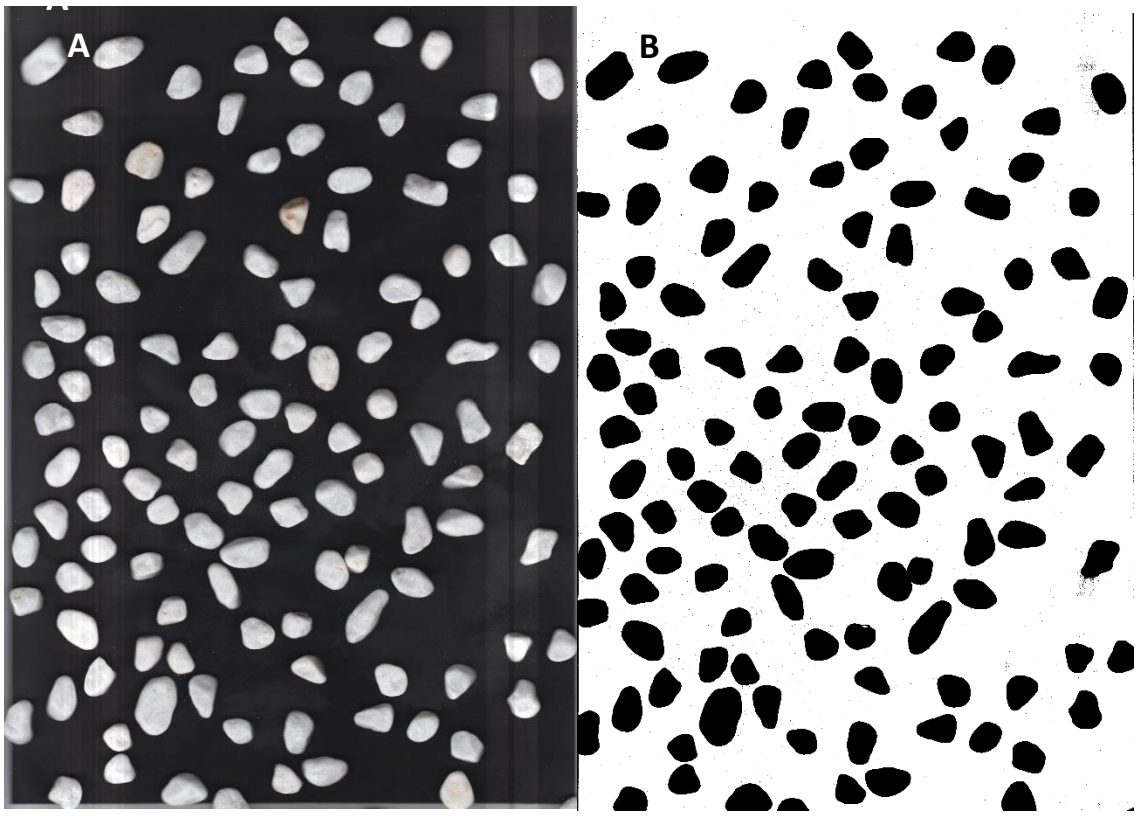

Fig. C1. A, Image of particles. B, Auto-identification of particles using a binary threshold prior to analysis, fraction 1

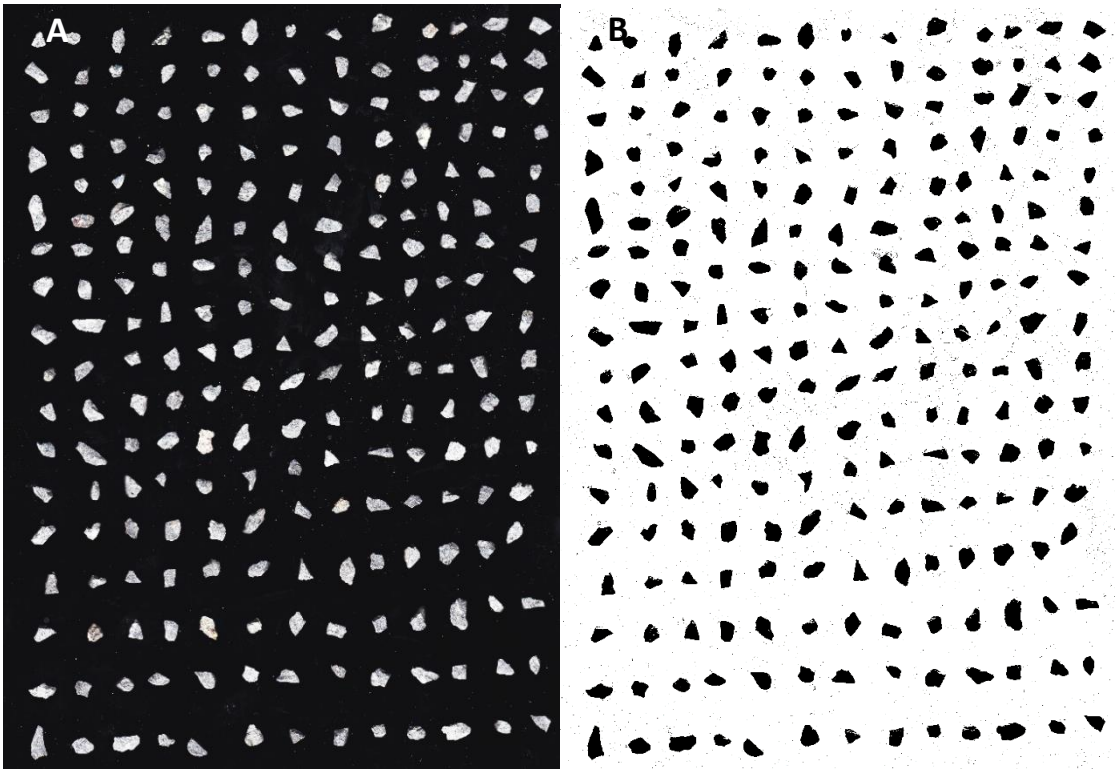

Fig. C2. A, Image of particles. B, Auto-identification of particles using a binary threshold prior to analysis, fraction 2

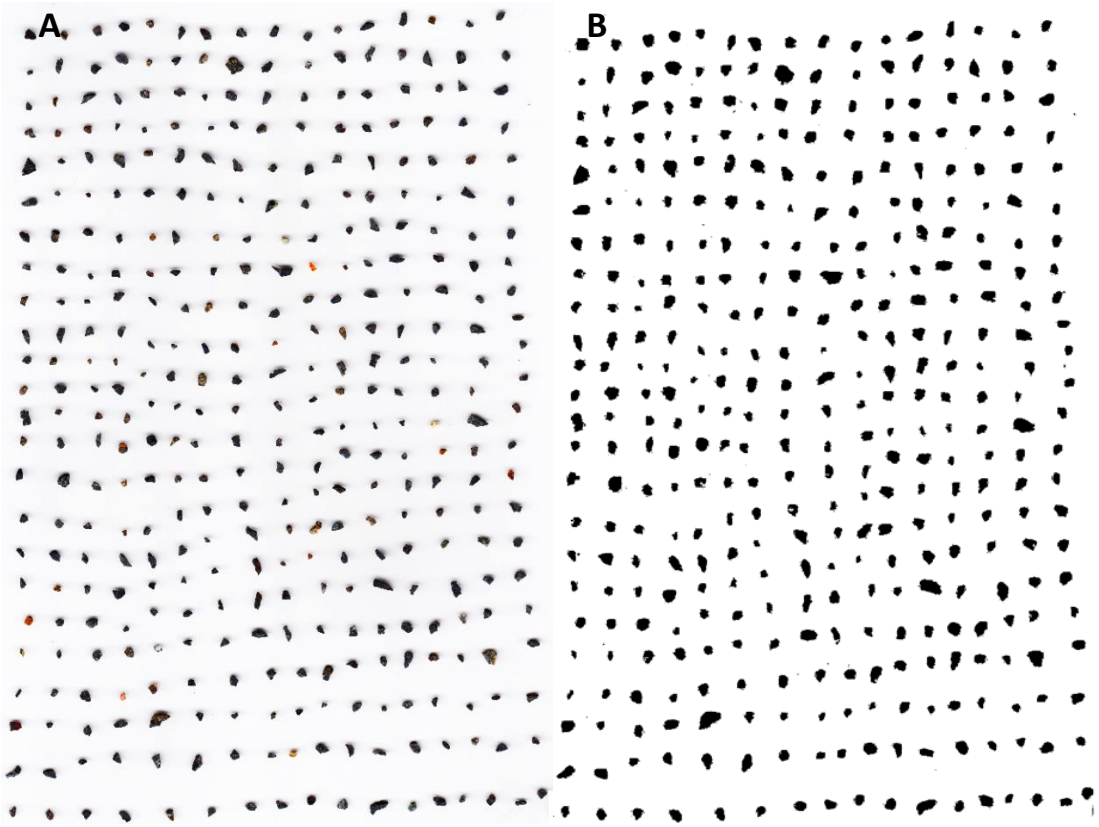

Fig. C3. A, Image of particles. B, Auto-identification of particles using a binary threshold prior to analysis, fraction 3

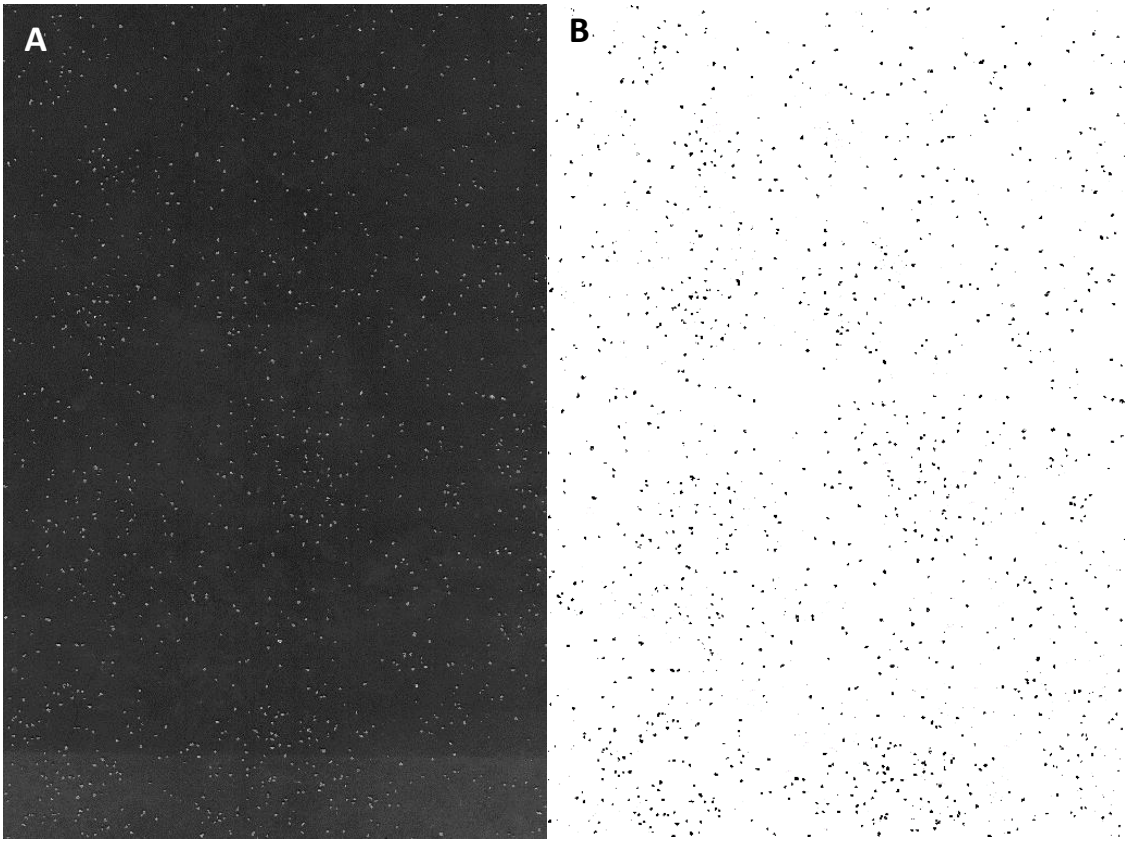

Fig. C4. A, Image of particles. B, Auto-identification of particles using a binary threshold prior to analysis, fraction 4

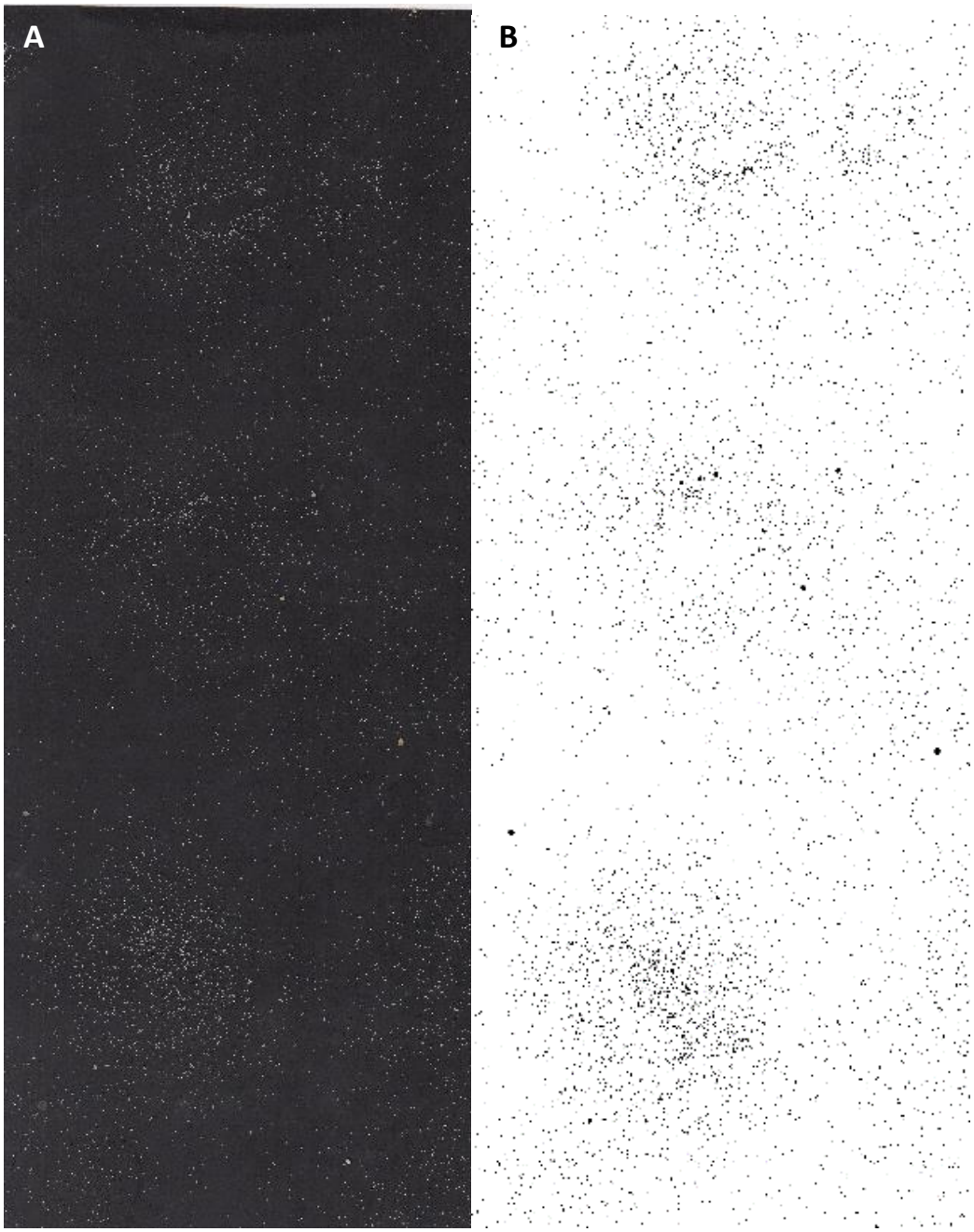

Fig. C5. A, Image of particles. B, Auto-identification of particles using a binary threshold prior to analysis, fraction 5

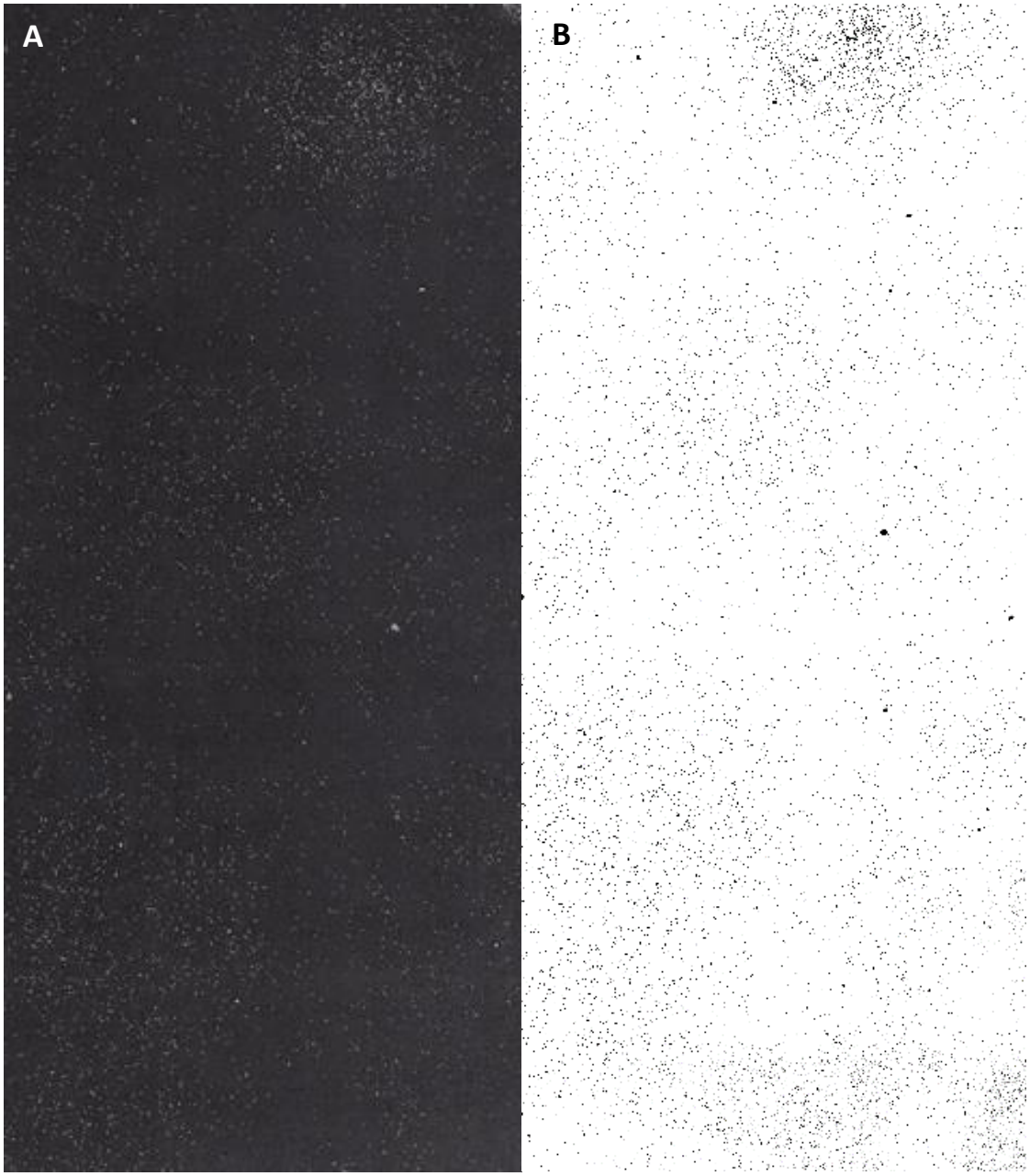

Fig. C6. A, Image of particles. B, Auto-identification of particles using a binary threshold prior to analysis, fraction 5